



**THE DEVELOPMENT OF
A POINT OF CARE DEVICE FOR
MEASURING BLOOD AMMONIA**

by

Niamh T. Brannelly

**A thesis submitted in partial fulfilment of the requirements of the
University of the West of England, Bristol for the degree of Doctor
of Philosophy**

July 2016

Supervisors:

Prof. Anthony J. Killard

&

Prof. Julian P. Hamilton-Shield

DECLARATION

I hereby certify that this material, which I now submit for assessment on the programme of study leading to the award of PhD, is entirely my own work, that I have exercised reasonable care to ensure that the work is original, and does not to the best of my knowledge breach any law copyright, and has not been taken from the work of others save and to the extent that such work has been cited and acknowledged within the text of my work.

ACKNOWLEDGEMENTS

The first person I would like to thank is Prof. Tony Killard. Thank you for your encouragement and guidance through the highs and lows of this research.

Thank you to my second supervisor Prof. Julian Hamilton-Shield.

I would also like to thank Dr. Laura Gonzalez-Macia. Your friendship and support during this time meant so much to me. Thank you for the long scientific discussions and guidance. You were always there for me and I am ever grateful.

Thank you to Dr. Roy Pemberton and Dr. Timothy Cox for their help in preparing for my *viva voce* examination. Their time and advice was sincerely appreciated.

To Hanan Alabouh and Maya El Hindy, thank you *habibati* for the laughter and tears shared. The personal journeys we ventured while in Bristol are those I will never forget.

I would like to mention my all of my friends in UWE, especially Matt Harris for his positive encouragement and Eleni Siasou for her humour. Thank you to George Papaharalabos who kindly provided technical support.

Thank you also to Fiona Rice, true friends are never apart.

I would like to thank Carmel Ryan for her kindness, love and support.

A special thank you to Derek Conway. Without you, I would not have started, let alone finish. Thank you for wiping all of my tears, listening to my obsessive science talk and for the necessary distractions with many happy weekends away from Bristol.

Finally, I would like to thank my family. To my Mother - you are incredible! You ground and strengthen me to strive and continue on the path of my dreams. Thank you also to my sister, Ciara and brother, Liam for their continued love and support. Thank you all for the daily phone calls which cheered me up and kept me going.

DEDICATION

To my Grandfather, James P.A. Kenny (1939 - 2007)

TABLE OF CONTENTS

DECLARATION	I
ACKNOWLEDGEMENTS	III
DEDICATION	III
TABLE OF CONTENTS	IV
ABBREVIATIONS	V
ABSTRACT	IX
CHAPTER 1	1
BLOOD AMMONIA AND ITS CURRENT AND POTENTIAL USE IN CLINICAL DIAGNOSTICS	1
1.1. THE CURRENT STATUS OF CLINICAL BLOOD AMMONIA TESTING	2
1.1.1. The role of the liver in ammonia metabolism	6
1.1.2. The role of the kidneys in nitrogen metabolism.....	11
1.1.3. The effects of ammonia on the central nervous system	12
1.1.4. The digestive system	13
1.1.5. The relationship between the lungs and ammonia	15
1.1.6. Muscle metabolism and exercise and their association with ammonia.....	16
1.2. TECHNIQUES FOR AMMONIA DETERMINATION	17
1.2.1. Test kits and POC devices	20
1.2.2. Conducting polymers such as polyaniline used as ammonia sensing materials	22
1.2.3. The reaction mechanism of ammonia and polyaniline.....	25
1.3. CONCLUSIONS.....	26
1.4. THESIS OUTLINE.....	28
1.5. REFERENCES.....	30

CHAPTER 2	42
MATERIALS AND METHODS	42
2.1. MATERIALS	43
2.2. INSTRUMENTATION.....	44
2.3. SOFTWARE	45
2.4. METHODS	45
2.4.1. Buffer.....	45
2.4.2. Electrode fabrication via screen printing.....	45
2.4.3. Polyaniline nanoparticle synthesis	46
2.4.4. Inkjet printing of polyaniline nanoparticles	46
2.4.5. Assembly of the aqueous ammonia sensing device	47
2.4.6. Characterisation techniques.....	49
2.4.7. Cyclic voltammetric analysis of polyaniline dispersions	49
2.4.8. Electrochemical impedance spectroscopic measurement of ammonia	50
2.4.8.1. Ratiometric method.....	50
2.4.9. Spectrophotometric measurement of ammonia	50
2.4.10. Bradford protein assay.....	50
2.4.11. Oil red O analysis for cellular lipids	51
2.5. REFERENCES.....	52
CHAPTER 3	53
OPTIMISATION AND CHARACTERISATION OF POLYANILINE NANOPARTICLE INK PRODUCTION AND SENSOR FABRICATION	53
3.1. INTRODUCTION	54
3.1.1. Polyaniline nanoparticle synthesis and processability	54
3.1.2. Electrochemical impedance spectroscopic analysis	55
3.2. RESULTS AND DISCUSSION	57

3.2.1. Fabrication and characterisation of polyaniline nanoparticles	57
3.2.2. Screen printed silver interdigitated electrode design as part of the inkjet-printed polyaniline sensor.....	61
3.2.3. Impedimetric assessment of polyaniline sensors.....	63
3.2.4. Impact of the synthesis method on particle size and its effect on sensor impedance.....	66
3.2.5. Impact of the synthesis method on zeta-potential and its effect on sensor impedance.....	68
3.2.6. Characterisation of the ammonia sensor in response to liquid samples	71
3.2.6.1. The use of a hydrophobic membrane for ammonia gas measurement from a liquid sample.....	72
3.2.6.2. Ammonia sensor reproducibility and drift	74
3.2.6.3. Investigation of the polyaniline nanoparticle inkjet printing process on the characterisation and performance of the ammonia sensor	75
3.2.7. Electrochemical characterisation of inkjet-printed polyaniline films	81
3.3. CONCLUSIONS.....	85
3.4. REFERENCES.....	86
CHAPTER 4	91
DESIGN AND TESTING OF THE AQUEOUS AMMONIA DEVICE	91
4.1. INTRODUCTION	92
4.2. RESULTS AND DISCUSSION	93
4.2.1. Impedance spectroscopic characterisation of the prototype ammonia measurement device	93
4.2.2. Strategies to eliminate solvent interferents	97
4.2.2.1. Investigation of the effect of membrane composition.....	97
4.2.2.2. Ammonia sensor recovery	99
4.2.2.3. Investigation of sample exposure time in the sampling chamber	103

4.2.2.4. Investigation of the effect of sample pH	105
4.2.3. Time course analysis of the ammonia measurement process	110
4.2.4. Sensor pre-calibration	112
4.3. CONCLUSION	116
4.4. REFERENCES	118
CHAPTER 5	121
CHARACTERISATION AND VALIDATION OF THE BLOOD AMMONIA SENSOR DEVICE	121
5.1. INTRODUCTION	122
5.1.1. Blood buffering capacity	122
5.1.2. Consideration of sample interferences	123
5.2. RESULTS AND DISCUSSION	124
5.2.1. Spectrophotometric analysis of ammonia in solution using the Berthelot reaction	124
5.2.2. Validation of the device using the Abcam® spectrophotometric assay	125
5.2.3. Interference study	131
5.2.4. Characterisation of sample matrix effects on ammonia measurement	134
5.2.4.1. Determination of ammonia in a protein sample matrix	134
5.2.4.2. Ammonia analysis in serum	136
5.2.4.3. Spectrophotometric assessment of protein and lipid assay interference	139
5.2.4.4. Delipidated and deproteinated serum as a matrix for ammonia determination using the ammonia device	142
5.2.5. Lifetime study of the blood ammonia device	149
5.3. CONCLUSIONS	151
5.4. REFERENCES	153

CHAPTER 6	157
FUTURE DEVELOPMENTS	157
6.1. FURTHER DEVELOPMENTS OF THE BLOOD AMMONIA DEVICE	158
6.1.1. Reflections and lessons	159
6.1.1.1. Limitations	159
6.1.1.2. Sensitivity and reproducibility	159
6.1.1.3. Optimisations	160
6.1.3. Further matrix and interference assessments.....	161
6.2. INTEGRATED SENSING SYSTEMS	162
6.3. OTHER APPLICATIONS AND ALTERNATIVE TECHNIQUES	162
6.3.1. Wearable sensors	162
6.3.2. Clinical and environmental gas-based ammonia measurements	163
6.3.3. Enzymatic biosensors	163
6.3.4. Alternative techniques to impedimetric ammonia analysis.....	164
6.4. REFERENCES.....	166
CHAPTER 7	169
OVERALL CONCLUSIONS	169
7.1. CONCLUSIONS.....	170
7.2. CLOSING STATEMENT.....	171
LIST OF PUBLICATIONS AND PRESENTATIONS.....	173
1. SCIENTIFIC PUBLICATIONS.....	174
2. ORAL PRESENTATIONS	174
3. POSTER PRESENTATIONS	175
APPENDIX.....	178

ABBREVIATIONS

a.c.	Alternating current
ADP	Adenosine diphosphate
Ag/AgCl	Silver/silver chloride
ALF	Acute liver failure
APS	Ammonium persulphate
ATP	Adenosine-5-triphosphate
BCAAs	Branched chain amino acids
BSA	Bovine serum albumin
BUN	Blood urea nitrogen
CF	Cystic fibrosis
CNS	Central nervous system
CPS-1	Carbamoyl phosphate synthetase-1
CV	Cyclic voltammetry
<i>D</i>	Diffusion coefficient
DBSA	Dodecylbenzene sulphonic acid
d.c.	Direct current
DLS	Dynamic light scattering
E	Emeraldine
EC	Ethyl cellulose
EIS	Electrochemical impedance spectroscopy
ESRD	End stage renal disease
<i>f</i>	Frequency
FBS	Foetal bovine serum
GCE	Glassy carbon electrode
GCS	Glasgow Coma Scale
GLDH	Glutamate dehydrogenase
GS	Glutamine synthetase

HE	Hepatic encephalopathy
HM	Hepatic myelopathy
<i>H. pylori</i>	Helicobacter pylori
I	Current
IDEs	Interdigitated electrodes
ICP	Increased intracranial pressure
L	Leucoemeraldine
LED	Light-emitting diode
LOD	Limit of detection
MELD	Model for End-Stage Liver Disease
M	Mean
M_n	Number average molar mass
M_w	Weight average molar mass
NADPH	Nicotinamide adenine dinucleotide phosphate
NAG	N-acetylglutamate
NMDA	N-methyl-D-aspartate
OTC	Ornithine transcarbamylase
ϕ	Phase shift
P	Pernigraniline
<i>P</i>	Permeation
PBS	Phosphate buffered saline solution
PDI	Polydispersity index
PET	Polyethylene terephthalate
pKa	Acid dissociation constant
POC	Point of care
ppbv	parts-per-billion volume
PPI	Proton pump inhibitor
ppm	Parts-per-million
PSA	Pressure sensitive adhesive

PTFE	Polytetrafluoroethylene
PVDF	polyvinyl fluoride
QC	Quality control
R	Pearson product-moment correlation coefficient
R^2	Coefficient of determination
RBCs	Red blood cells
Refs	References
RSD	Relative standard deviation
S	Solubility coefficient
SD	Standard deviation
SDS	Sodium dodecyl sulfate
SEM	Scanning electron microscopy
TCA	Trichloroacetic acid
t_e	Ejection time
TEM	Transmission electron microscopy
TIPS	Transjugular intrahepatic portosystemic shunt
TMT	Trail Making Test
UCD	Urea cycle disorder
UTI	Urinary tract infection
UV	Ultra violet
V	Voltage
VOCs	Volatile organic compounds
v/v%	volume/volume percent
WHC	West Haven Criteria
Z	Impedance
Z'	Real impedance
Z''	Imaginary impedance
$ Z $	Absolute impedance
Z_{air}	Impedance in air

Zd

Average diameter of a nanoparticle

ABSTRACT

Ammonia is produced in the body during the metabolism of amino acids. In the liver, it is converted to urea via the urea cycle and excreted by the kidneys as urine. Normal levels are between 11 to 50 μM , whereas a blood ammonia level of approximately 100 μM indicates pathology. Elevated blood ammonia is associated with a number of pathological conditions including liver and kidney dysfunction. Conditions such as these can affect brain function and can be fatal. Current blood ammonia analysis requires a laboratory blood test. Few, if any of the techniques used are suitable for point of care (POC) testing. The development of a reliable and simple method for blood ammonia determination is essential for clinical diagnosis and management of patient progress in order to prevent further debilitating illnesses developing, and extending life. This is particularly critical in many disorders such as hyperammonaemia of the new-born, inborn errors of metabolism including urea cycle defects, organic acidaemias, hyperinsulinism/hyperammonaemia, liver disease and other causes of hyperammonaemic encephalopathy. This thesis investigates the development of an electrochemical sensor for the measurement of ammonia in blood.

Polyaniline has a known affinity for ammonia which operates on the deprotonation of the polyaniline backbone forming an ammonium ion. In this work, polyaniline nanoparticles were fabricated and inkjet-printed onto silver screen printed electrodes. The sensors were then incorporated into devices containing a gas-permeable membrane, which facilitated the measurement of gaseous ammonia from a liquid sample (blood) using electrochemical impedance spectroscopy. The combination of impedance spectroscopy with a gas-permeable membrane allowed the measurement of gaseous ammonia from solution.

The ammonia device developed possessed refinements to enhance its sensitivity and included careful optimisation of other aspects of the measurement. For example, an air purge through the device gas chamber was employed to remove matrix interferences from the sensor and improve the specificity to ammonia. The pH of the sample to be analysed was modified in order to increase the mass of ammonia in solution, thus lowering the limit of detection (LOD) of the device. Finally, assay timings were optimised in order to increase the impedimetric response

of ammonia. These optimisations resulted in the effective detection of ammonia in a liquid sample down to the lowest clinically relevant levels found in blood.

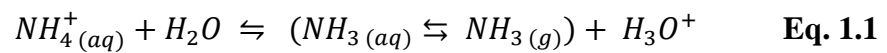
The devices displayed an impedimetric baseline intra- and inter-variability of 25 and 6.9%, respectively for $n = 15$ over a period of 160 s. A calculated limit of LOD of 12 μM was achieved for human serum measurements, with a coefficient of determination of 0.9984, slope of 0.0046 and an intercept of 1.1534 across the linear range of 25 to 200 μM ammonia ($n = 3$). The device was validated against a commercial spectrophotometric assay which resulted in excellent correlation (0.9699, $p < 0.0001$) with a slope of 1.4472 and an intercept of 0.5631 between both methods ($n = 3$). The devices could be stored in desiccant for up to five months and displayed minimal variation (0.64%) over time ($n = 12$).

CHAPTER 1

BLOOD AMMONIA AND ITS CURRENT AND POTENTIAL USE IN CLINICAL DIAGNOSTICS

1.1. THE CURRENT STATUS OF CLINICAL BLOOD AMMONIA TESTING

Ammonia is an important analyte in clinical diagnostics. It is an inorganic nitrogen compound found naturally in the body and is involved in many metabolic processes. It is produced from the deamination of amino acids in the liver, muscle and kidneys. It is also produced by bacteria in the colon and small intestine and also from the metabolic breakdown of dietary proteins (Huizenga *et al.*, 1996). It may be combined with glutamate to form glutamine, which is an important metabolic fuel for some tissues {{142 Adeva, Maria M. 2012}}. The importance of ammonia in metabolism has been known for a very long time. (Dawson, 1978) It is neurotoxic and can penetrate biological membranes such as the blood-brain barrier. It is detoxified by converting it to urea via the urea cycle in the liver and excreted by the kidneys as urine, so maintaining a low concentration of ammonia in the body. Impaired clearance of ammonia results in rising ammonium ion (NH_4^+) levels in the blood. Levels exceeding 1 mM are toxic (Barsotti, 2001) and often affect the central nervous system, deteriorating brain, liver, kidney, stomach and lung function (Brusilow and Maestri, 1996). Blood ammonia is in the form of either ammonium ions (NH_4^+) or aqueous ammonia ($\text{NH}_3(\text{aq})$) which is in equilibrium with dissolved gaseous ammonia ($\text{NH}_3(\text{g})$). Throughout this thesis, unless stated otherwise, we will refer to these interchangeably as ammonia. Ammonia has a pKa of 9.3 and a pKb of 4.7 and so under normal physiological conditions (pH 7.4) above 98% of ammonia is present as an aqueous species, as determined by the Henderson-Hasselbalch equation (Solga *et al.*, 2013):



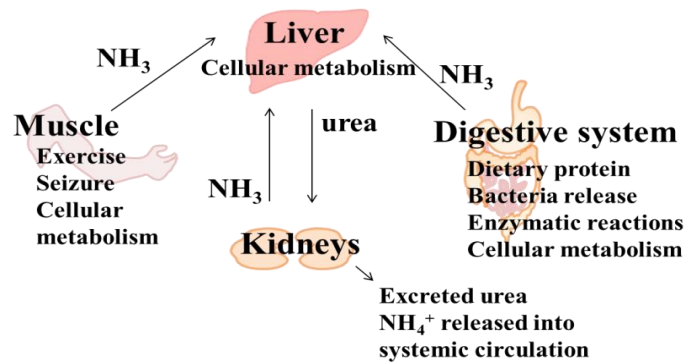
$$K_a = \frac{[\text{H}_3\text{O}^+][\text{NH}_3]}{\text{NH}_4^+}$$

$$\text{when } [\text{NH}_4^+] = [\text{NH}_3], \text{ then } K_a = [\text{H}_3\text{O}^+]$$

$$pK_a(\text{NH}_4^+) = 9.3 \text{ and } pK_b(\text{NH}_3) = 14.0 - 9.3 = 4.7$$

Under normal conditions, ammonia-rich blood is transported via the portal vein to the liver which goes on to be detoxified via the urea cycle and excreted by the kidneys as urea in urine, thus maintaining nitrogen homeostasis (Fig. 1.1).

Normal ammonia metabolism



Liver dysfunction

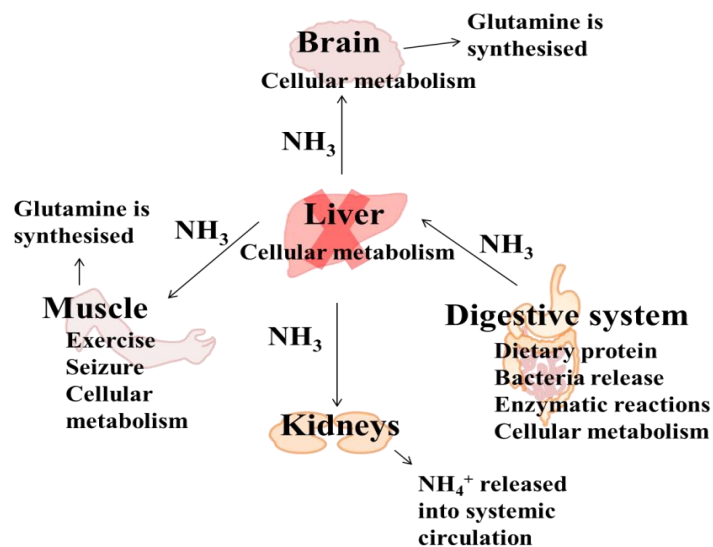


Figure 1.1. Schematic of ammonia metabolism in the body under normal conditions and during liver dysfunction. Endogenous or exogenous ammonia is transferred to the liver and detoxified. It is then transferred to the kidneys and excreted as urea. During liver dysfunction ammonia is not detoxified and accumulates in the body, passing through the blood-brain barrier. Skeletal muscle begins to use up excess ammonia, generating glutamine.

Blood ammonia levels are typically in the range of 11 to 50 μM . Levels may vary between venous, capillary and arterial blood (Ong *et al.*, 2003, Mehmood *et al.*, 2013). When ammonia homeostasis is affected, there can be an increase in systemic ammonia (hyperammonaemia). Hyperammonaemia is not itself a diagnosis but a prompt for further investigation to find the underlying cause which may be inherited or acquired (Elgouhari and O'Shea, 2009). Ammonia toxicity can affect all organs,

especially the brain. Levels exceeding 100 μM may trigger a cascade of pathological events in which the liver, kidney, stomach, lung and central nervous system (CNS) may be irreversibly affected, leading to encephalopathy with associated neurological and cognitive impairment across a broad spectrum of severity (Pita *et al.*, 2004, Bosoi and Rose, 2009). Congenital hyperammonaemia is a neonatal emergency. Ammonia levels should be measured in seemingly healthy neonates with unexplained non-specific systemic illness with neurological symptoms (Leonard and Morris, 2006). There is often no definitive cure for most hyperammonaemic conditions. However, restriction of dietary protein intake and prevention of catabolism through high calorie diets and supplements can prevent encephalopathy (Lee *et al.*, 2015). Current treatment of hyperammonaemia involves lowering ammonia levels immediately by treating any ammonia producing processes (stopping gastrointestinal bleeding, treating infections, kidney failure, and electrolyte abnormalities). Management of ammonia levels then takes place by inhibiting ammonia production in the gut and targeting ammonia removal pathways. Management requires tailored intake of protein and a provision of carbohydrates (to stop catabolism and promote anabolism) and intake of ammonia scavenging drugs (sodium benzoate, sodium phenylbutyrate and arginine hydrochloride) (Broomfield and Grunewald, 2012). Severe cases may require haemofiltration or dialysis. Medicines containing ammonium (including certain antacids) should also be avoided. Table 1.1 presents numerous pathological conditions associated with hyperammonaemia.

Chapter 1

Table 1.1. Pathological conditions associated with hyperammonaemia.

Classification	Underlying causes	Ammonia (μM)	Details	Treatment
Congenital	Transient hyperammonaemia of new-borns	>1500		Lactitol, carglumic acid
	Urea cycle disorders	>600	Enzyme and transporter defects, citrin deficiency, hyperornithinaemia hyperammonaemia homocitrullinuria, lysinuric protein intolerance	Sodium benzoate, branched chain amino acids (BCAAs), glycerol phenylbutyrate. Liver (Mukhtar <i>et al.</i> , 2013) and/or kidney (Bezinover <i>et al.</i> , 2010) transplant
	Organic acidaemias	100-150	Pyruvate dehydrogenase deficiency, Type B pyruvate carboxylase deficiency Propionic, methylmalonic, isovaleric	Biotin, thiamine, dichloroacetate, citrate
	Respiratory alkalosis	~600 ~200	Hepatic glutamine synthetase deficiency, primary pulmonary hypertension and high nitrogen load	Lung transplant (Hocker <i>et al.</i> , 2011, Lichtenstein <i>et al.</i> , 2000)
	Fatty acid oxidation disorders	200-600	Carnitine palmitoyltransferase-1/ long chain 3-hydroxyacyl-CoA dehydrogenase deficiency/ very long chain hydroxyacyl-CoA dehydrogenase deficiency/ glutaric aciduria type II/ carnitine deficiency	Bone marrow transplant (Davies <i>et al.</i> , 1996)
Acquired	Hyperinsulinism hyperammonaemia syndrome	~250	Hypoglycaemia and hyperinsulinaemia	Diazoxide, K_{ATP} antagonist, epigallocatechin gallate
	Sepsis, liver dysfunction	<200		BCAAs, L-ornithine, L-aspartate, glycerol phenylbutyrate

1.1.1. The role of the liver in ammonia metabolism

The liver maintains nitrogen homeostasis. It does this by converting nitrogenous compounds produced via the breakdown of amino acids into less toxic soluble forms which can be safely removed by the urea cycle (Fig. 1.2) and excreted by the kidneys (Adeva *et al.*, 2012). The liver is subject to a number of congenital or acquired disorders, which can affect its ability to effectively metabolise ammonia to urea. A urea cycle disorder (UCD) is a genetic mutation in one of the six enzymes that control the cycle: N-acetylglutamate synthase (NAGS), carbamoyl phosphate synthetase-1 (CPS-1), ornithine transcarbamylase (OTC), argininosuccinate synthetase-1, argininosuccinate lyase, arginase-1 hydrolysis (Table 1.2). Protein breakdown results in an increase in glutamate concentration, which signals the up-regulation of N-acetylglutamate synthase (NAGS) and thus the entire cycle. The remaining enzymatic steps are controlled by their substrate concentrations. Impaired enzymatic function obstructs the cycle causing hyperammonaemia (Voet and Voet, 2004). Half of patients with UCD present in the neonatal period with non-specific symptoms which develop into hyperammonaemic crisis and which results in severe intellectual disability (Leonard and Morris, 2002). Effective neonatal monitoring for elevated ammonia could reduce associated morbidity and mortality. Acquired UCD can present at any time. It is usually brought on by pregnancy, infectious illnesses or fasting with subsequent catabolism or the use of sodium valproate which unmasks latent CPS-1 or OTC deficiency (Gropman *et al.*, 2007). Sodium valproate is known to cause hyperammonaemia (Aires *et al.*, 2011). Diagnosis of an acquired UCD is performed by measuring ammonia levels and enzyme activity in leukocytes or cultured fibroblasts. Timely detection, close monitoring, diet and drug management are used to maintain blood ammonia at physiological levels (Daniotti *et al.*, 2011). Patients with UCD and other chronic hyperammonaemic conditions have no effective means of monitoring their condition as blood ammonia self-testing is not effective. The use of a reliable POC test could allow effective self-monitoring.

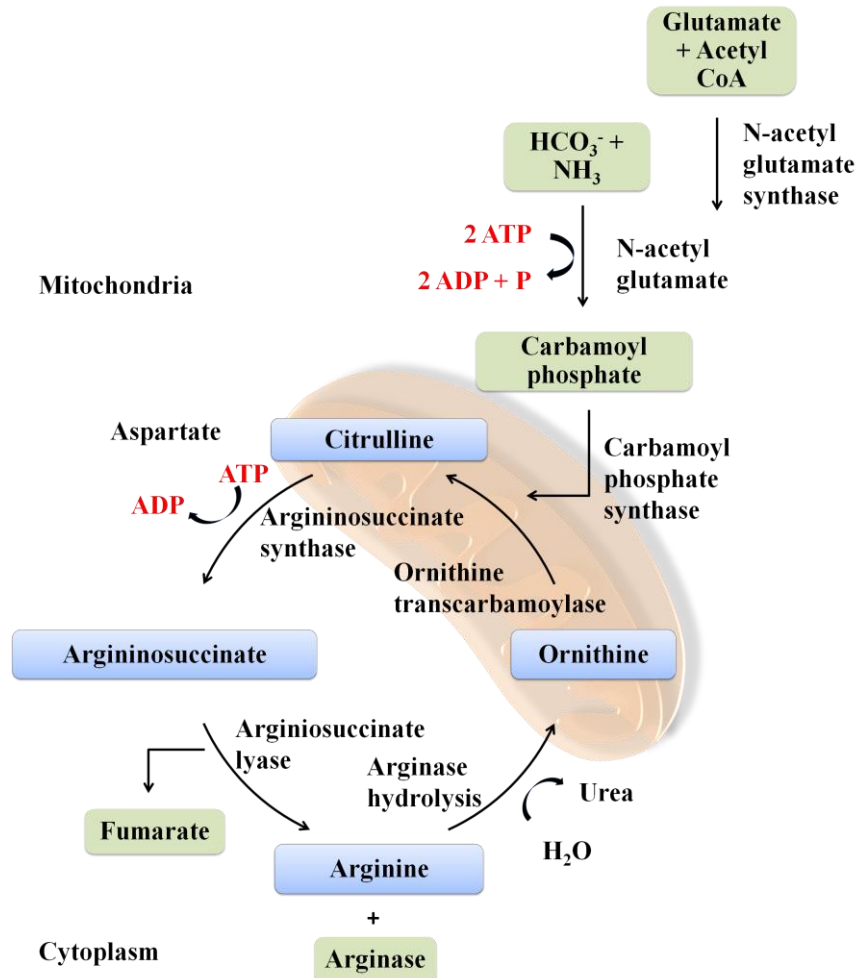


Figure 1.2. The urea cycle. N-acetylglutamate (NAG) is synthesised from glutamate and acetyl-CoA by N-acetylglutamate synthase (NAGS). This activates carbamoyl phosphate synthetase-1 (CPS-1) to initiate the urea cycle. Ammonia is first absorbed into the liver and combined with bicarbonate to form carbamoyl phosphate in the mitochondrial matrix. This enters the urea cycle and combines with ornithine (from the cytoplasm) to form citrulline. In the cytosol, amino acids are fed into the cycle by aspartate which combines with citrulline to form argininosuccinate. Arginiosuccinate is then split into fumarate (which is fed into the citric acid cycle) and arginine. Arginine then reacts with arginase and water to produce urea and regenerated ornithine. This travels from the mitochondrial matrix via the ornithine transporter, so completing the cycle.

Table 1.2. A list of the enzymes associated with the urea cycle, along with the causes of their disorders and symptoms.

Enzyme	Role and deficiency	Symptoms
N-acetylglutamate synthase (NAGS)	Catalyses synthesis of NAG from acetyl-CoA-1 and glutamate which activates CPS-1	Congenital: Respiratory alkylolosis, hyperammonaemia, coma Acquired: Acute attacks of hyperammonaemia, neurological, gastrointestinal and psychiatric clinical signs. May be developed secondary to carnitine deficiency
Carbamoylphosphate synthetase-1 (CPS-1)	Catalyses the first step of the urea cycle; synthesis of carbamoyl phosphate from HCO_3^- , ATP, and NH_3 using NAGS Urea cycle cannot proceed without carbamoylphosphate	Congenital: Hyperammonaemia, coma, delayed development, intellectual disability Acquired: Secondary to hyperinsulinism/hyperammonaemia syndrome
Ornithine transcarbamylase (OTC)	Catalyses the synthesis of citrulline from carbamoyl phosphate and ornithine that enters the mitochondria from the cytosol	Congenital: Hyperammonaemia, respiratory alkalosis and cerebral oedema Acquired: Triggered by catabolism
Argininosuccinate synthetase-1	Combines citrulline and aspartate in the cytosol generating arginosuccinate	Type 1 citrullinemia, cancer
Argininosuccinate lyase	Catalyses the breakdown of arginosuccinate to arginine, arginase and fumarate	Argininosuccinic aciduria, HE, respiratory alkalosis with neurological manifestations, reduced arginine synthesis
Arginase-1	Catalyses the hydrolysis of arginine to ornithine and urea	May go undiagnosed until later in life and recognised as cerebral palsy, spastic tetraplegia in children

Cirrhosis is scarring of the liver tissue as a result of long-term damage. This scarring cuts down on blood flowing through the liver, causing a loss of function. Severity is measured with the Child Pugh or Model for End-Stage Liver Disease (MELD) scores which are a measure of the prevalence of portosystemic shunting and redistribution of organ blood flow. The portal vein is a blood vessel from the gastrointestinal tract and spleen to the liver. In healthy individuals, ammonia levels in the portal vein are higher than in the hepatic vein because ammonia is removed by the liver. Patients with liver disease may develop portal collateral veins (varices) that bypass the liver and divert portal blood with high ammonia levels to systemic circulation (Imran *et al.*, 2012, Frontera, 2014, Luo *et al.*, 2014) (Fig. 1.3).

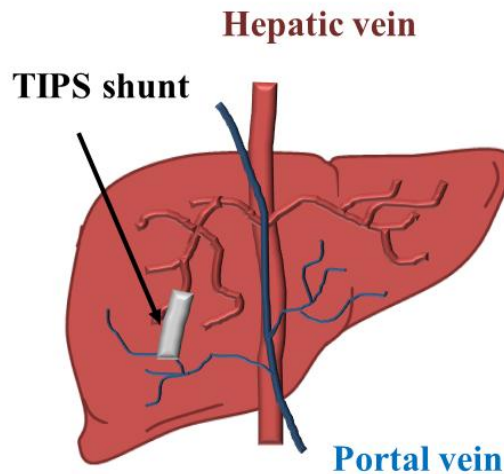


Figure 1.3. Blood from the gastrointestinal tract and spleen is carried by the portal vein and diverted to the hepatic vein, bypassing the liver via a transjugular intrahepatic portosystemic shunt (TIPS).

Noiret *et al.* have developed a mathematical model of portosystemic shunting in cirrhosis to monitor hyperammonaemia to be used in conjunction with other monitoring techniques such as ammonia levels (Noiret *et al.*, 2014). Ammonia has also been shown to drive dendritic immune cells into dysfunction which contributes to the immunocompromised state of cirrhosis (Auffermann-Gratzinger *et al.*, 2001) and tumour patients (Luo *et al.*, 2014).

Hepatic myelopathy (HM) is an unusual complication of chronic liver disease which manifests as cirrhosis and portosystemic shunts (Utku *et al.*, 2005). It is characterised by spastic paraparesis which results in patients being confined to a

wheelchair (Ben Amor *et al.*, 2014). Ammonia has been identified as a major contributor to the development of HM (Campellone *et al.*, 1996). Although ammonia-lowering treatment has not been shown to help, liver transplantation along with Lioresal treatment has been shown to improve patient mobility (Campellone *et al.*, 1996, Weissenborn *et al.*, 2003, Endre *et al.*, 2011).

Reye's syndrome is a rare encephalopathy that causes swelling in the liver and brain. It is characterised by cerebral oedema which often occurs during recovery from viral infection. It has also been linked to the use of aspirin. Changes occur to liver cells and so diagnosis is carried out via liver biopsy. Reye's syndrome also features hyperammonaemia of unclear cause and increased blood concentration of fatty and lactic acids (DeLong and Glick, 1982).

Acute liver failure (ALF) is a rare but life threatening illness. It may rapidly lead to adverse events including systemic inflammatory response, renal failure, hyperammonaemia, cerebral oedema, hepatic encephalopathy (HE), increased intracranial pressure (ICP), coma and death mainly due to ammonia toxicity (Cauli *et al.*, 2014). While HE (Endre *et al.*, 2011) and blood ammonia (Zhao *et al.*, 2014) are used as markers for ALF, its diagnosis is quite complicated. It is important to note that encephalopathy can be delayed in some cases of ALF. Cirrhotic patients that present with neurological symptoms may be misdiagnosed with Parkinson's disease (Noone *et al.*, 2008). Patients that present with high blood ammonia levels without liver disease may have an underlying liver issue such as cirrhosis or ALF which is often also associated with coagulopathy and hyperbilirubinaemia (Elgouhari and O'Shea, 2009). Liver disorders may also be asymptomatic until severe late stages of the disease and can develop into cancer. It is therefore imperative to monitor those with a history of hepatitis virus.

Blood ammonia has the potential to diagnose, support and treat patients with underlying problems related to the liver such as those discussed above. When symptoms are life-threatening a liver transplant may be considered. Ammonia should be monitored throughout a transplant to avoid elevations during the procedure. Future hopes for a definitive cure for ALF lie in gene replacement therapy, which could again be supported by blood ammonia monitoring.

Most pharmaceutical drugs are metabolised by the liver and so impact on liver function. Many drugs are hepatotoxic, while others are used to treat liver dysfunction and associated hyperammonaemia. Blood ammonia could also be used as a tool for studying the metabolism of other drugs for potential hepatotoxic effects so as to allow dosage to be optimised for individual patients; using a personalised or precision medicine approach (Finberg and Guharoy, 2012, Poh and Chang, 2012).

1.1.2. The role of the kidneys in nitrogen metabolism

Along with the liver, the kidneys also play an important role in nitrogen homeostasis (Weiner *et al.*, 2014). Urea is passed into the blood stream by the liver and is absorbed by the kidneys via the glomerulus. The kidneys filter the blood urea. Excess ammonia is divided between the ureter for excretion as urine and the renal vein to be used in cellular metabolism. The kidneys play an important role in correcting acidosis by enhanced production or excretion of ammonia. A large acid load initiates ammonia excretion while a basic load initiates ammonia production (Garibotto *et al.*, 2004).

Numerous pathological conditions result in chronic kidney disease. It may result in end stage renal disease (ESRD), uraemia, acidosis/alkalosis or oedema. Creatinine, blood urea nitrogen (BUN) and glomerular filtration rate are important indicators of kidney function. Currently, those with ESRD are managed using dialysis. Principally, haemodialysis is used, which is typically performed in a hospital or clinic. However, home dialysis and continuous ambulatory peritoneal dialysis are becoming increasingly used (Castledine *et al.*, 2013). Ammonia has been used as a marker to indicate haemodialysis efficacy (Narasimhan *et al.*, 2001, Gouma *et al.*, 2010, Neri *et al.*, 2012, Hibbard *et al.*, 2013) and uraemia breath during haemodialysis (Romero-Gomez *et al.*, 2001, Mochalski *et al.*, 2014). Treatment for kidney damage may include blocking N-methyl-D-aspartate (NMDA) receptors which delay kidney damage by allowing the improvement of glomerulus filtration and ammonia elimination in order to delay hyperammonaemia. This treatment reduces changes in cerebral blood flow and brain lactate, allowing time for kidney transplant or regeneration (Cauli *et al.*, 2014).

A urinary tract infection (UTI) develops when part of the urinary tract becomes infected, usually by urease-producing bacteria. Urease breaks down urea,

releasing ammonia into the systemic circulation. This may overwhelm the urea cycle, resulting in hyperammonaemia and coma (Samtoy and Debeukelaer, 1980, De Jonghe *et al.*, 2002, Sato *et al.*, 2008). Blood ammonia has the potential to serve as a diagnostic tool for UTIs and monitor treatment.

1.1.3. The effects of ammonia on the central nervous system

As previously discussed, several dysfunctions of ammonia metabolism may lead to hyperammonaemia and consequent HE and that most of the impact of hyperammonaemic disease is on the CNS, predominantly the brain (Ong *et al.*, 2003). Ammonia can cross the blood-brain barrier to reach levels over 400 μM in the CNS, leading to neurological deterioration (Munoz *et al.*, 2000, Felipo and Butterworth, 2002). Congenital defects such as UCDs and organic acidaemias are rare and are frequently undiagnosed at birth until significant and irreparable neurological impairment has occurred (Leonard and Morris, 2002, Prasad *et al.*, 1997). It is not yet fully understood why the brain is more susceptible to permanent damage from elevated ammonia than other organs (Rose, 2014). Ammonia is also a product of synthesis of glutamate from glutamine at nerve endings located in the CNS (Daniotti *et al.*, 2011) (Fig. 1.4).

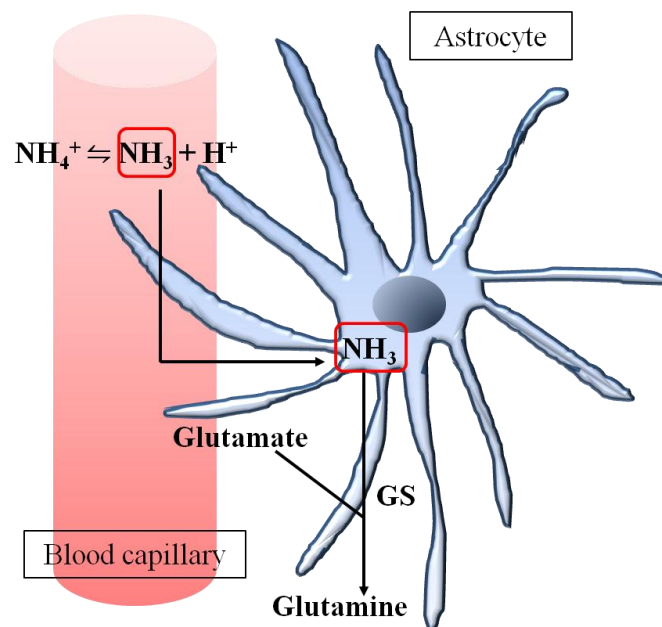


Figure 1.4. Ammonia can pass through the blood-brain barrier and into brain astrocytes. Here, ammonia may be metabolized to glutamine via glutamine synthetase (GS).

HE is a metabolic disorder which presents as a spectrum of neurological symptoms, principally as a consequence of hepatic dysfunction (Ferenci *et al.*, 2002, Cordoba and Minguez, 2008, Amodio *et al.*, 2013). The pathogenesis is not fully understood. Ammonia accumulation brought about by hepatic dysfunction and portosystemic shunting has been described as a primary cause. HE may be triggered by the intake of too much protein, dehydration, abnormal electrolyte homeostasis, gastrointestinal bleeding, infections and low blood oxygen. Elevated serum ammonia levels are detected in up to 80% of HE patients (Frontera, 2014). HE occurs in 30-45% of cirrhotic patients (Romero-Gomez *et al.*, 2001) and 10 to 50% of those with TIPS (Boyer and Haskal, 2010). The diagnosis is typically confirmed by blood ammonia determinations and electrophysical methods such as EEG (Eklou-Lawson *et al.*, 2009). Psychometric tests can then be used to grade HE such as the Trail Making Test (TMT), West Haven Criteria (WHC), and the Glasgow Coma Scale (GCS). Newer techniques such as positron emission tomography and magnetic resonance imaging are then used to confirm diagnosis. Management of HE is broken into five steps; stabilisation, addressing modifiable factors, lowering blood ammonia, managing ICP and managing complications (Frontera, 2014). Drug treatment options include lactose and neomycin, along with a combination of Rifaximin and lactulose (Sharma *et al.*, 2013). A liver transplant is considered to be a successful long-term therapy for HE. However, recipients who have HE at the time of a transplant are at high risk of neurological complications due to their susceptibility to stress of surgery and the neurotoxicity of drugs used in treatment (Dhar *et al.*, 2008).

1.1.4. The digestive system

The digestive system breaks down food into their basic forms such as sugars, amino acids and fatty acids. These are absorbed into the blood stream and provide energy where required. Food passes through the gastrointestinal tract which is made up of the oral cavity, pharynx, oesophagus, stomach, small and large intestines. The digestive system has long been acknowledged as a major source of ammonia. Ammonia is produced by protein breakdown and amino acid metabolism in the gastrointestinal tract. Bacteria in the gastrointestinal tract may also produce ammonia (Aprea *et al.*, 2012).

The oral cavity contains a large and diverse microbial flora. As microbes accumulate, they form biofilms. Bacteria reside in these biofilms producing numerous volatile organic compounds (VOCs). When bacterial levels are excessive due to poor oral hygiene, halitosis can result. This oral malodour is mostly due to by-products of microbial metabolism, principally sulphur and nitrogen compounds (Amano *et al.*, 2002). Several studies have shown that oral bacteria contribute to ammonia levels measured in breath (Wang *et al.*, 2008, Smith *et al.*, 2008, Hibbard and Killard, 2011). In order to measure the correlation between blood ammonia and breath ammonia relating to physiological processes and not to bacteria in the mouth, antibacterial mouth rinses have been used (Solga *et al.*, 2013). The contribution made by oral bacteria in the measurement of ammonia levels in breath sampling remains an issue of some debate in breath research (Schmidt *et al.*, 2013). The clinically accepted way to determine ammonia relating to a biological process is blood analysis.

Helicobacter pylori (*H. pylori*) are a Gram negative spirillum bacillus, often found infecting the stomach and duodenum. Infection may be contracted from food or water. The bacteria can survive in the acidic environment of the stomach by secreting urease enzymes which generate ammonia to neutralise acids (Moblely *et al.*, 1991). This weakens the lining tissue of the stomach causing ulcers. The ammonia produced may be released into systemic circulation causing hyperammonaemia. *H. pylori* infection is the main cause of peptic ulcer, chronic atrophic gastritis, gastric MALT lymphoma and gastric cancer. Elimination of *H. pylori* is performed in order to treat peptic ulcers, and is achieved using a combination of antibiotics (amoxicillin, clarithromycin, metronidazole) and a proton pump inhibitor (PPI) (lansoprazole and omeprazole), allowing the ulcer to heal naturally.

In the intestines, the majority of ammonia production is due to digestive amino acid breakdown, predominantly glutamine (Turner *et al.*, 2006). Significant levels of ammonia are also produced by bacterial breakdown of amino acids and urea (Damink *et al.*, 2009). Amino acids, nucleotide bases, and other nitrogenous compounds then diffuse into the blood and are transported to the liver (Berg *et al.*, 2002). The highest ammonia concentration in the body is found in the colon. As ammonia is absorbed through the colonic epithelium, levels of *L*-glutamine and *L*-arginine in the portal blood are increased (Eklou-Lawson *et al.*, 2009). Thus, there

may be a metabolic link between colon mucosa and liver biosynthesis. Small intestinal bacterial overgrowth in patients with liver cirrhosis is more frequent in alcoholic liver cirrhosis cases.

Diet also affects ammonia metabolism and can be used as a tool to manage many disorders associated with hyperammonaemia (Lee *et al.*, 2015). It has been found that ammonia emissions from the skin and blood concentrations increased after protein intake and reached maximum levels after two hours (Tsuda *et al.*, 2011). Protein intolerances and related deficiencies (as mentioned in Table 1.1) can prevent normal ammonia metabolism, causing severe and often irreversible damage (Shaw *et al.*, 1989, Sebastio *et al.*, 2011). Blood ammonia along with other metabolites has the potential to analyse gastrointestinal physiology (Spacek *et al.*, 2015).

Glutamate dehydrogenase (GLDH) has been used as a marker of liver function as well as for a marker for recent alcohol consumption in alcoholics (Kravos and Malesic, 2010). This reaction proceeds towards the direction of oxidative deamination of glutamate, which releases ammonia, normally with an activity of 6.4 U/L for women and 11.0 U/L for men. However, these values are higher in alcoholics (Jung *et al.*, 1985). GLDH and ammonia levels decrease rapidly after cessation of alcohol (Smith *et al.*, 2002). There is the potential to replace the current GLDH assay with a blood ammonia test which could be used to monitor and screen for liver dysfunction and alcohol activity (Adeva *et al.*, 2012). *H. pylori* infection is also common in alcoholics (Lieber, 1998). Mutations of glutamate dehydrogenase 1 (GDH1) can occur. This may cause hyperinsulinism/hyperammonaemia which is characterised by hypoglycaemic hyperinsulinemia along with elevated blood ammonia, which requires monitoring and management.

1.1.5. The relationship between the lungs and ammonia

Hyperventilation is an early sign of the metabolic crisis associated hyperammonaemia, followed by encephalopathy. Hyperventilation can occur as a response to acidosis in order to improve carbon dioxide removal (Tizianello *et al.*, 1977). Liver disease, together with an abnormal pH balance is likely to cause respiratory alkalosis. Altered consciousness along with respiratory alkalosis/acidosis

should prompt the determination of blood ammonia (Msall *et al.*, 1984, Krivitzky *et al.*, 2009). Blood ammonia with transaminases should also be considered for perinatal asphyxia markers (Esque-Ruiz *et al.*, 2003).

Breath ammonia has been linked to cystic fibrosis (CF) and blood ammonia monitoring may contribute to its management (Newport *et al.*, 2009). Although, ammonia is not likely to compete with the current means of diagnosis which is based on salt in sweat.

1.1.6. Muscle metabolism and exercise and their association with ammonia

Since the early 1920s it has been known that ammonia is released during skeletal muscle movement. However, the importance of skeletal muscle in ammonia homeostasis was not recognised until the 1970s (Dawson, 1978). Abnormal nitrogen metabolism is caused by increased production of ammonia (seizure with increased movement of muscle) or impaired clearance of ammonia (kidney and liver dysfunction, portosystemic shunting) causing hyperammonaemia. The skeletal muscle becomes the most important organ in ammonia homeostasis during liver and/or kidney dysfunction (Lockwood *et al.*, 1979). Skeletal muscle has a large mass capacity to remove ammonia produced during the purine nucleotide cycle by forming glutamine through the enzyme glutamine synthetase (Sabina *et al.*, 1984). At rest, there is no uptake or release of ammonia by skeletal muscle. The intensity of exercise governs how ammonia is released into the venous blood of the exercising limb, either by the purine nucleotide cycle during brief exercise or by increased metabolism of branched chain amino acid (BCAA) breakdown during prolonged exercise (Lowenstein, 1990, Maclean *et al.*, 1992, Derave *et al.*, 1997).

Physical exercise has been used to study ammonia metabolism (Wilkinson *et al.*, 2010, Solga *et al.*, 2014). Ammonia produced during exercise has been shown to induce immune and inflammatory responses (Gleeson, 2007). To counter these responses, arginine supplements have been shown to decrease hyperammonaemia and lymphocyte response during intense exercise. The use of amino acids has also been used to modify metabolism during exercise (Goncalves *et al.*, 2012). In order to evaluate, monitor and prescribe exercise intensity for conditioning programmes, ammonia and lactate levels may be used (Gorostiaga *et al.*, 2010). However, gender

and age need to be considered when compiling a conditioning programme (Lourenco and Turner, 2014).

1.2. TECHNIQUES FOR AMMONIA DETERMINATION

Blood plasma is the clinical standard sample for determination of systemic ammonia levels. It can also be measured in whole blood, erythrocytes, breath, saliva, sweat and urine (Green, 1988). While arterial blood ammonia is accepted as being most representative of systemic ammonia levels, sampling arterial blood is challenging (Metz, 2014). Venous ammonia levels varies somewhat from arterial ammonia, but is routinely used (Adeva *et al.*, 2012). Ammonia levels may spontaneously increase in a blood sample (Maranda *et al.*, 2007). Difficult venepuncture, haemolysis of red blood cells (RBCs) and changes in metabolism can cause a sudden rise in the ammonia levels of the blood sample (Conway, 1935). Factors such as anxiety, exercise, smoking, and food and alcohol intake may also affect systemic ammonia levels. A major limitation of blood ammonia measurement is the complexity involved in the correct drawing and handling of the sample. When collected for transportation to the hospital laboratory, the sample should be kept below 0°C and separated from RBCs within 15 min of collection. Once separated, the plasma ammonia is stable for four hr at 4°C. Analysis should be repeated at the same time of day and under the same conditions to confirm the result due to the high risk of false positives. This urgency in time requires the patient to be close to a clinical laboratory (Huizenga *et al.*, 1994).

Numerous techniques have been developed to quantify ammonia in blood, most of which are covered in a comprehensive review of blood ammonia measurement by Barsotti (2001). A number of wet chemistry methods have been available for the purpose of determining blood ammonia and urea. They include distillation, micro-diffusion and ion-exchange chromatography which require the release or capture of ammonia from the blood sample before they can be used to quantify ammonia levels. More modern methods such as the enzymatic method and spectrophotometric titration quantify ammonia levels present in the blood sample which is why they are most commonly used.

Chapter 1

Distillation is one of the earliest techniques for measurement of ammonia. It involves the addition of an alkaline buffer to the blood sample, followed by vacuum distillation. The vacuum lowers the pressure which lowers the boiling point of the sample. The released ammonia gas is collected in a trap containing dilute acid which converts the gas into ammonium ions. Although a vacuum is used the method is still slow compared to others. It requires a subsequent quantification step and is also dependent on the pH environment. For these reasons the technique is rarely used today.

Another old technique is the micro-diffusion method which liberates ammonia from a blood sample by alkalisation (Conway and Cooke, 1939). It is performed using two Pyrex 'Petri dishes', one inside the other. The sample is placed in the outer chamber and a known amount of strong base is added and gaseous ammonia is released from the alkaline solution and travels through an air gap into the other chamber and absorbed by an ammonium indicator. The change in colour is measured by reflectance spectroscopy (Obrink, 1955). The micro-diffusion method is not very accurate or precise. It is also time consuming and is seldom used.

Ion exchange methods have also long been used for the determination of ammonia in blood (Dienst, 1961, Fenton, 1962, Fenton and Williams, 1968). Strong acidic cation exchange resin captures ammonium ions. They are then eluted with sodium chloride or a dilute alkali. Quantification of ammonia is performed by spectrophotometric analysis. Long determinations and a second quantification step prevent this method from being widely used.

After release or capture of ammonia by distillation, micro-diffusion or ion exchange chromatography, the Berthelot reaction, which is a spectrophotometric reaction step used to quantify ammonia. The formation of a blue colour on mixing ammonium ions, hypochlorite and phenol was described by Berthelot as early as 1859. Berthelot developed the reaction which was given his name (Fig. 1.5) to detect aniline. This is now used as a reference method for the determination of ammonia. The reaction is selective and suitable at low concentrations (Hioki *et al.*, 1991). From the Beer-Lambert Law ammonia concentration is related to the light absorption at the absorption maximum of indophenol blue (670 nm). The reaction consists of two steps. The first is a fast second order reaction in which hypochlorite transforms all

ammonia into chloramine. The rate and products of this reaction are highly dependent on the pH of the environment. The second step is the rate limiting step which involves the addition of phenol to chloramines forming indophenol (Searle, 1984). At room temperature the reaction takes 15 min, although heating will accelerate this.

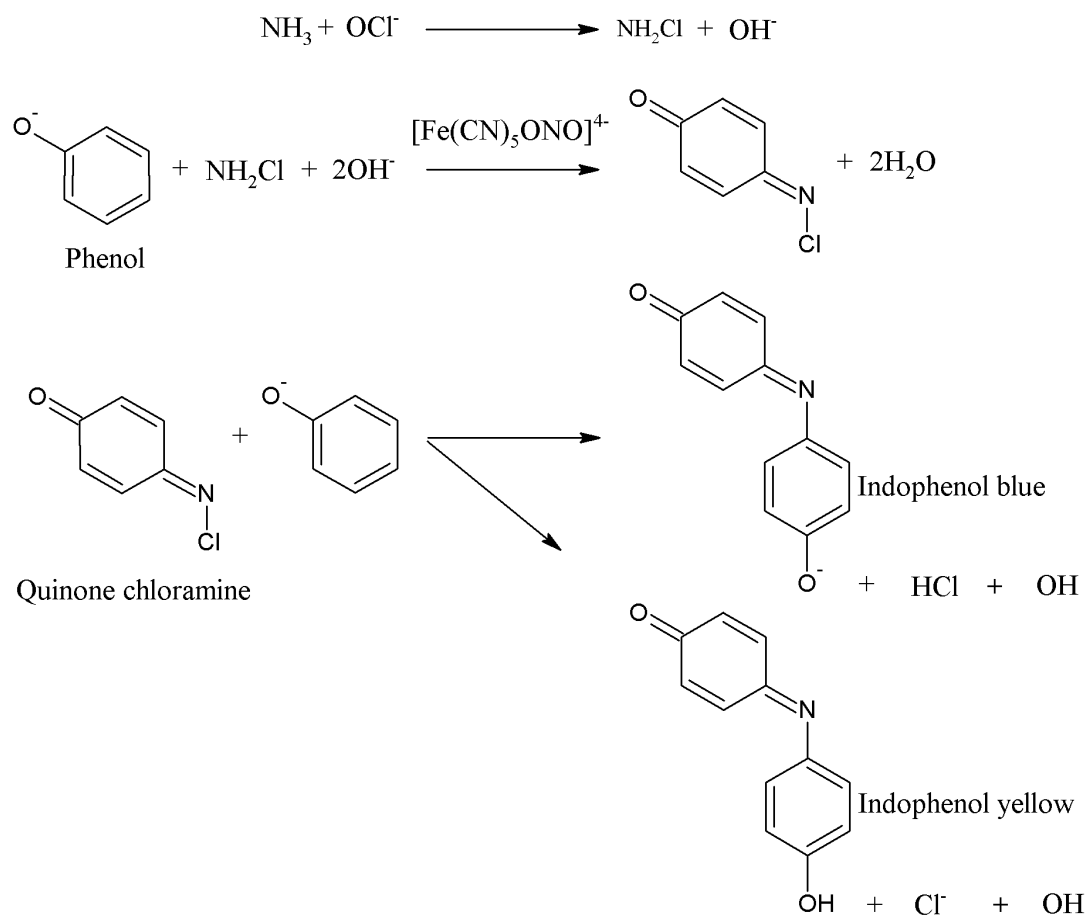
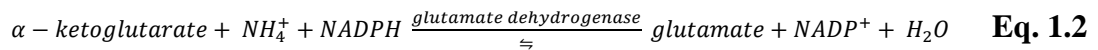


Figure 1.5. The Berthelot reaction which can be used to quantify ammonia levels via colorimetric analysis.

In the UK, the enzymatic method is the most commonly used technique to quantify blood ammonia and is capable of direct measurement, measuring levels over a broad range (12 μM to 1 mM) (Hawke, 2012). It catalyses the reaction of ammonium with α -ketoglutarate and nicotinamide adenine dinucleotide phosphate (NADPH) with glutamate dehydrogenase to form glutamate, NADP^+ and water. An absorbance change can then be used to measure the oxidation of NADPH, which is

proportional to ammonia concentration. In the reaction UV absorbance of NADPH co-factor is measured as it is converted to NADP⁺.



Although the enzymatic method is the most commonly used method of clinical quantification of ammonia it is not suitable to *in situ* measurements.

1.2.1. Test kits and POC devices

Major improvements have been made to these older techniques focusing on the production of commercial test kits and POC devices, see Table 1.3. Wet chemistry kits dominate the commercial field however solid absorptive supports (test strip devices) have gained attention because of their POC advantage such as simple use and easy disposal (Tanzer, 1997). The absorbent layer is often impregnated with alkaline reagents to convert ammonium ions to gaseous ammonia (Hrboticka, 2005). Most of these kits and devices are made for use in a clinical setting by trained personnel, requiring sample treatment, additional chemicals and instrumentation. In addition, the nature of the methods available contributes to additional pre-analytical errors due to issues such as sample transportation and handling. They may detect over the clinical range but require expensive equipment and not all can be used in whole blood.

Table 1.3. Analytical performance characteristics of a range of commercial kits and devices for ammonia

Product Name	Technique	LOD (μM)	Range (μM)	Analysis Time (min)	Sample Volume (μL)	Operational Temperature ($^{\circ}\text{C}$)	Method Limitations	Refs
PocketChem™ BA and ammonia test kit II	Berthelot	Not specified	2-285	~6	20	10-35	Memory capacity is 50 measurements.	(Arkray, 2016)
Vitros® Chemistry Products AMON Slides	Berthelot	Not specified	8.7-500	5	10	37	Anticoagulant, centrifugation, calibrators and QC materials required.	(Ortho- Clinical Diagnostics Inc., 2015)
Abcam® Ammonia Assay Kit - Modified Berthelot	Berthelot	>10	Not specified	30	100	37	Centrifugation, colorimetric microplate reader, orbital shaker, required. Phenol is used.	(Abcam Plc., 2016)
Sekisui Ammonia L3K®	Enzymatic	4.1	8.8-1174	Not specified	Not specified	Not Specified	Anticoagulant, colorimetric microplate reader, calibrators and QC materials required.	(Sekisui Diagnostics (UK) Ltd., 2013)
Sigma Aldrich® Ammonia Assay Kit	Enzymatic	12	12-881	20	10-200	18-35	Anticoagulants, colorimetric plate reader and cuvettes required	(Sigma- Aldrich Co. LLC., 2015)

1.2.2. Conducting polymers such as polyaniline used as ammonia sensing materials

Conducting polymers have been an area of intense interest over the past 30 years, culminating in the 2000 Nobel Prize in Chemistry to MacDiarmid, Heeger and Shirakawa (Nobelprize.org, 2013). In recent decades, conducting polymers have received attention as the active layer in sensors due to their conductive, electrical and optical properties. Their multi-functionality has led to developments in sensing devices as well as actuators, batteries, corrosion science, light-emitting diode (LEDs), membranes and photovoltaics. Their utility has been further improved with new nanostructured fabrication and deposition techniques (Weng *et al.*, 2010). Selectivity and lack of interference from atmospheric gases such as H₂, CH₄, CO and CO₂ make these polymers very attractive gas sensing materials.

Polyaromatic polymers such as polyaniline, polypyrrole, polythiophene and polyphenylene are redox-active. Alteration of the electron density on the polymer backbone (by means of (a) doping/de-doping, (b) interactions of ions, functional groups, lone pairs, or (c) charge transfer between polar molecules) can change their conductivity (for example, Fig. 1.6 polyaniline). Conductivity of the polymer depends on two factors; the ability of the polymer backbone to transport charge carriers and the carriers hopping between different polymer chains (Fratoddi *et al.*, 2015). Conducting polymers show almost no conductivity in their neutral (uncharged) state. They may be doped (oxidised) into a more conductive form, creating a positive charge on the conjugated backbone, to behave as a p-type conductor. Polyaniline has three forms; emeraldine (E), pernigraniline (P) leucoemeraldine (L) which may exist as a base (B) or a salt (S). EB is the half oxidised form, it can either be fully oxidised to PB which is an insulator or instead be reduced to LB which is also an insulator. ES is the only conductive form and is formed by the protonation of EB by exposure to protonic acids, upon oxidation of LB or reduction of PB. ES has positively charged local centres located at nitrogen atoms through which valence electrons can hop, giving rise to conduction. It has a broad conductivity range, for example 14 S cm⁻¹ (Stejskal *et al.*, 1999), 28.4 S cm⁻¹ (Jang *et al.*, 2007) and 32 mS cm⁻¹ (Ngamna *et al.*, 2007).

Polypyrrole has been used widely in the literature as an active material for ammonia. Polypyrrole films have been synthesised and combined with gold electrodes for the resistance measurement of gaseous ammonia (4 to 80 ppm) at room temperature (Joshi *et al.*, 2011). Polypyrrole nanowires have also been used to determine the resistance response upon exposure to ammonia (40 to 300 ppm) in argon carried gas (Hernandez *et al.*, 2007). Research involving dip coated polypyrrole colloidal suspensions onto non-conducting substrates, such as acrylic, (Ratcliffe, 1990) has resulted in the determination of volatile amines, including ammonia, across the range of 1 to 1000 ppm (Costello *et al.*, 1996).

The main advantage of using polyaniline over other aromatic conducting polymers, such as polypyrrole, is its processability. Polyaniline is easily synthesised into an aqueous nanoparticle ink and inkjet print deposited. There are very few examples in the literature of inkjet-printed polypyrrole. This is most likely because polypyrrole is difficult to disperse and process into stable printable formulations (Weng *et al.*, 2011). Although, Weng *et al.* (2011) have developed printable polypyrrole nanodispersions formed in the presence of novel gemini surfactants. These dispersions were formed by controlling particle size, size distribution, viscosity and surface tension to ensure that the requirements for inkjet printing systems were met and resulted in relatively high conductive and stable ink formulation.

Chapter 1

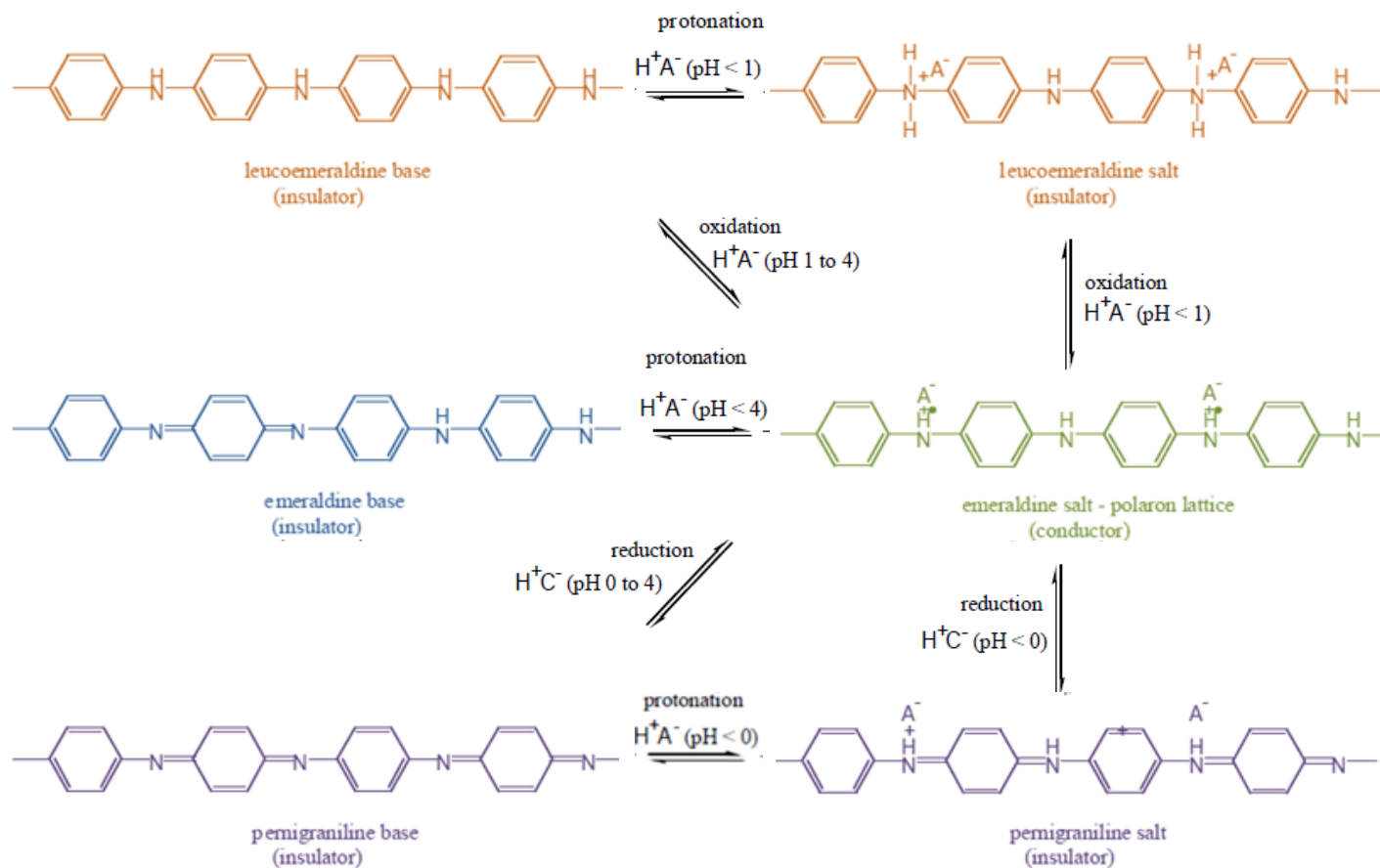


Figure 1.6. The protonation and reactions between the various forms of polyaniline and their associated colours. Reproduced with permission from CRC Press (Wallace *et al.*, 2003) and adapted.

1.2.3. The reaction mechanism of ammonia and polyaniline

The principle feature of polyaniline as ammonia sensor material lies in the affinity of the ES form for ammonia due to a distinct similarity of the coordinative roles of nitrogen atoms in both compounds. Nitrogen atoms of the polymer chains serve as adsorption centres for ammonia molecules, which are deprotonated. When the ES form of polyaniline (PANIH^+) interacts with ammonia the following reaction occurs (Fig. 1.7):



Ammonia de-protonates ES polyaniline to form energetically favourable ammonium ions (Kukla *et al.*, 1996). It is this deprotonation that causes changes in the observable conductive behaviour.

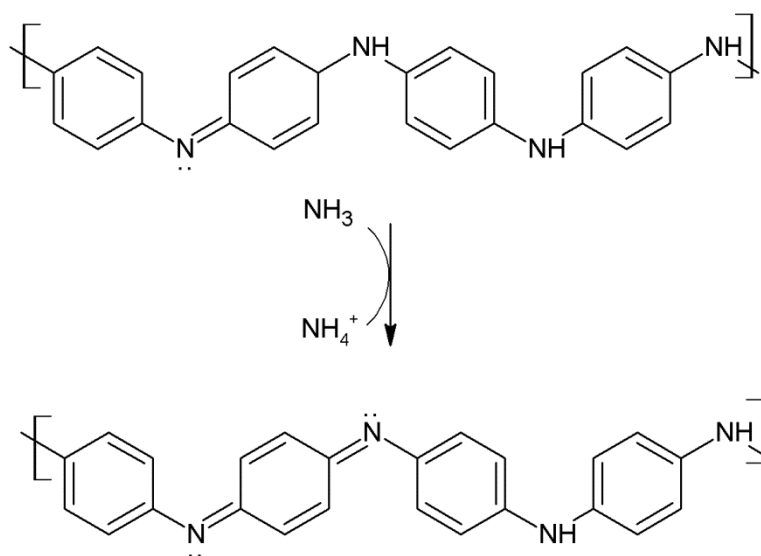


Figure 1.7. Schematic of the ES polyaniline interaction with ammonia. Polyaniline is deprotonated by ammonia generating the EB polyaniline form.

Much research has been performed on the ES form of polyaniline when exposed to ammonia, as observed by electrochemistry or spectroscopy (Kukla *et al.*, 1996, Wu *et al.*, 2000, Dhawan *et al.*, 1997). There are many polyaniline-based aqueous ammonia sensors in the literature, with a wide variety of fabrication techniques and sensing applications. For example, an optical detector in combination with polyaniline coated silica micro-capillaries has been used for the detection of aqueous ammonia (Florea *et al.*, 2013). Optical sensing has also been used to

quantify aqueous ammonia utilising chemically synthesised polyaniline and deposited onto glass substrates (Castrellon-Urbe *et al.*, 2009). Amperometric analysis of aqueous ammonia has been reported within a flow injection system including electropolymerised polyaniline modified platinum electrode (Trojanowicz *et al.*, 1997). Our group have reported a number of biosensors and chemical sensors produced using inkjet printable polyaniline nanodispersion for the determination of aqueous ammonia in a variety of matrices. The application of the inkjet polyaniline nanoparticles has been illustrated in a sensor for aqueous ammonia in refrigerant waste water via an amperometric flow injection system (Crowley *et al.*, 2008). The system was found to have good performance and stability. An ammonia measurement probe for continuous monitoring of secondary refrigerants has also been developed. Impedimetric analysis was used to generate a strong calibration in the industrially relevant range of 0 to 100 parts-per-million (ppm) (0 to 560 mM) (Subramanian *et al.*, 2013). All of these technologies are useful in an industrial setting. However, they are not all suitable to miniaturised on-site environmental testing or POC bedside monitoring of pathological diseases relating to ammonia. Miniaturisation and reconfiguration of these technologies is required for them to be adapted for environmental and clinical applications.

1.3. CONCLUSIONS

Ammonia is involved in many processes in the body. As a consequence, it may potentially be used to diagnose and monitor a number of conditions, either alone, or in combination with other tests and biomarker profiles. Blood ammonia may be used as a minimally invasive means of diagnosis. New technology is required which has excellent analytical performance and accurate measurement across the diagnostically relevant range. Few, if any, of the available POC kits and assays are suitable to patient testing. Most are limited to use by trained personnel as they require high volumes and/or sample handling and preparation. Ultimately they are too complex, bulky and expensive to be developed as viable POC technologies.

Application of a suitable sensor technology, followed by clinical evidencing has the potential to lead to a broad range of screening, monitoring and diagnostic solutions for the conditions discussed. Sensor technology has

Chapter 1

gained a reputation as the answer to many analytical problems, especially in the clinical arena where many laboratory techniques fail to reach the diagnostically relevant ranges. Sensors provide a low cost, simple and rapid way to directly analyse low concentrations of analyte in complex matrices often with little or no sample preparation or handling (Komuro *et al.*, 2013). For these reasons they have potential for use in blood gas analysis.

1.4. THESIS OUTLINE

The purpose of this research was to develop a POC device for the quantification of aqueous ammonia in blood. This was achieved using a combination of printing processes to produce silver interdigitated electrodes modified with polyaniline nanoparticles, which were individually used in conjunction with a gas permeable membrane and encapsulated to form the device. This device may be capable of diagnosis, treatment and monitoring of pathological conditions associated with blood ammonia.

Chapter 1 presents a literature survey on the topic of blood ammonia. The importance of blood ammonia testing is outlined and an overview of ammonia metabolism in the body is described. External factors that can influence ammonia metabolism are also highlighted. Current techniques to determine blood ammonia are discussed along with new technologies capable of being utilised as POC blood ammonia tests.

In Chapter 2, the materials, instrumentation and methods used throughout this thesis are outlined.

Chapter 3 describes the initial development of polyaniline-modified silver screen-printed interdigitated electrodes for the application of ammonia sensing. The materials used to produce these sensors were characterised and optimised using a range of optical and electrical techniques. The sensors were then electrochemically assessed with the use of electrochemical impedance spectroscopy.

Chapter 4 details the design and testing of the aqueous ammonia device with the use of a gas-permeable membrane to allow contact with ammonia in solution. The device required a sample pH change to detect ammonia and an air purge to remove matrix interferences.

The clinical viability of the device is discussed in Chapter 5 with efforts focused on matrix effects and interferences. The device was then validated against a commercially available kit.

Chapter 1

Recommendations for future work and developments emerging from this thesis are discussed in Chapter 6. Overall conclusions of the thesis are presented in Chapter 7.

1.5. REFERENCES

Abcam Plc. (2016) *Ammonia Assay Kit - Modified Berthelot - (Colorimetric) (ab102509)*. Available from: <http://www.abcam.com/ammonia-assay-kit-modified-berthelot-colorimetric-ab102509.html>.

Adeva, M.M., Souto, G., Blanco, N. and Donapetry, C. (2012) Ammonium metabolism in humans. *Metabolism-Clinical and Experimental*. 61 (11), pp.1495-1511.

Aires, C.C.P., van Cruchten, A., Ijlst, L., de Almeida, I.T., Duran, M., Wanders, R.J.A. and Silva, M.F.B. (2011) New insights on the mechanisms of valproate-induced hyperammonemia: Inhibition of hepatic N-acetylglutamate synthase activity by valproyl-CoA. *Journal of Hepatology*. 55 (2), pp.426-434.

Amano, A., Yoshida, Y., Oho, T. and Koga, T. (2002) Monitoring ammonia to assess halitosis. *Oral Surgery Oral Medicine Oral Pathology Oral Radiology and Endodontics*. 94 (6), pp.692-696.

Amodio, P., Bemeur, C., Butterworth, R., Cordoba, J., Kato, A., Montagnese, S., Uribe, M., Vilstrup, H. and Morgan, M.Y. (2013) The Nutritional Management of Hepatic Encephalopathy in Patients With Cirrhosis: International Society for Hepatic Encephalopathy and Nitrogen Metabolism Consensus. *Hepatology*. 58 (1), pp.325-336.

Apra, E., Morisco, F., Biasioli, F., Vitaglione, P., Cappellin, L., Soukoulis, C., Lembo, V., Gasperi, F., D'Argenio, G., Fogliano, V. and Caporaso, N. (2012) Analysis of breath by proton transfer reaction time of flight mass spectrometry in rats with steatohepatitis induced by high-fat diet. *Journal of Mass Spectrometry*. 47 (9), pp.1098-1103.

Arkray, I. (2016) *Blood Ammonia Meter PocketChem BA PA-4140*. Available from: <http://www.arkray.co.jp/english/products/pdf/pa4140.pdf>.

Auffermann-Gratzinger, S., Keeffe, E.B. and Levy, S. (2001) Impaired dendritic cell maturation in patients with chronic, but not resolved, hepatitis C virus infection. *Blood*. 97 (10), pp.3171-3176.

Barsotti, R. (2001) Measurement of ammonia in blood. *Journal of Pediatrics*. 138 (1), pp.S11-S19.

Ben Amor, S., Saied, M.Z., Harzallah, M.S. and Benammou, S. (2014) Hepatic myelopathy with spastic paraparesis: report of two cases and review of the literature. *European Spine Journal*. 23 pp.S167-S171.

Berg, J.M., Tymoczko, J.L. and Stryer, L. (2002) *Biochemistry*. 5th ed. New York: W.H. Freeman and Company.

Chapter 1

Bezinover, D., Douthitt, L., McQuillan, P.M., Khan, A., Dalai, P., Stene, J., Uemura, T., Kadry, Z. and Janicki, P.K. (2010) Fatal Hyperammonemia After Renal Transplant due to Late-Onset Urea Cycle Deficiency: A Case Report. *Transplantation Proceedings*. 42 (5), pp.1982-1985.

Bosoi, C.R. and Rose, C.F. (2009) Identifying the direct effects of ammonia on the brain. *Metabolic Brain Disease*. 24 (1), pp.95-102.

Boyer, T.D. and Haskal, Z.J. (2010) Role of Transjugular Intrahepatic Portosystemic Shunt (TIPS) in the Management of Portal Hypertension: Update 2009. *Hepatology*. 51 (1), pp.306.

Broomfield, A. and Grunewald, S. (2012) How to use serum ammonia. *Archives of Disease in Childhood-Education and Practice Edition*. 97 (2), pp.72-77.

Brusilow, S.W. and Maestri, N.E. (1996) Urea cycle disorders: diagnosis, pathophysiology, and therapy. *Advances in Pediatrics*. 43 pp.127-170.

Campellone, J.V., Lacomis, D., Giuliani, M.J. and Kroboth, F.J. (1996) Hepatic myelopathy - Case report with review of the literature. *Clinical Neurology and Neurosurgery*. 98 (3), pp.242-246.

Castledine, C.I., Gilg, J.A., Rogers, C., Ben-Shlomo, Y. and Caskey, F.J. (2013) Renal centre characteristics and physician practice patterns associated with home dialysis use. *Nephrology Dialysis Transplantation*. 28 (8), pp.2169-2180.

Castrellon-Uribe, J., Nicho, M.E. and Reyes-Merino, G. (2009) Remote optical detection of low concentrations of aqueous ammonia employing conductive polymers of polyaniline. *Sensors and Actuators B-Chemical*. 141 (1), pp.40-44.

Cauli, O., Gonzalez-Usano, A., Cabrera-Pastor, A., Gimenez-Garzo, C., Lopez-Larrubia, P., Ruiz-Sauri, A., Hernandez-Rabaza, V., Duszczuk, M., Malek, M., Lazarewicz, J.W., Carratala, A., Urios, A., Miguel, A., Torregrosa, I., Carda, C., Montoliu, C. and Felipo, V. (2014) Blocking NMDA Receptors Delays Death in Rats with Acute Liver Failure by Dual Protective Mechanisms in Kidney and Brain. *Neuromolecular Medicine*. 16 (2), pp.360-375.

Conway, E.J. (1935) Apparatus for the micro-determination of certain volatile substances: The blood ammonia, with observations on normal human blood. *The Biochemical Journal*. 29 (12), pp.2755-2772.

Conway, E.J. and Cooke, R. (1939) Blood ammonia. *The Biochemical Journal*. 33 (4), pp.457-78.

Cordoba, J. and Minguez, B. (2008) Hepatic encephalopathy. *Seminars in Liver Disease*. 28 (1), pp.70-80.

Costello, B., Evans, P. and Ratcliffe, N. (1996) Preparation of polypyrrole composites and the effect of volatile amines on their electrical properties. *Analyst*. 121 (6), pp.793-797.

Chapter 1

Crowley, K., O'Malley, E., Morrin, A., Smyth, M.R. and Killard, A.J. (2008) An aqueous ammonia sensor based on an inkjet-printed polyaniline nanoparticle-modified electrode. *Analyst*. 133 (3), pp.391-399.

Damink, S.W.M.O., Jalan, R. and Dejong, C.H.C. (2009) Interorgan ammonia trafficking in liver disease. *Metabolic Brain Disease*. 24 (1), pp.169-181.

Daniotti, M., la Marca, G., Fiorini, P. and Filippi, L. (2011) New developments in the treatment of hyperammonemia: emerging use of arglucic acid. *International Journal of General Medicine*. 4 pp.21-28.

Davies, S.M., Szabo, E., Wagner, J.E., Ramsay, N.K.C. and Weisdorf, D.J. (1996) Idiopathic hyperammonemia: A frequently lethal complication of bone marrow transplantation. *Bone Marrow Transplantation*. 17 (6), pp.1119-1125.

Dawson, A.M. (1978) Regulation of Blood Ammonia. *Gut*. 19 (6), pp.504-509.

De Jonghe, B., Janier, V., Abderrahim, N., Hillion, D., Lacherade, J.C. and Outin, H. (2002) Urinary tract infection and coma. *Lancet*. 360 (9338), pp.996-996.

de Keijzer, M.H., Jakobs, B.S., Brandts, R.W., Hofs, M.T.W., Trijbels, F.J.M. and Smeitink, J.A.M. (1997) Rapid and reliable measurement of highly elevated blood ammonia concentrations in children. *European Journal of Clinical Chemistry and Clinical Biochemistry*. 35 (11), pp.353-354.

DeLong, G.R. and Glick, T.H. (1982) Ammonia Metabolism in Reye Syndrome and the Effect of Citrulline. *Annals of Neurology*. 11 (1), pp.53-58.

Derave, W., Bouckaert, J. and Pannier, J.L. (1997) Gender differences in blood ammonia response during exercise. *Archives of Physiology and Biochemistry*. 105 (2), pp.203-209.

Dhar, R., Young, G.B. and Marotta, P. (2008) Perioperative neurological complications after liver transplantation are best predicted by pre-transplant hepatic encephalopathy. *Neurocritical Care*. 8 (2), pp.253-258.

Dhawan, S.K., Kumar, D., Ram, M.K., Chandra, S. and Trivedi, D.C. (1997) Application of conducting polyaniline as sensor material for ammonia. *Sensors and Actuators B-Chemical*. 40 (2-3), pp.99-103.

Dienst, S.G. (1961) An ion exchange method for plasma ammonia concentration. *The Journal of Laboratory and Clinical Medicine*. 58 pp.149-155.

Eklou-Lawson, M., Bernard, F., Neveux, N., Chaumontet, C., Bos, C., Davila-Gay, A., Tome, D., Cynober, L. and Blachier, F. (2009) Colonic luminal ammonia and portal blood l-glutamine and l-arginine concentrations: a possible link between colon mucosa and liver ureagenesis. *Amino Acids*. 37 (4), pp.751-760.

Elgouhari, H.M. and O'Shea, R. (2009) What is the utility of measuring the serum ammonia level in patients with altered mental status? *Cleveland Clinic Journal of Medicine*. 76 (4), pp.252-254.

Endre, Z.H., Pickering, J.W., Storer, M.K., Hu, W.-., Moorhead, K.T., Allardyce, R., McGregor, D.O. and Scotter, J.M. (2011) Breath ammonia and trimethylamine allow real-time monitoring of haemodialysis efficacy. *Physiological Measurement*. 32 (1), pp.115-130.

Esque-Ruiz, M.T., Figueras-Aloy, J., Salvia-Roiges, M.D. and Carbonell-Estrany, X. (2003) Blood ammonia and transaminases in full-term infants suffering from perinatal asphyxia. *Revista De Neurologia*. 36 (9), pp.801-805.

Felipo, V. and Butterworth, R.F. (2002) Neurobiology of ammonia. *Progress in Neurobiology*. 67 (4), pp.259-279.

Fenton, J.C. (1962) The estimation of plasma ammonia by ion exchange. *Clinica Chimica Acta; International Journal of Clinical Chemistry*. 7 pp.163-175.

Fenton, J.C. and Williams, A.H. (1968) Improved method for the estimation of plasma ammonia by ion exchange. *Journal of Clinical Pathology*. 21 (1), pp.14-18.

Ferenci, P., Lockwood, A., Mullen, K., Tarter, R., Weissenborn, K., Blei, A.T. and Members of the Working Party (2002) Hepatic encephalopathy-definition, nomenclature, diagnosis, and quantification: Final report of the working party at the 11th World Congresses of Gastroenterology, Vienna, 1998. *Hepatology*. 35 (3), pp.716-721.

Finberg, R.W. and Guharoy, R. (2012) *Clinical use of Anti-Infective Agents: A Guide on how to Prescribe Drugs used to Treat Infections*. New York: Springer Science and Business Media.

Florea, L., Diamond, D. and Benito-Lopez, F. (2013) Polyaniline coated micro-capillaries for continuous flow analysis of aqueous solutions. *Analytica Chimica Acta*. 759 pp.1-7.

Fratoddi, I., Venditti, I., Cametti, C. and Russo, M.V. (2015) Chemiresistive polyaniline-based gas sensors: A mini review. *Sensors and Actuators B-Chemical*. 220 pp.534-548.

Frontera, J.A. (2014) Management of Hepatic Encephalopathy. *Current Treatment Options in Neurology*. 16 (6), pp.297.

Garibotto, G., Sofia, A., Robaudo, C., Saffioti, S., Sala, M.R., Verzola, D., Vettore, M., Russo, R., Procopio, V., Deferrari, G. and Tessari, P. (2004) Kidney protein dynamics and ammoniogenesis in humans with chronic metabolic acidosis. *Journal of the American Society of Nephrology*. 15 (6), pp.1606-1615.

Gleeson, M. (2007) Immune function in sport and exercise. *Journal of Applied Physiology*. 103 (2), pp.693-699.

Chapter 1

Goncalves, L.C., Bessa, A., Freitas-Dias, R., Luzes, R., Saar Werneck-de-Castro, J.P., Bassini, A. and Cameron, L. (2012) A sportomics strategy to analyze the ability of arginine to modulate both ammonia and lymphocyte levels in blood after high-intensity exercise. *Journal of the International Society of Sports Nutrition*. 9 pp.30.

Gorostiaga, E.M., Asiain, X., Izquierdo, M., Postigo, A., Aguado, R., Alonso, J.M. and Ibanez, J. (2010) Vertical jump performance and blood ammonia and lactate levels during typical training sessions in elite 400-m runners. *Journal of Strength and Conditioning Research*. 24 (4), pp.1138-1149.

Gouma, P., Kalyanasundaram, K., Yun, X., Stanacevic, M. and Wang, L. (2010) Nanosensor and Breath Analyzer for Ammonia Detection in Exhaled Human Breath. *Ieee Sensors Journal*. 10 (1), pp.49-53.

Green, A. (1988) When and how should we Measure Plasma Ammonia. *Annals of Clinical Biochemistry*. 25 pp.199-209.

Gropman, A.L., Summar, M. and Leonard, J.V. (2007) Neurological implications of urea cycle disorders. *Journal of Inherited Metabolic Disease*. 30 (6), pp.865-879.

Hawke, L. (2012) *Ammonia (Plasma, Blood)*. Available from: <http://www.acb.org.uk/docs/NHLM/Ammonia.pdf>.

Hernandez, S.C., Chaudhuri, D., Chen, W., Myung, N.V. and Mulchandani, A. (2007) Single polypyrrole nanowire ammonia gas sensor. *Electroanalysis*. 19 (19-20), .

Hibbard, T. and Killard, A.J. (2011) Breath ammonia levels in a normal human population study as determined by photoacoustic laser spectroscopy. *Journal of Breath Research*. 5 (3), pp.037101.

Hibbard, T., Crowley, K., Kelly, F., Ward, F., Holian, J., Watson, A. and Killard, A.J. (2013) Point of Care Monitoring of Hemodialysis Patients with a Breath Ammonia Measurement Device Based on Printed Polyaniline Nanoparticle Sensors. *Analytical Chemistry*. 85 (24), pp.12158-12165.

Hioki, A., Kubota, M. and Kawase, A. (1991) Accuracy in the Precise Coulometric Titration of Ammonia and Ammonium Ion with Electrogenerated Hypobromite. *Talanta*. 38 (4), pp.397-404.

Hocker, S., Rabinstein, A.A. and Wijdicks, E.F.M. (2011) Pearls & Oy-sters: Status epilepticus from hyperammonemia after lung transplant. *Neurology*. 77 (10), pp.E54-E56.

Hrboticka, E. (2005) EP1566632A1 One step tester for ammonia. *Anmeldung*.

Huizenga, J.R., Gips, C.H. and Tangerman, A. (1996) The contribution of various organs to ammonia formation: A review of factors determining the arterial ammonia concentration. *Annals of Clinical Biochemistry*. 33 pp.23-30.

Chapter 1

Huizenga, J.R., Tangerman, A. and Gips, C.H. (1994) Determination of Ammonia in Biological-Fluids. *Annals of Clinical Biochemistry*. 31 pp.529-543.

Imran, M., Shah, Y., Nundlall, S., Roberts, N.B. and Howse, M. (2012) Is blood ammonia influenced by kidney function? A prospective study. *Clinical Biochemistry*. 45 (4-5), pp.363-365.

Jang, J., Ha, J. and Kim, S. (2007) Fabrication of polyaniline nanoparticles using microemulsion polymerization. *Macromolecular Research*. 15 (2), pp.154-159.

Joshi, A., Gangal, S.A. and Gupta, S.K. (2011) Ammonia sensing properties of polypyrrole thin films at room temperature. *Sensors and Actuators B-Chemical*. 156 (2), pp.938-942.

Jung, K., Pergande, M., Rej, R., Schreiber, G. and Schimmelpfennig, W. (1985) Mitochondrial-Enzymes in Human-Serum - Comparative Determinations of Glutamate-Dehydrogenase and Mitochondrial Aspartate-Aminotransferase in Healthy-Persons and Patients with Chronic Liver-Diseases. *Clinical Chemistry*. 31 (2), pp.239-243.

Komuro, N., Takaki, S., Suzuki, K. and Citterio, D. (2013) Inkjet printed (bio)chemical sensing devices. *Analytical and Bioanalytical Chemistry*. 405 (17), pp.5785-5805.

Kravos, M. and Malesic, I. (2010) Glutamate Dehydrogenase as a Marker of Alcohol Dependence. *Alcohol and Alcoholism*. 45 (1), pp.39-44.

Krivitzky, L., Babikian, T., Lee, H., Thomas, N.H., Burk-Paull, K.L. and Batshaw, M.L. (2009) Intellectual, Adaptive, and Behavioral Functioning in Children With Urea Cycle Disorders. *Pediatric Research*. 66 (1), pp.96-101.

Kukla, A.L., Shirshov, Y.M. and Piletsky, S.A. (1996) Ammonia sensors based on sensitive polyaniline films. *Sensors and Actuators B-Chemical*. 37 (3), pp.135-140.

Lee, B., Diaz, G.A., Rhead, W., Lichter-Konecki, U., Feigenbaum, A., Berry, S.A., Le Mons, C., Bartley, J.A., Longo, N., Nagamani, S.C., Berquist, W., Gallagher, R., Bartholomew, D., Harding, C.O., Korson, M.S., McCandless, S.E., Smith, W., Cederbaum, S., Wong, D., Merritt, J.L., II, Schulze, A., Vockley, G., Kronn, D., Zori, R., Summar, M., Milikien, D.A., Marino, M., Coakley, D.F., Mokhtarani, M. and Scharschmidt, B.F. (2015) Blood ammonia and glutamine as predictors of hyperammonemic crises in patients with urea cycle disorder. *Genetics in Medicine*. 17 (7), pp.561-568.

Leonard, J.V. and Morris, A.A.M. (2006) Diagnosis and early management of inborn errors of metabolism presenting around the time of birth. *Acta Paediatrica*. 95 (1), pp.6-14.

Leonard, J.V. and Morris, A.A.M. (2002) Urea cycle disorders. *Seminars in Neonatology* : SN. 7 (1), pp.27-35.

Chapter 1

Lichtenstein, G.R., Yang, Y.X., Nunes, F.A., Lewis, J.D., Tuchman, M., Tino, G., Kaiser, L.R., Palevsky, H.I., Kotloff, R.M., Furth, E.E., Bavaria, J.E., Stecker, M.M., Kaplan, P. and Berry, G.T. (2000) Fatal hyperammonemia after orthotopic lung transplantation. *Annals of Internal Medicine*. 132 (4), pp.283-287.

Lieber, C.S. (1998) Gastritis in the alcoholic: relationship to gastric alcohol metabolism and *Helicobacter pylori*. *Addiction Biology*. 3 (4), pp.423-433.

Lockwood, A.H., McDonald, J.M., Reiman, R.E., Gelbard, A.S., Laughlin, J.S., Duffy, T.E. and Plum, F. (1979) Dynamics of Ammonia Metabolism in Man - Effects of Liver-Disease and Hyper-Ammonemia. *Journal of Clinical Investigation*. 63 (3), pp.449-460.

Lourenco, C. and Turner, C. (2014) Breath analysis in disease diagnosis: methodological considerations and applications. *Metabolites*. 4 (2), pp.465-98.

Lowenstein, J.M. (1990) The Purine Nucleotide Cycle Revised. *International Journal of Sports Medicine*. 11 pp.S37-S46.

Luo, C., Shen, G., Liu, N., Gong, F., Wei, X., Yao, S., Liu, D., Teng, X., Ye, N., Zhang, N., Zhou, X., Li, J., Yang, L., Zhao, X., Yang, L., Xiang, R. and Wei, Y. (2014) Ammonia Drives Dendritic Cells into Dysfunction. *Journal of Immunology*. 193 (4), pp.1080-1089.

Maclean, D.A., Spriet, L.L. and Graham, T.E. (1992) Plasma Amino-Acid and Ammonia Responses to Altered Dietary Intakes Prior to Prolonged Exercise in Humans. *Canadian Journal of Physiology and Pharmacology*. 70 (4), pp.420-427.

Maranda, B., Cousineau, J., Allard, P. and Lambert, M. (2007) False positives in plasma ammonia measurement and their clinical impact in a pediatric population. *Clinical Biochemistry*. 40 (8), pp.531-535.

Mehmood, M.A., Waseem, T., Ahmad, F.Z. and Humayun, M.A. (2013) Measuring Partial Pressure of Ammonia in Arterial or Venous Blood VS total Ammonia Levels in Hepatic Encephalopathy. *J. Gastroenterol. Hepatol. Res*. 2 pp.602-606.

Metz, M.P. (2014) Ammonia, a troublesome analyte. *Clinical Biochemistry*. 47 (9), pp.753-753.

Mobley, H.L., Hu, L.T. and Foxal, P.A. (1991) *Helicobacter pylori* urease: properties and role in pathogenesis. *Scandinavian Journal of Gastroenterology. Supplement*. 187 pp.39-46.

Mochalski, P., King, J., Haas, M., Unterkofler, K., Amann, A. and Mayer, G. (2014) Blood and breath profiles of volatile organic compounds in patients with end-stage renal disease. *Bmc Nephrology*. 15 (1), pp.43.

Msall, M., Batshaw, M.L., Suss, R., Brusilow, S.W. and Mellits, E.D. (1984) Neurologic Outcome in Children with Inborn-Errors of Urea Synthesis - Outcome of

Urea-Cycle Enzymopathies. *New England Journal of Medicine*. 310 (23), pp.1500-1505.

Mukhtar, A., Dabbous, H., El Sayed, R., Aboulfetouh, F., Bahaa, M., Abdelaal, A., Fathy, M. and El-Meteini, M. (2013) A Novel Mutation of the Ornithine Transcarbamylase Gene Leading to Fatal Hyperammonemia in a Liver Transplant Recipient. *American Journal of Transplantation*. 13 (4), pp.1084-1087.

Munoz, M.D., Monfort, P., Gaztelu, J.M. and Felipo, V. (2000) Hyperammonemia impairs NMDA receptor-dependent long-term potentiation in the CA1 of rat hippocampus in vitro. *Neurochemical Research*. 25 (4), pp.437-441.

Narasimhan, L.R., Goodman, W. and Patel, C.K.N. (2001) Correlation of breath ammonia with blood urea nitrogen and creatinine during hemodialysis. *Proceedings of the National Academy of Sciences of the United States of America*. 98 (8), pp.4617-4621.

Neri, G., Lacquaniti, A., Rizzo, G., Donato, N., Latino, M. and Buemi, M. (2012) Real-time monitoring of breath ammonia during haemodialysis: use of ion mobility spectrometry (IMS) and cavity ring-down spectroscopy (CRDS) techniques. *Nephrology Dialysis Transplantation*. 27 (7), pp.2945-2952.

Newport, S., Amin, N. and Dozor, A.J. (2009) Exhaled Breath Condensate pH and Ammonia in Cystic Fibrosis and Response to Treatment of Acute Pulmonary Exacerbations. *Pediatric Pulmonology*. 44 (9), pp.866-872.

Ngamna, O., Morrin, A., Killard, A.J., Moulton, S.E., Smyth, M.R. and Wallace, G.G. (2007) Inkjet printable polyaniline nanoformulations. *Langmuir*. 23 (16), pp.8569-8574.

Nobelprize.org (2013) *The Nobel Prize in Chemistry 2000*. Available from: http://www.nobelprize.org/nobel_prizes/chemistry/laureates/2000.

Noiret, L., Baigent, S. and Jalan, R. (2014) Arterial ammonia levels in cirrhosis are determined by systemic and hepatic hemodynamics, and by organ function: a quantitative modelling study. *Liver International*. 34 (6), pp.E45-E55.

Noone, M.L., Kumar, V.G.P., Ummer, K., Achambat, L. and Salam, K.A. (2008) Cirrhosis presenting as Parkinsonism. *Annals of Indian Academy of Neurology*. 11 (3), pp.179-181.

Obrink, K.J. (1955) A modified Conway unit for microdiffusion analysis. *The Biochemical Journal*. 59 (1), pp.134-136.

Ong, J.P., Aggarwal, A., Krieger, D., Easley, K.A., Karafa, M.T., Van Lente, F., Arroliga, A.C. and Mullen, K.D. (2003) Correlation between ammonia levels and the severity of hepatic encephalopathy. *American Journal of Medicine*. 114 (3), pp.188-193.

Chapter 1

Ortho-Clinical Diagnostics Inc. (2015) *Vitros Chemistry Products AMON Slides*. Available from: https://www.cmmc.org/cmmclab/IFU/AMON_MP2-90_EN_I.pdf.

Pita, A.M., Fernandez-Bustos, A., Rodes, M., Arranz, J.A., Fisac, C., Virgili, N., Soler, J. and Wakabayashi, Y. (2004) Orotic aciduria and plasma urea cycle-related amino acid alterations in short bowel syndrome, evoked by an arginine-free diet. *Journal of Parenteral and Enteral Nutrition*. 28 (5), pp.315-323.

Poh, Z. and Chang, P.E.J. (2012) A current review of the diagnostic and treatment strategies of hepatic encephalopathy. *International Journal of Hepatology*. 2012 pp.480309-480309.

Prasad, A.N., Breen, J.C., Ampola, M.G. and Rosman, P. (1997) Argininemia: A treatable genetic cause of progressive spastic diplegia simulating cerebral palsy: Case reports and literature review. *Journal of Child Neurology*. 12 (5), pp.301-309.

Ratcliffe, N. (1990) Polypyrrole-Based Sensor for Hydrazine and Ammonia. *Analytica Chimica Acta*. 239 (2), pp.257-262.

Romero-Gomez, M., Boza, F., Garcia-Valdecasas, M.S., Garcia, E. and Aguilar-Reina, J. (2001) Subclinical hepatic encephalopathy predicts the development of overt hepatic encephalopathy. *American Journal of Gastroenterology*. 96 (9), pp.2718-2723.

Rose, C.F. (2014) Ammonia: more than a neurotoxin? *Liver International*. 34 (5), pp.649-651.

Sabina, R.L., Swain, J.L., Olanow, C.W., Bradley, W.G., Fishbein, W.N., Dimauro, S. and Holmes, E.W. (1984) Myoadenylate Deaminase Deficiency - Functional and Metabolic Abnormalities Associated with Disruption of the Purine Nucleotide Cycle. *Journal of Clinical Investigation*. 73 (3), pp.720-730.

Samtoy, B. and Debeukelaer, M.M. (1980) Ammonia Encephalopathy Secondary to Urinary-Tract Infection with *Proteus-Mirabilis*. *Pediatrics*. 65 (2), pp.294-297.

Sato, S., Yokota, C., Toyoda, K., Naganuma, M. and Minematsu, K. (2008) Hyperammonemic encephalopathy caused by urinary tract infection with urinary retention. *European Journal of Internal Medicine*. 19 (8), pp.e78-9.

Schmidt, F.M., Vaitinen, O., Metsala, M., Lehto, M., Forsblom, C., Groop, P.-. and Halonen, L. (2013) Ammonia in breath and emitted from skin. *Journal of Breath Research*. 7 (1), pp.017109.

Searle, P.L. (1984) The Berthelot Or Indophenol Reaction and its use in the Analytical-Chemistry of Nitrogen - a Review. *Analyst*. 109 (5), pp.549-568.

Sebastio, G., Sperandeo, M.P. and Andria, G. (2011) Lysinuric Protein Intolerance: Reviewing Concepts on a Multisystem Disease. *American Journal of Medical Genetics Part C-Seminars in Medical Genetics*. 157C (1), pp.54-62.

Sekisui Diagnostics (UK) Ltd. (2013) *Ammonia L3K®*. Available from: http://www.sekisuidiagnostics.com/writable/product_documents/files/Ammonia_L3K_SS_80-7440-00-02.pdf.

Sharma, B.C., Sharma, P., Lunia, M.K., Srivastava, S., Goyal, R. and Sarin, S.K. (2013) A Randomized, Double-Blind, Controlled Trial Comparing Rifaximin Plus Lactulose With Lactulose Alone in Treatment of Overt Hepatic Encephalopathy. *American Journal of Gastroenterology*. 108 (9), pp.1458-1463.

Shaw, P.J., Dale, G. and Bates, D. (1989) Familial Lysinuric Protein Intolerance Presenting as Coma in 2 Adult Siblings. *Journal of Neurology Neurosurgery and Psychiatry*. 52 (5), pp.648-651.

Sigma-Aldrich Co. LLC. (2015) *Ammonia Assay Kit*. Available from: <https://www.sigmaaldrich.com/content/dam/sigmaaldrich/docs/Sigma/Bulletin/aa0100bul.pdf>.

Smith, D., Wang, T.S. and Spanel, P. (2002) On-line, simultaneous quantification of ethanol, some metabolites and water vapour in breath following the ingestion of alcohol. *Physiological Measurement*. 23 (3), pp.477-489.

Smith, D., Wang, T., Pysanenko, A. and Spanel, P. (2008) A selected ion flow tube mass spectrometry study of ammonia in mouth- and nose-exhaled breath and in the oral cavity. *Rapid Communications in Mass Spectrometry*. 22 (6), pp.783-789.

Solga, S.F., Mudalel, M., Spacek, L.A., Lewicki, R., Tittel, F.K., Loccioni, C., Russo, A., Ragnoni, A. and Risby, T.H. (2014) Changes in the concentration of breath ammonia in response to exercise: a preliminary investigation. *Journal of Breath Research*. 8 (3), pp.037103.

Solga, S.F., Mudalel, M., Spacek, L.A., Lewicki, R., Tittel, F., Loccioni, C., Russo, A. and Risby, T.H. (2013) Factors influencing breath ammonia determination. *Journal of Breath Research*. 7 (3), pp.037101.

Spacek, L.A., Mudalel, M.L., Lewicki, R., Tittel, F.K., Risby, T.H., Stoltzfus, J., Munier, J.J. and Solga, S.F. (2015) Breath ammonia and ethanol increase in response to a high protein challenge. *Biomarkers*. 20 pp.149-156.

Stejskal, J., Sapurina, I., Prokes, J. and Zemek, J. (1999) In-situ polymerized polyaniline films. *Synthetic Metals*. 105 (3), pp.195-202.

Su, X.L., Yu, B.S., Tan, H.W., Yang, X.R., Nie, L.H. and Yao, S.Z. (1998) Flow-injection determination of total ammonia and total carbon dioxide in blood based on gas-diffusion separation and with a bulk acoustic wave impedance sensor. *Journal of Pharmaceutical and Biomedical Analysis*. 16 (5), pp.759-769.

Subramanian, R., Crowley, K., Morrin, A. and Killard, A.J. (2013) A sensor probe for the continuous in situ monitoring of ammonia leakage in secondary refrigerant systems. *Anal. Methods*. 5 (1), pp.134-140.

Chapter 1

Tanzer, D. (1997) 542839 Means and method for the determination of ammonium ions (5620900).

Tizianello, A., Deferrari, G., Gurreri, G. and Acquarone, N. (1977) Effects of Metabolic Alkalosis, Metabolic-Acidosis and Uremia on Whole-Body Intracellular Ph in Man. *Clinical Science and Molecular Medicine*. 52 (2), pp.125-135.

Trojanowicz, M., Krawczyk, T.K.V., Zmorzynska, M. and Campanella, L. (1997) Amperometric sensing of ammonia in aqueous solutions using a polyaniline-modified electrode in flow injection systems. *Electroanalysis*. 9 (14), pp.1062-1066.

Tsuda, T., Ohkuwa, T. and Itoh, H. (2011) Findings of Skin Gases and Their Possibilities in Healthcare Monitoring. In: Yoshikawa, T.N.,Y., ed. (2011) *Gas Biology Research in Clinical Practice*. Basel: Karger, pp.125-132.

Turner, C., Spanel, P. and Smith, D. (2006) A longitudinal study of ammonia, acetone and propanol in the exhaled breath of 30 subjects using selected ion flow tube mass spectrometry, SIFT-MS. *Physiological Measurement*. 27 (4), pp.321-337.

Utku, U., Asil, T., Balci, K., Uzunca, I. and Celik, Y. (2005) Hepatic myelopathy with spastic paraparesis. *Clinical Neurology and Neurosurgery*. 107 (6), pp.514-516.

Voet, D. and Voet, J.G. (2004) *Biochemistry*. 3rd ed. USA: John Wiley & Sons, Inc.

Wallace, G., Spinks, G.M., Kane-Maguire, L.A.P. and Teasdale, P.R., (2003) *Conductive Electroactive Polymers - Intelligent Materials Systems*. 2nd ed. USA: CRC Press.

Wang, T., Pysanenko, A., Dryahina, K., Spanel, P. and Smith, D. (2008) Analysis of breath, exhaled via the mouth and nose, and the air in the oral cavity. *Journal of Breath Research*. 2 (3), pp.037013.

Weiner, I.D., Mitch, W.E. and Sands, J.M. (2014) Urea and Ammonia Metabolism and the Control of Renal Nitrogen Excretion. *Clin J Am Soc Nephrol*. 10 (8), pp.1444-1458.

Weissenborn, K., Tietge, U.J.F., Bokemeyer, M., Mohammadi, B., Bode, U., Manns, M.P. and Caselitz, M. (2003) Liver transplantation improves hepatic myelopathy: Evidence by three cases. *Gastroenterology*. 124 (2), pp.346-351.

Weng, B., Shepherd, R.L., Crowley, K., Killard, A.J. and Wallace, G.G. (2010) Printing conducting polymers. *Analyst*. 135 (11), pp.2779-2789.

Weng, B., Shepherd, R., Chen, J. and Wallace, G.G. (2011) Gemini surfactant doped polypyrrole nanodispersions: an inkjet printable formulation. *Journal of Materials Chemistry*. 21 (6), pp.1918-1924.

Wilkinson, D.J., Smeeton, N.J. and Watt, P.W. (2010) Ammonia metabolism, the brain and fatigue; revisiting the link. *Progress in Neurobiology*. 91 (3), pp.200-219.

Chapter 1

Wu, S., Zeng, F., Li, F. and Zhu, Y. (2000) Ammonia sensitivity of polyaniline films via emulsion polymerization. *European Polymer Journal*. 36 (4), pp.679-683.

Zhao, P., Wang, C., Liu, W., Wang, X., Yu, L. and Sun, Y. (2014) Acute liver failure in Chinese children: a multicenter investigation. *Hepatobiliary & Pancreatic Diseases International*. 13 (3), pp.276-280.

CHAPTER 2

MATERIALS AND METHODS

2.1. MATERIALS

Acetaminophen (AC100) and *L*-ascorbic acid (BDH9242) were purchased from the British Drug House Ltd. (Poole, UK).

Calcium chloride (BP510), ethanol (BP2818500), hydrochloric acid (11355890), magnesium chloride (M35), methanol (A41120), potassium chloride (P/4280/53), potassium dihydrogen orthophosphate (P/4800/53), 2-propanol (A461), sodium chloride (S/3160/60), sodium dodecyl sulphate (S/5200/53), sodium hydroxide (S/4920/60), disodium hydrogen orthophosphate (S/4520/53), toluene (T324) and Vivaspin 20 centrifuge tubes (10015804) with a molecular weight cut off (MWCO) of 3 kDa were purchased from Fisher Scientific UK Ltd. (Loughborough, UK).

Ammonium chloride (326372), ammonium persulphate (A7460), aniline (132934; distilled and stored frozen under nitrogen before use), bovine serum albumin (BSA) lyophilized powder (A2153), Brij® S10 (388890), cellulose acetate dialysis tubing 22 mm width with a molecular weight cut off of 14 kDa (D9777), Coomassie blue G dye (B0770), creatinine anhydrous (C4255), ethyl cellulose (433837), foetal bovine serum (F7524), *L*-glutamic acid monosodium salt monohydrate (49621), Oil red O stain (O0625), paraformaldehyde (P6148), phosphoric acid (P6560), uric acid (U2625) and Whatman® 0.2 µm polytetrafluoroethylene (PTFE) membrane filters (WHA10411411) were purchased from Sigma-Aldrich Company Ltd. (Dorset, UK).

Other materials were obtained as follows: Ammonia Assay Kit – Modified Berthelot (ab102509) was purchased from Abcam® Plc. (Cambridge, UK). Carbon SPE (DRP-110) with 3 mm carbon working electrode, carbon counter electrode and silver reference electrode were provided by DropSens (Asturias, Spain). Compressed air was provided by BOC (British Oxygen Company Ltd., Manchester, UK). Dodecylbenzene sulphonic acid (DBSA) soft type (D0989) was purchased from TCI Europe N.V. (Zwijndrecht, Belgium). Pooled delipidated processed serum (S139) was purchased from Scipac Ltd. (Kent, UK). Glassy carbon electrodes (GCE) with 3 mm diameter (010763) were sourced from IJ Cambria Scientific Ltd. (Llanelli, Wales, UK). Rubber o-rings (BS013 Viton) were purchased from Polymax Ltd.

(Hampshire, UK). Polyester pressure sensitive adhesive (PSA, ARcare 92712) of 48 μm thickness were supplied by Adhesives Research Inc. (Limerick, Ireland). Preshrunk polyethylene terephthalate (PET) substrates of 175 μm thickness were supplied by HiFi Industrial Film Ltd. (Hertfordshire, UK). Sericol (ZT639) was purchased from Fujifilm Dimatix Inc. (Santa Clara, CA). Electrodag PF-410 silver conductive ink was purchased from NorCote International, Ltd. (Hampshire, UK).

2.2. INSTRUMENTATION

During ammonia sensor production and assessment the following instrumentation was used. Screen printing was performed with a semi-automated DEK-248 printing machine (DEK International, Dorset, UK). Inkjet printing was carried out using a Dimatix Materials Printer DMP-2831 with Dimatix Drop Manager DMP-2800 series software (Fujifilm Dimatix Inc., Santa Clara, CA). The MEMS-based Dimatix cartridge with 16 nozzles (20 μm diameter) spaced at 254 μm was used. Centrifugation of polyaniline nanoparticles was carried out using a Beckman Coulter Allerga X-22R Centrifuge with a Beckman C0650 conical rotor head. A Graphtec CE5000-40 Craft Robo Pro cutting plotter (Graphtec GB Ltd., Wrexham, UK) and Robo Master-Pro software were used to prepare the PSA patterns for encapsulation of the sensor. All electrochemical protocols were performed on a Metrohm Autolab PGSTAT 128N potentiostat (Metrohm UK Ltd., Cheshire, UK) with Nova 1.6 software equipped with a FRA2 electrochemical impedance analyser. A glassy carbon electrode with a silver/silver chloride (Ag/AgCl) reference electrode and a platinum mesh auxiliary electrode were used during voltammetric experiments. Unless otherwise stated all measurements were performed at room temperature $25 \pm 3^\circ\text{C}$.

To characterise the materials produced and the fabricated sensors the following instrumentation was used. Particle sizing and zeta potential analysis was performed using a Malvern Zetasizer Nano ZS (Malvern Instruments Ltd., Worcestershire, UK). Scanning electron microscopy (SEM) was performed using a Phillips X230 scanning electron microscope. Transmission electron microscopy (TEM) was performed using a Phillips CM10 transmission electron microscope. The UV-vis results were observed using a Perkin Elmer Lambda XLS spectrometer. A Fluostar Optima spectrophotometer was used to analyse spectrophotometric results

(BMG LabTech Ltd., Buckinghamshire, UK). Serum centrifugation was carried out using an ALC PK 120 centrifuge with an ALC T534 rotor.

2.3. SOFTWARE

AutoCAD 2008 was used to design screen printed electrodes, inkjet-printed patterns and PSA designs for device encapsulation. AutoCAD was also used to present the device assembly in Fig. 2.3. ACD/ChemSketch was used to draw chemical structures printed throughout the thesis. SigmaPlot version 10.0 was used for all data analysis and graphic presentations.

2.4. METHODS

2.4.1. Buffer

0.1 M phosphate buffered saline solution (PBS) was prepared by dissolving 13.609 g of potassium dihydrogen orthophosphate (0.1 M), 8 g of sodium chloride (0.137 M) and 0.2 g of potassium chloride (2.7 mM) in 1 L deionised water. A 1 L solution was made up in deionised water containing 14.196 g of disodium hydrogen orthophosphate (0.1 M), 8 g of sodium chloride (0.137 M) and 0.2 g of potassium chloride (2.7 mM). The second solution was gradually added to the first until pH 7.4 was reached.

2.4.2. Electrode fabrication via screen printing

Silver screen printed interdigitated electrodes (IDEs) were fabricated using a DEK-248 screen printer with a polyester screen with a mesh thickness 77 T (filaments per cm) and mounted at 45° to the print stroke (Crowley *et al.*, 2008a). Electrodag PF-410 silver ink was deposited onto a 175 µm thick PET substrate and cured at 120°C for five min. Silver screen printed IDEs were designed in a two electrode configuration. The design of the IDE used in this work is illustrated in Fig. 2.1. At one end of the structure is a set of IDEs which occupy an area of approximately 14 × 14 mm, each with a width of 0.2 mm and a pitch of 0.75 mm, respectively. Bonding pads are located at the other end of the electrode.

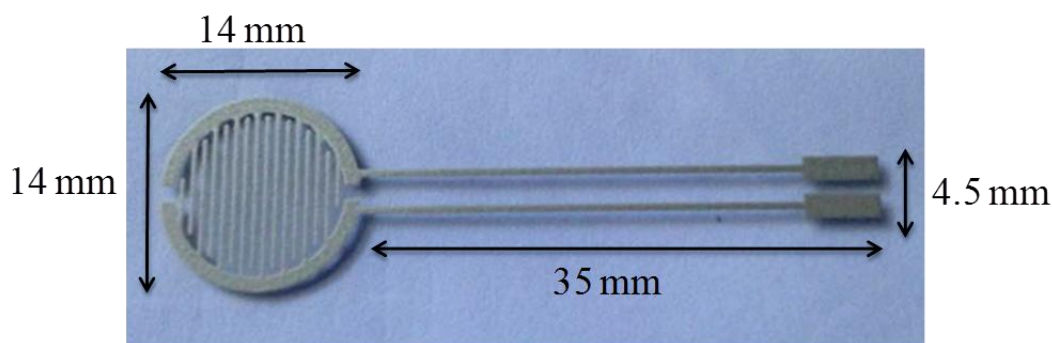


Figure 2.1. Image of a silver interdigitated screen printed electrode with 14×14 mm head dimensions containing an interdigitate width of 0.2 mm and pitch of 0.75 mm. The electrode legs are 35 mm long with bonding pads located at the end of the structure.

2.4.3. Polyaniline nanoparticle synthesis

Polyaniline nanoparticles were synthesised using the rapid mixing method (Ngamna *et al.*, 2007). Synthesis was as follows: dodecylbenzene sulphonic acid (DBSA; 3.6 g) was made up to 40 mL with deionised water and ammonium persulphate (APS; 0.36 g) was dissolved in 20 mL of the DBSA solution. The remaining 20 mLs of the DBSA solution was stirred at 20°C whilst aniline (0.6 mL) was added, followed quickly by the DBSA-APS solution. The mixture was left stirring for 2.5 hours at 300 rpm. A 0.05 M solution of sodium dodecyl sulphate (SDS) was prepared by dissolving 14.4 g of SDS in deionised water. After stirring, 20 mL of SDS was added to the polyaniline dispersion which was centrifuged for 30 min at $3,000 \times g$. The supernatant was finally dialyzed for 48 hours against 500 mL of SDS to remove excess material such as unwanted aniline. The final product was a dark green aqueous solution that was inkjet-printed onto the screen printed electrodes using a Dimatix Drop Manager-2381 Inkjet Printer.

2.4.4. Inkjet printing of polyaniline nanoparticles

A Dimatix 2381 printer based on piezoelectric technology was used to print the polyaniline nanoparticle layer. Previous work by our group detailed the technique of inkjet-printed polyaniline nanoparticles (Crowley *et al.*, 2008b). In brief, polyaniline nanoparticles were syringed into a Fujifilm Dimatix ink cartridge using a Thermo Syringe combined with an Acrodisc polyvinyl fluoride (PVDF) syringe filter (0.2 μm) and needle to inject 2 mL of the polyaniline nanoparticulate solution.

The Fujifilm Dimatix inkjet printer cartridges contain 16 nozzles that eject 10 pL of ink. The cartridge was placed into the Dimatix inkjet printer at a head angle of 4.5° where ten layers were printed onto the silver IDEs. The operating conditions were optimised with a voltage of 18 V and pitch density spacing set to 20 µm. The substrate conditions were set to a print height of 1 mm and at ambient conditions. After printing, the sheets of dry sensors were lightly rinsed with deionised water to remove residual SDS. The sensors were then placed in a dry-heat oven at 70°C for 30 min. A resulting sensor is shown in Fig. 2.2.

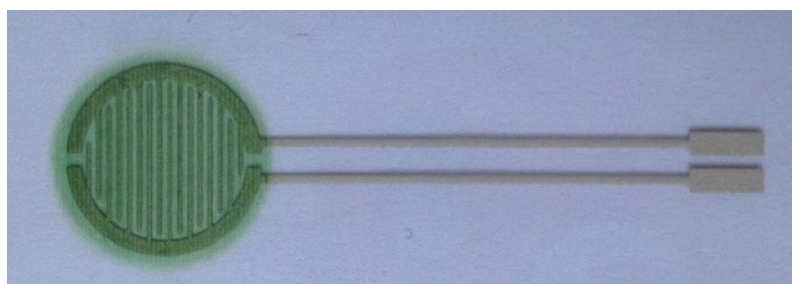


Figure 2.2. Image of a silver interdigitated screen printed electrode modified with ten inkjet-printed layers of polyaniline nanoparticles.

2.4.5. Assembly of the aqueous ammonia sensing device

The printed ammonia sensors were further assembled into a device suitable for measuring ammonia in solution. A Graphtec Robo Pro S (Model no. CE50000-4-CRP) cutting plotter and Robo Master Pro software (Wrexham, UK) were used to prepare the PSA patterns for sensor and device fabrication. Patterns were drawn using AutoCAD and uploaded into the Robo Master software. To create the headspace between the sensor and the sample solution, an o-ring with a thickness of 1.78 mm was adhered to the modified sensor using PSA, with a thickness of 48 µm and a gas-permeable PTFE membrane, with a 0.2 µm pore size and a diameter of 25 mm, was fixed above the o-ring using PSA to create a headspace of 247 mm³. The distance between the sensor and membrane was 1.88 mm. The sensor and headspace along with the PTFE membrane was encapsulated with PSA and a lid was then attached to create a sample chamber with a capacity of 52 µL. Air inlet and outlet ports were created using two hypodermic needles inserted into the o-ring at opposite sides of the device to allow the passage of compressed air over the sensor surface. An exploded version of the device is shown in Fig. 2.3.

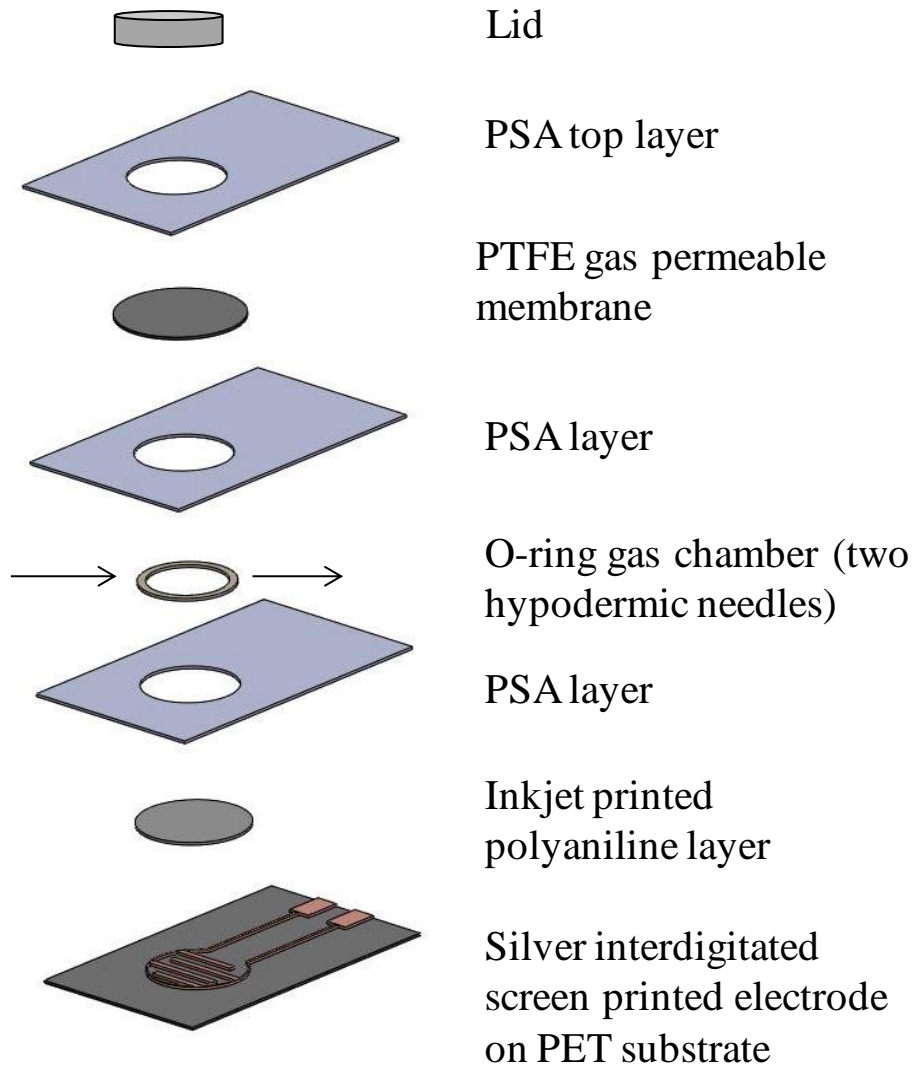


Figure 2.3. Design layout of the sensing device assembly. A silver screen printed interdigitated electrode deposited onto PET substrate was inkjet print modified with ten layers polyaniline creating an ammonia sensor. A gas headspace of 247 mm³ was created above the sensor using a PTFE membrane and a 1.78 mm thick o-ring (with air inlet and outlet ports created using two hypodermic needles inserted into the o-ring at opposite sides of the device to allow the passage of compressed air over the sensor surface) adhered together using 48 μm thick PSA. This gas headspace chamber was adhered to the modified sensor using PSA. The sensor and headspace along with the PTFE membrane was then encapsulated using PSA and a lid was attached to create a sample chamber with a capacity of 52 μL.

2.4.6. Characterisation techniques

UV-visible spectroscopy was carried out on the polyaniline aqueous nanodispersions. They were diluted in deionised water at a ratio of 1:100 and analysed in the range of 300 to 900 nm.

Irradiation at 632.8 nm using a He-Ne laser was used to perform particle size and zeta potential analysis. The polyaniline nanodispersions were diluted in deionised water at a ratio of 1:100. In order for the Zetasizer to apply Mie theory, optical properties are required such as refractive index of both the dispersed particles and dispersant and the imaginary refractive index (absorption) of the dispersed particles (Malvern Instruments Ltd., 2016). Mie theory predicts the scattering intensity of light upon exposure to an extremely dilute suspension of particles. It is based on Maxwell's electromagnetic field equations and uses the refractive index difference between the particle and the dispersing medium to predict the intensity of the scattered light. It also describes how the absorption characteristics of a particle affect the amount of light which is transmitted through the particle which may be either absorbed or refracted.

Optical parameters used were taken from recommendations by Escubed Ltd. for the measurement of polyaniline in deionised water. They were as follows:

Refractive index of particles	1.52
Imaginary refractive index of particles	0.1
Refractive index of dispersant	1.33

2.4.7. Cyclic voltammetric analysis of polyaniline dispersions

Cyclic voltammetry was performed on polyaniline films by drop casting 7 μL of the polymer dispersion onto GCEs cycled in 1 M HCl at a scan rate of 0.1 V s^{-1} from -0.2 to 0.9 V vs. Ag/AgCl.

Inkjet-printed polyaniline films were studied on DropSens carbon screen printed electrodes in 1 M HCl at a scan rate of 0.1 V s^{-1} from -0.2 to 0.9 V vs. Ag/AgCl.

2.4.8. Electrochemical impedance spectroscopic measurement of ammonia

Impedance spectroscopic measurements were carried out on the encapsulated ammonia devices. The devices were exposed to ammonia as ammonium chloride in 0.1 M PBS, unless otherwise stated. PBS was initially made at pH 7.4, upon the addition of ammonia it was altered to pH 11.0 using 5 M NaOH ready for device exposure. A sample volume of 52 μL was left to incubate on the electrode surface for 15 min and removed before 5 psi of compressed air was passed over the sensor surface for 1 min. Impedance was measured across the range of 0.1 Hz to 100 kHz, at 5 mV amplitude and a 1 s sampling rate. For impedimetric single frequency experiments 1 kHz was applied using the same parameters.

2.4.8.1. Ratiometric method

Each individual device response was normalised (Z/Z_{air}) with respect to its initial baseline (Z_{air}) and its response to ammonia (Z). This gave rise to a value which was due to the response of ammonia alone as opposed to the inherent differences due different devices being compared to each other.

2.4.9. Spectrophotometric measurement of ammonia

The Abcam® ammonia assay kit which utilises the Berthelot reaction was used for the spectrophotometric assays carried out to validate the ammonia device. Unless otherwise stated, 100 μL of ammonia chloride standards (25 to 200 μM) were prepared using a provided calibrator stock of 1 mM ammonia. Standards were made up in 0.1 M PBS pH 7.4 and were analysed in triplicate in a 96 well plate. To the standards, 80 μL of Assay Reagent 1 (nitroferricyanide, 2-phenylphenol) and 40 μL of Assay Reagent 2 (sodium hypochlorite) were added and incubated for 30 min at room temperature and measured at 650 nm.

2.4.10. Bradford protein assay

The Bradford assay was used to measure the protein concentration of biological samples. A stock dye of Coomassie blue G dye (330 mg Coomassie blue G dye dissolved in 100 mL phosphoric acid/ethanol 2:1) was prepared fresh. The working solution was prepared from 3% stock dye, 8% phosphoric acid and 3.8% ethanol in deionised water. BSA protein standards (0.25 to 1.25 $\mu\text{g } \mu\text{L}^{-1}$) were prepared from a BSA stock of 1 $\mu\text{g } \mu\text{L}^{-1}$ and added in triplicate to a 96 well plate.

Working dye solution (200 μL) was added to each well and the absorbance was monitored at 620 nm (Bradford, 1976).

2.4.11. Oil red O analysis for cellular lipids

Oil red-O was used to measure the lipid content of serum samples. Serum samples were dried onto glass slides, then washed in PBS and fixed in 2.5% paraformaldehyde (PFA) and then stained for lipids. A stock solution of 0.5% (v/v) (saturated) Oil red-O in 2-propanol was freshly diluted (three parts stock solution in two parts deionised water) and filtered. The serum samples were stained for 30 min at 37°C then briefly de-stained in 60% (v/v) 2-propanol and washed in water before mounting in PBS/glycerol (Moffitt *et al.*, 2005). Imaging was carried out under a light microscope.

2.5. REFERENCES

Bradford, M.M. (1976) Rapid and Sensitive Method for Quantitation of Microgram Quantities of Protein Utilizing Principle of Protein-Dye Binding. *Analytical Biochemistry*. 72 (1-2), pp.248-254.

Crowley, K., Morrin, A., Hernandez, A., O'Malley, E., Whitten, P.G., Wallace, G.G., Smyth, M.R. and Killard, A.J. (2008a) Fabrication of an ammonia gas sensor using inkjet-printed polyaniline nanoparticles. *Talanta*. 77 (2), pp.710-717.

Crowley, K., O'Malley, E., Morrin, A., Smyth, M.R. and Killard, A.J. (2008b) An aqueous ammonia sensor based on an inkjet-printed polyaniline nanoparticle-modified electrode. *Analyst*. 133 (3), pp.391-399.

Malvern Instruments Ltd. (2016) Zeta Potential and Electrokinetic Phenomena. *Zetasizer Nano Course*.

Moffitt, J.H., Fielding, B.A., Evershed, R., Berstan, R., Currie, J.M. and Clark, A. (2005) Adverse physicochemical properties of tripalmitin in beta cells lead to morphological changes and lipotoxicity in vitro. *Diabetologia*. 48 (9), pp.1819-1829.

Ngamna, O., Morrin, A., Killard, A.J., Moulton, S.E., Smyth, M.R. and Wallace, G.G. (2007) Inkjet printable polyaniline nanoformulations. *Langmuir*. 23 (16), pp.8569-8574.

CHAPTER 3

OPTIMISATION AND CHARACTERISATION OF POLYANILINE NANOPARTICLE INK PRODUCTION AND SENSOR FABRICATION

3.1. INTRODUCTION

Of the available tests and kits for blood ammonia detailed in Chapter 1, none utilise electrochemical methods. Few, if any, are suitable for *in situ* testing for blood ammonia. Thus, the concept of an impedimetric measurement of a liquid sample using a gas phase sensor was considered as a potential solution to the problem of aqueous (blood) ammonia measurement.

3.1.1. Polyaniline nanoparticle synthesis and processability

It was the aim of this work to develop a blood ammonia device based on the principal of the interaction of polyaniline with ammonia. Fabrication options available for conductive polyaniline were, in the past, limited to chemical or electrochemical polymerisation. Both of these techniques gave minimal control over film formation and morphology (Li *et al.*, 2005). The development of polyaniline sensors has been greatly facilitated by the work of Han *et al.* (2002). They demonstrated the chemical oxidative polymerization of aniline with APS in a DBSA micellar solution to obtain conductive nanoparticles with enhanced thermal stability, processability and conductivity (Fig. 3.1).

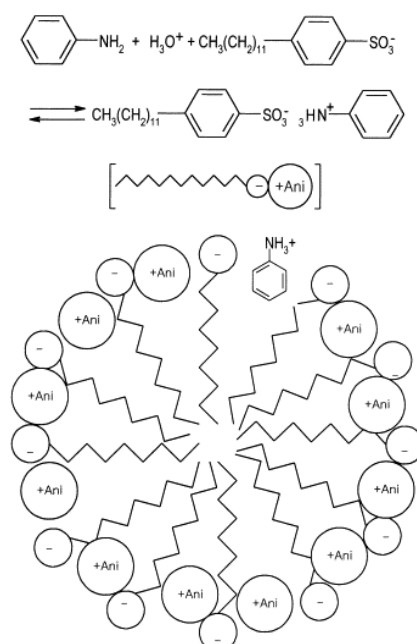


Figure 3.1. Reaction scheme of a polyaniline-dodecylbenzene sulphonic acid micellar structure. Reproduced with permission from Elsevier (Han *et al.*; 2002).

This method of polymerisation enables large numbers of sensors to be prepared simultaneously via inkjet printing which overcomes poor processability previously associated with the deposition of conducting polymers. Our group has focused research in the area of polymer science culminating in the development of inkjet printable polyaniline nanoformulations (Ngamna *et al.*, 2007). In this work, polyaniline nanodispersions were synthesised to produce an aqueous ‘nanoink’ which was then inkjet-printed using an Epson desktop printer for pattern deposition. Later work applied the inkjet-printed polyaniline nanoparticles to the development of a breath ammonia monitoring system known as AmBeR® (Hibbard *et al.*, 2013a). The AmBeR® technology quantifies ammonia across the clinically relevant range of 40 to 2175 parts-per-billion (ppbv) using electrochemical impedance by measuring impedance changes of the polyaniline film upon exposure to ammonia. Parallel to the AmBeR® technology, the quantification of aqueous ammonia leaks in secondary refrigerant systems was developed (Subramanian *et al.*, 2013). This system also utilised impedimetric measurement of ammonia, but employed a gas-permeable membrane allowing for gaseous ammonia measurements to be conducted in an aqueous environment. Current work discussed in this thesis is built upon the foundations of the AmBeR® technology and secondary refrigerant system ammonia probe. The development of a blood ammonia sensor using screen printed electrodes modified with inkjet-printed polyaniline nanoparticles in combination with a gas-permeable membrane was selected as the basis of the development of a sensing device for the measurement of ammonia in a liquid sample, particularly in blood.

3.1.2. Electrochemical impedance spectroscopic analysis

The fabricated ammonia sensor was characterised and analysed using electrochemical impedance spectroscopy. Electrochemical impedance spectroscopy is based on the opposition of the flow of an alternating current (a.c.) through a system. It is an extremely powerful technique for probing the behaviour of materials. It is used throughout the literature as an analytical measurement method providing a wealth of information about the physiochemical processes occurring at electrodes including ion migration, and charge distribution at the electrode/electrolyte interface and the velocity of the reaction. Impedance (Z) can be thought of as the ratio between an applied sinusoidal voltage (V) and a responding sinusoidal current (I) in

the frequency domain (Macdonald, 1992) (Fig. 3.2). It is a product of the resistance (Z_R) to the input function and the capacitive reactance (Z_C):

$$Z = Z_R + Z_C = R - j/\omega C \quad \text{Eq. 3.1}$$

where the resistance (R) is calculated by real impedance and the capacitance ($-j/\omega C$) is calculated by imaginary angular frequency. In the complex plane diagram (Nyquist plot) the capacitance (Z'') is on the y-axis and the resistance (Z') is found on the x-axis. Impedance has properties of magnitude and phase angle as portrayed in Fig 3.2. The sinusoidal ac input response is altered when a disturbance resulting from resistances, capacitances or inductances in the system result in changes to phase and magnitude.

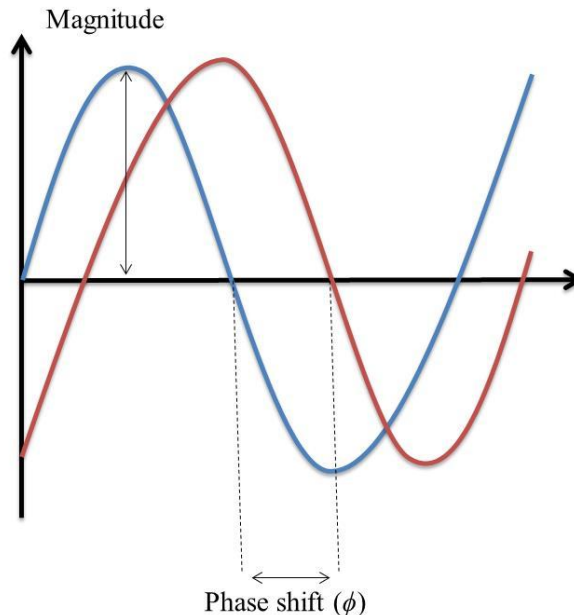


Figure 3.2. Sinusoidal representation of impedance - the change in magnitude represented by phase shift (ϕ) upon the introduction of a change to the system, i.e. the difference between the input voltage (red) and the output current (blue).

In the context of this study, the polyaniline sensor will have particular impedance characteristics which will be altered by the introduction of ammonia (Crowley *et al.*, 2008a). This impedimetric change is hypothesised to be proportional to the concentration of ammonia added to the device.

The fabrication of the ammonia sensor is described in this chapter. To achieve this, polyaniline nanoparticles were synthesised as an aqueous dispersion and piezoelectrically inkjet-printed onto silver screen printed IDEs on a PET substrate. The quality of the sensors produced was studied using optical and electrochemical techniques. For preliminary gas-phase measurements, the sensor was used without further modification. However, to allow characterisation with liquid samples it was initially combined with a PTFE membrane. This allowed the ammonia sensors to be studied and optimised in relation to the impedimetric measurement of ammonia derived from a liquid sample, but which was in the gas phase.

3.2. RESULTS AND DISCUSSION

3.2.1. *Fabrication and characterisation of polyaniline nanoparticles*

Micellar emulsion polymerisation was employed to produce aqueous polyaniline nanodispersions as described by Ngamna *et al.* (2007) and detailed in Chapter 2, Section 2.4.3. In brief, 3.6 g of DBSA was made up to 40 mL in deionised water. APS (0.36 g) was dissolved in 20 mL of the DBSA solution. The remaining DBSA solution was stirred at 20°C and 0.6 mL of aniline was added, followed quickly by the DBSA-APS solution. The mixture was left stirring for 2.5 hr. After stirring, 20 mL of a 0.05 M solution of SDS was added to the dispersion, which was then centrifuged for 30 min at $3,000 \times g$. The supernatant was finally dialyzed for 48 hours against 500 mL of SDS to remove excess material such as unwanted aniline and to stabilise the DBSA-polyaniline nanoparticles. Batches of polyaniline nanoparticles were subsequently characterised using a range of analytical techniques. Parameters such as absorbance, particle sizing and zeta (ζ)-potential were analysed to ensure batch quality.

Initially, UV-visible spectra were obtained for the aqueous polyaniline dispersions (1:100 polyaniline dilution in deionised water) over a wavelength range from 300 to 900 nm. In total, eleven polyaniline batches were synthesised throughout this study and the spectra for each is shown in Fig. 3.3. The UV-visible spectrum of polyaniline is very well established in the literature and so any deviations in batch production were easily identified. It is characteristic of the π - π^*

band to appear between 320 nm and 360 nm, the π -polaron band is expected to be seen between 400 nm and 420 nm and the localised polaron should be between 740 nm and 800 nm (Kim *et al.*, 2001). It can be seen from Fig. 3.3 that typical characteristics of the emeraldine salt form of polyaniline were observed for all eleven batches. There was no shift of features for any batch, meaning there was little deviation in batch to batch quality during synthesis or compared to the literature, but they do appear to vary significantly in overall concentration. This may have been caused during the centrifugation step of the synthesis. Subsequent to centrifugation, larger entities form a pellet. However, this pellet is not solid and leaks into the supernatant when decanting. Thus, altering the concentration of the polyaniline nanodispersion and resulting in absorbance intensity variations.

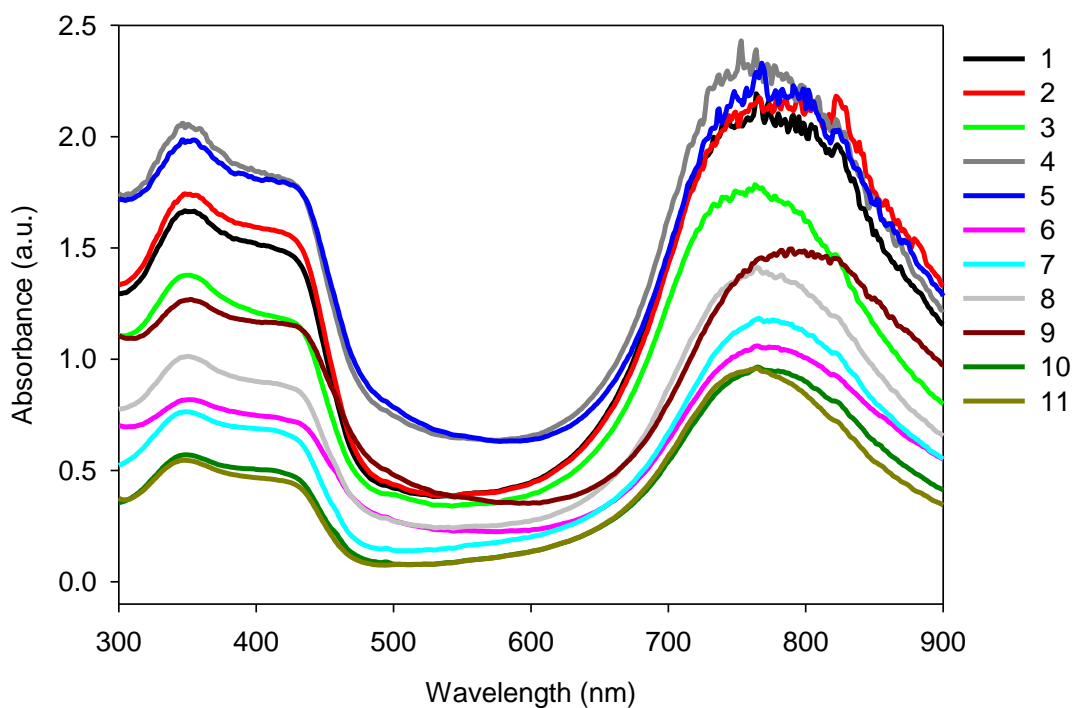


Figure 3.3. UV-visible spectra of 11 polyaniline nanoparticle dispersions in deionised water at a range of 300 to 900 nm. For all batches the π - π^* band was visible between 320 nm and 360 nm, the π -polaron band could be seen between 400 nm and 420 nm and the localised polaron was observed between 740 nm and 800 nm.

UV-Visible spectroscopy provided confirmation of the polyaniline form synthesised. However, this technique measures bulk optical properties and could not contribute nanoscale suspension information.

Particle sizing and ζ -potential provided nanoscale information for each of the diluted polyaniline batches synthesised. This information was investigated for links to the quality and processability of the inks produced. Polyaniline nanoparticle sizes were firstly analysed using TEM at 100 kV and 15.5 k \times magnification. The nanoparticles were diluted in deionised water and imaged on a carbon grid (Fig. 3.4). The morphology of the nanoparticles was spherical but did appear to vary in size, ranging from 30 to 388 nm. The average particle size was 157 nm for batch 1.

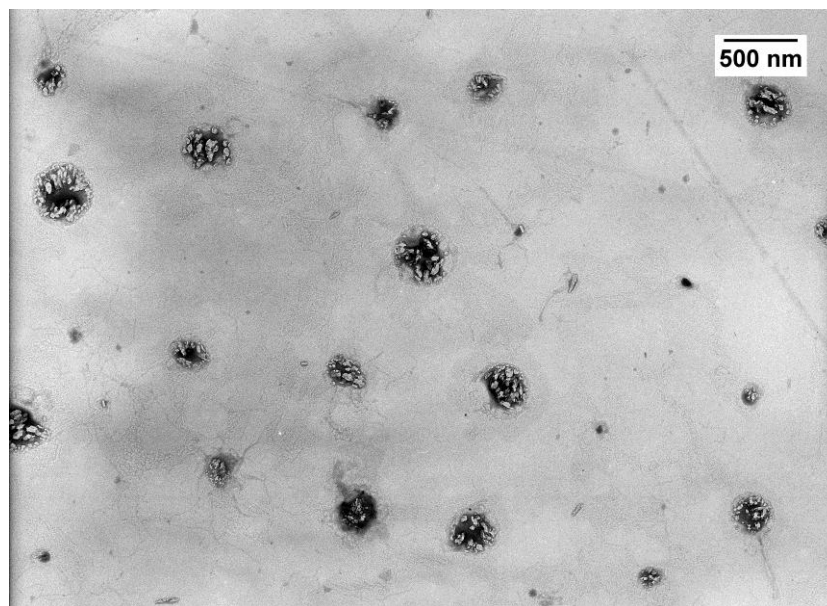


Figure 3.4. Transmission electron micrograph of diluted batch 1 polyaniline nanoparticles deposited onto a carbon grid and recorded at 100 kV and 15.5 k \times magnification.

The shape of the nanoparticles synthesised did appear to be similar to that reported for other polyaniline dispersions (Ngamna *et al.*, 2007, Han *et al.*, 2002, Moulton *et al.*, 2004, Morrin *et al.*, 2008). The quality of the images attained using TEM does not provide accurate or quantitative particle size information. Further particle size information was required to support the TEM results.

Particle size distribution using Dynamic Light Scattering (DLS) was carried out on the polyaniline nanoparticles. An example of the particle size distribution of a typical polyaniline batch can be seen in Fig. 3.5. A major distribution centred at approximately 77 nm and a smaller distribution at approximately 4800 nm was

observed. It can be seen that the majority of the dispersion was nanoparticulate with the second peak attributable to some aggregation of these nanoparticles.

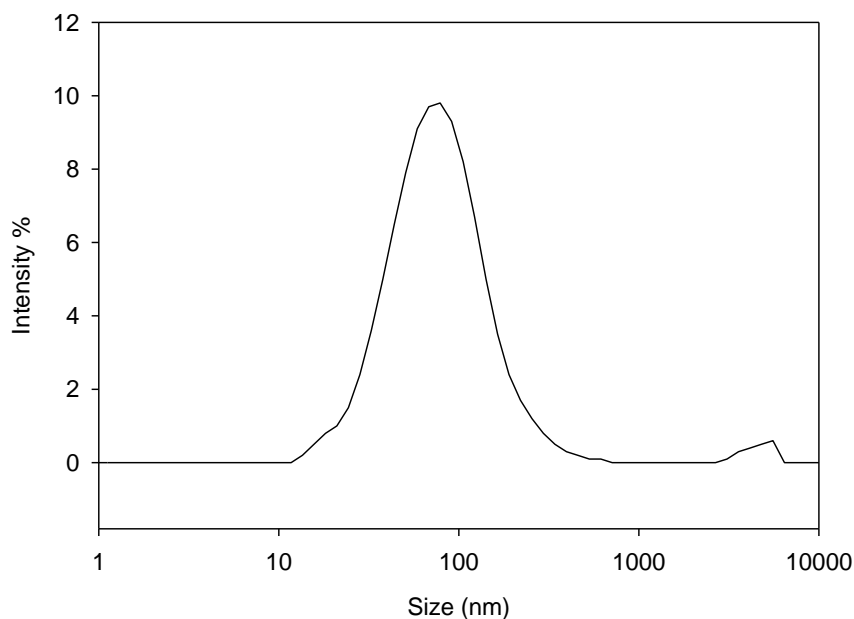


Figure 3.5. Size distribution of polyaniline nanodispersion batch 11 in deionised water. A major distribution can be seen for particles of 77 nm in diameter and a small distribution can be seen at 4800 nm.

The size of these nanoparticles was similar to the approximately 82 nm particle size reported for polyaniline dispersions generated by Ngamna *et al.* (2007). However, they are larger than those reported by Han *et al.* (2002) and Moulton *et al.* (2004) which were approximately 25 nm and 10 nm, respectively. The same synthesis methodology was used in all these studies. This suggests the micellar polymerisation is prone to particle size variations. In this study, each batch of polyaniline contained the same concentration of APS, DBSA and aniline and they were all treated in the same way. Thus, in theory the rate of the polymerisation reaction should have been similar. However, during the synthesis, temperature was difficult to control. According to the protocol produced by Ngamna *et al.* (2007) the temperature needed to be maintained at 20°C. It was difficult to achieve typical room temperature levels using a hot plate or a water bath and so it was decided that synthesis would take place at ambient temperature. Considering the variation due to time of day or season, the temperature would typically remain near 20°C in the absence of a reaction chamber. Sensitivity and activity and variability of reactive

reagents such as APS may also account for this variation which has also been seen in the literature.

The micellar synthesised polyaniline nanoparticles were inkjet-printed onto silver screen printed IDEs to produce polyaniline ammonia sensors. The impedimetric quality of these sensors was then assessed.

3.2.2. Screen printed silver interdigitated electrode design as part of the inkjet-printed polyaniline sensor

The IDE array design is one of the most common configurations in electroanalysis as it produces high currents from the redox cycling and feedback between the closely arranged interdigitated generators and collectors (Guajardo *et al.*, 2013). The currents generated between the interdigitates form dielectric fields which penetrate short depths (tens of nanometres) making them less dependent on cell geometry and allow the use of sensing layers for tailoring selectivity (de la Rica *et al.*, 2006). Polyaniline was synthesised into a nanoparticulate aqueous ink which was readily inkjet-printed as a thin film (~30 nm) (Morrin *et al.*, 2008). IDEs are compatible with thin films such as inkjet-printed polyaniline (Zaretsky *et al.*, 1988, Sheppard *et al.*, 1993). Thus, the IDE array design was chosen for the impedimetric measurement of ammonia using polyaniline. Silver was chosen as the electrode material, principally due to the combination of conductivity, chemical reactivity, printability and price. It has been used as a sensing material for gaseous ammonia determination, most commonly in the nanoparticulate form (Dubas and Pimpan, 2008). Silver nanoparticles have also been used as part of a composite for ammonia detection. Composite materials used in combination with silver nanoparticles include silicon (Guo and Tao, 2007), graphene oxide (Kavinkumar and Manivannan, 2016), pyrrole (Karmakar *et al.*, 2013) and polyaniline (Detsri and Popanyasak, 2015). The IDE was designed in a two-electrode configuration. A two electrode system facilitates a truly planar, solid-state configuration which is simpler to fabricate. In addition, the planar diffusion characteristics can be superior to bulk electrolytic devices, particularly for gas sensing (Mamishv *et al.*, 2004). The silver IDEs used in this study were fabricated using screen printing. Screen printing has been used as the basis of electrode sensors for more than 20 years (Weng *et al.*, 2010). It is a rapid and low cost way to mass produce highly reproducible electrodes for the

determination of a wide range of analytes (Wang, 1994). It provides a platform with broad applicability (Renedo *et al.*, 2007).

The screen printed electrodes fabricated during this study were modified with polyaniline nanoparticles via inkjet printing. Drop-on-demand piezoelectric inkjet printing has also displayed great promise in sensor development. In combination with conducting polymers it allows for the production of flexible electronics (Tekin *et al.*, 2008). Piezoelectric inkjet printing is a digital, non-contact printing technology that facilitates high resolution prints (Weng *et al.*, 2010). It is based on piezoelectric technology, involving the controlled ejection of pL volumes of ink from a micrometer-size nozzle via application of an electric field applied to a piezoelectric crystal (Magdassi, 2010, Magdassi and Ben Moshe, 2003) (Fig. 3.6). It has been shown to produce films with comparable conductivity and electroactivity to those electrochemically deposited (Morrin *et al.*, 2008). The modification of chemical polymerisation methods to produce nano-structured forms of polyaniline has allowed the deposition technique of inkjet printing to be explored (Ngamna *et al.*, 2007).

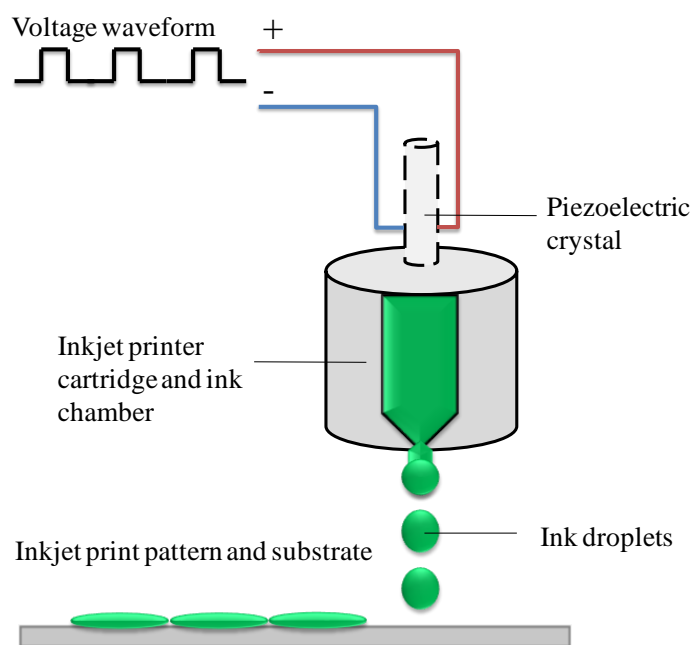


Figure 3.6. Principle of piezoelectric inkjet printing - the application of an electrical field in a waveform across the piezoelectric crystal causes its expansion to control the volume of ink being deposited onto the substrate.

3.2.3. Impedimetric assessment of polyaniline sensors

In electrochemical impedance spectroscopy, an ideal resistor will exhibit real impedance (Z') in the complex plane (Nyquist plot) equal in magnitude to the value of the resistance. It will have no imaginary impedance ($Z'' = 0$) and will have a constant absolute impedance (summation of resistive and capacitive properties, $|Z|$) at all frequencies, equal to the value of resistance. Phase angle (ϕ) will also be 0° at all frequencies. By contrast, a perfect capacitor will exhibit imaginary impedance with no real impedance components. It will display a $|Z|$ slope of -1 and a -90° phase shift at a frequency dependent on the magnitude of capacitance (Fernandez-Sanchez *et al.*, 2005). Combinations of resistors and capacitors in series and in parallel will exhibit more complex impedance characteristics.

Printed ammonia sensors were combined with a PTFE membrane and an o-ring spacer to allow solutions of ammonia to interact with the sensor. The sensors were assessed and optimised in response to these ammonia solutions using impedance spectroscopy. However, initial experiments were performed in air, which displayed both resistive and capacitive properties corresponding to the components that make up the sensor such as the IDE and the polyaniline layer. Impedance spectra were recorded in air across a frequency range of 0.1 Hz to 100 kHz at 5 mV rms. This can be observed in Fig. 3.7 represented by (a) Nyquist (insert displays the Nyquist plot on the same axis scale), Bode (b) modulus and (c) phase (ϕ) plots. The polyaniline sensor displayed a small capacitance ($-Z''$) value at approximately 20Ω and a series resistance (Z') offset value of 2980Ω . Thus, the polyaniline sensor displays predominantly resistive characteristics. This is evident from the Bode plots (b and c). At low frequencies $|Z|$ can be seen as a nearly straight line at 2980Ω and the phase angle was 0° . At high frequencies, capacitive properties of the polyaniline sensors were observed as a decrease in the total impedance from 2970 to 2951Ω , this was accompanied by a decrease in phase shift from 0° to -1.4° above 1 kHz.

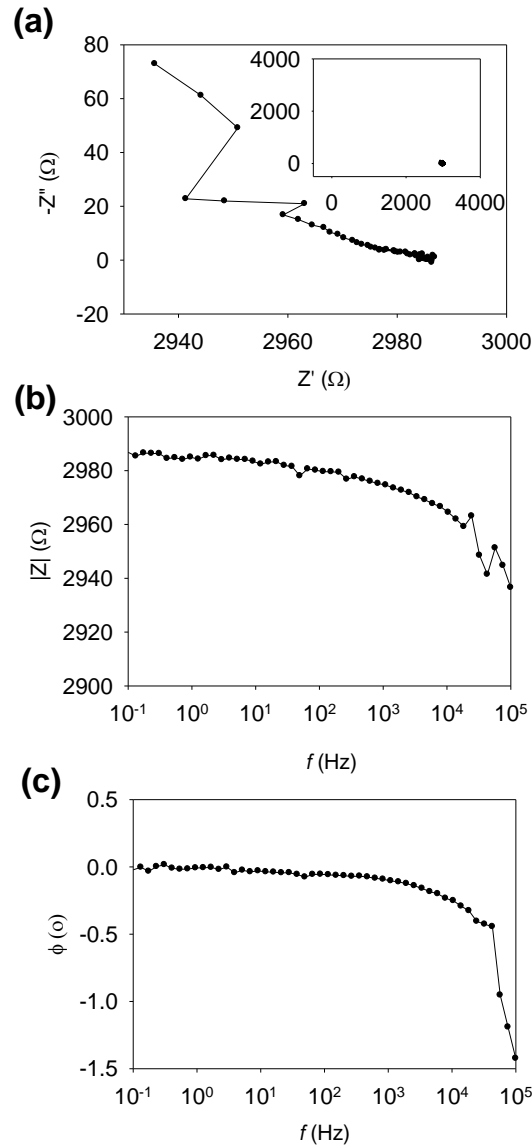


Figure 3.7. Impedance spectra of a polyaniline sensor in air, (a) Nyquist (insert displays the Nyquist plot on the same axis scale), Bode (b) modulus and (c) phase plots across a frequency range of 0.1 Hz to 100 kHz.

The characteristics of the printed polyaniline sensor were similar to results obtained by Hibbard *et al.* (2013b) which used a similar polyaniline sensor platform. They used a two-electrode gas phase set-up and observed almost identical behaviours. For example, a small capacitance up to 20 Ω and an offset resistance of 1 kHz for Nyquist data. Bode plots showed a decrease from the main resistance data which appeared as a straight line at 956 Ω $|Z|$ and 0° phase to 951 Ω $|Z|$ and -1.8° phase. The impedimetric data gathered in this study was also comparable to data collected by Kalaji and Peter (1991) in which polyaniline films were grown on

indium-doped tin oxide coated glass as part of a three-electrode cell containing redox active systems. For polyaniline films, the imaginary impedance was near 0Ω and resistance lay at approximately 10Ω on the Nyquist plots which displayed a typical arc (Kalaji and Peter, 1991).

An a.c. frequency of 1 kHz was chosen at which to probe the polyaniline film for resistive behaviour as the polyaniline becomes deprotonated by ammonia, forming the more stable ammonium ion and resulting in increased resistance within the polyaniline film (Kukla *et al.*, 1996). It is at this frequency that time-based measurements were carried out during this work. It is important to note that the polyaniline sensor acts as a bulk resistor in series with a negligible capacitance and the focus of the interaction with ammonia is on the polymer's deprotonation. Polyaniline has been widely used as a super-capacitor (Snook *et al.*, 2011). However, in the current context it appears to possess low capacitance. This is perhaps due to the nature of the films formed from the deposition of the doped polymer nanoparticles which may result in low surface concentration of charged sites within the polymer, leading to low capacitance (Hibbard *et al.*, 2013b).

The equivalent circuit of the polyaniline sensor was interpreted and drawn as shown in Fig. 3.8 (a). It was interpreted as a resistor in series with a parallel capacitor and resistor. These components represented the resistance of the IDEs and their connection with the polymer and the resistance and capacitance associated with the polymer. The polyaniline sensor was mapped using Nova 1.6 software and the equivalent circuit presented can be seen in Fig. 3.8 (b) represented by (i) Nyquist, Bode (ii) modulus and (iii) phase. The generated equivalent circuit may be compared to the impedance spectra of a polyaniline sensor in air (Fig. 3.7). in which the characteristics are similar. For example, both display small capacitance values of approximately 20Ω and a series resistance offset at 2980Ω for the experiment and 2033.5Ω for the equivalent circuit. Both display predominantly resistive characteristics which can be seen as a straight line at 2033.5Ω and a shift from 0° to 0.8° in the Bode plots of the equivalent circuit and a nearly straight line at 2980Ω and a shift from 0° to -1.4° in the Bode plots of the polyaniline sensor in air impedance spectra.

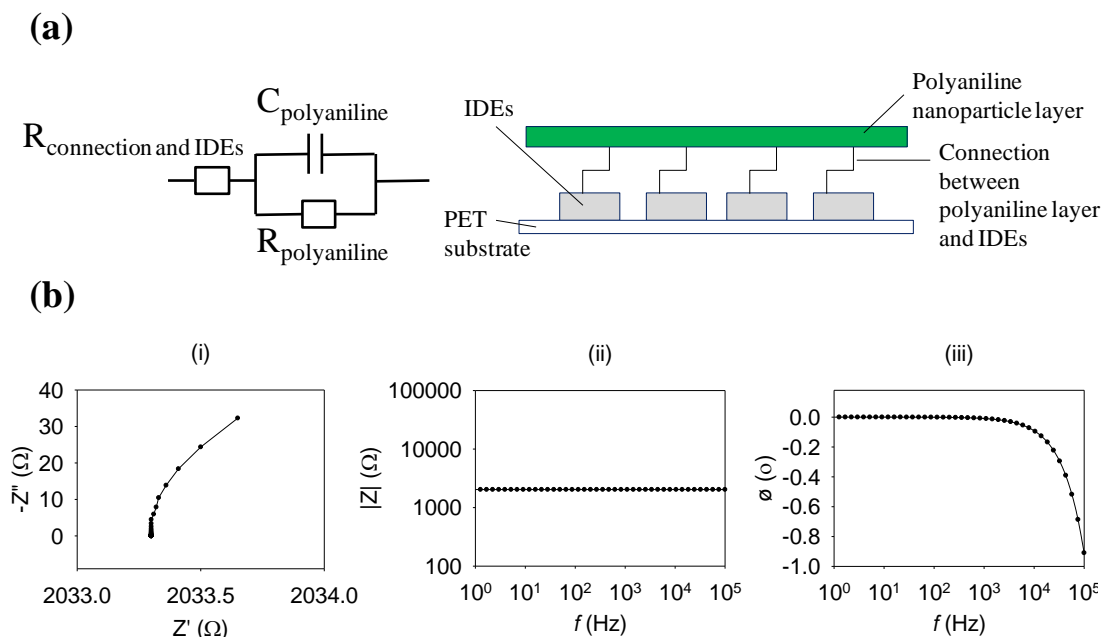


Figure 3.8. (a) Interpretation of the equivalent circuit of a polyaniline sensor and (b) the mapped equivalent circuit of the polyaniline sensor using Nova 1.6 software including (i) Nyquist, Bode (ii) modulus and (iii) phase.

3.2.4. Impact of the synthesis method on particle size and its effect on sensor impedance

The purpose of the polyaniline nanoparticles synthesised in this study was to be used as inkjet-printed semi-conductive sensing films. It was hypothesised that nanoparticle size may affect the impedance of the printed sensors. In order to investigate this, polyaniline batches with an associated particle size were inkjet-printed onto silver IDEs and analysed impedimetrically. Ten layers of polyaniline nanoparticles were inkjet-printed at a voltage of 18 V at room temperature. Fig. 3.9 shows the relationship between $|Z|$ in air versus particle size for five polyaniline batches. Average particle sizes of these five polyaniline batches ranged from 77 to 412 nm. There was no significant difference in the impedances of the films with respect to particle size. Indeed, other factors appear to contribute more to variations in impedance than particle size.

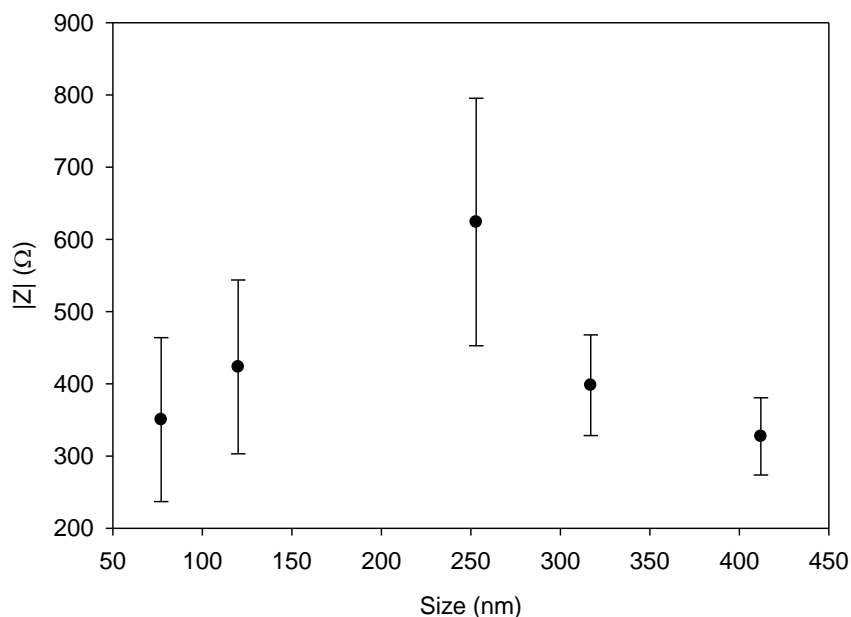


Figure 3.9. Polyaniline nanoparticle size (nm) versus inkjet-printed film absolute impedance $|Z|$ for five synthesised batches, $n = 4, 11, 6, 9, 6$ from left to right, respectively.

The relationship between particle size and polydispersity index (PDI) was also investigated. Polydispersity is a measure of the distribution of molecular mass throughout a sample. It is calculated using the PDI. For a given polymer sample the PDI is defined as the ratio of the weight average molar mass (M_w) to its number average molar mass (M_n) (Vieville *et al.*, 2011). Malvern DLS software system of the DLS instrument performed this calculation as a dimensionless measure of the broadness of the size distribution calculated from cumulant analysis of the Gaussian distribution related to standard deviation (SD) and the average diameter (Zd) of the particle size (Malvern Instruments Ltd., 2016), according to Eq. 3.2.

$$PDI = \frac{SD^2}{Zd^2} \quad \text{Eq. 3.2}$$

Acquired PDI values greater than 1 are typically too polydisperse for DLS analysis, with values less than 0.05 being regarded as monodisperse. It can be seen in Fig. 3.10 that the PDI of a number of polyaniline batches had a positive correlation with particle size, demonstrating that an increase in particle size was also accompanied by an increase in polydispersity.

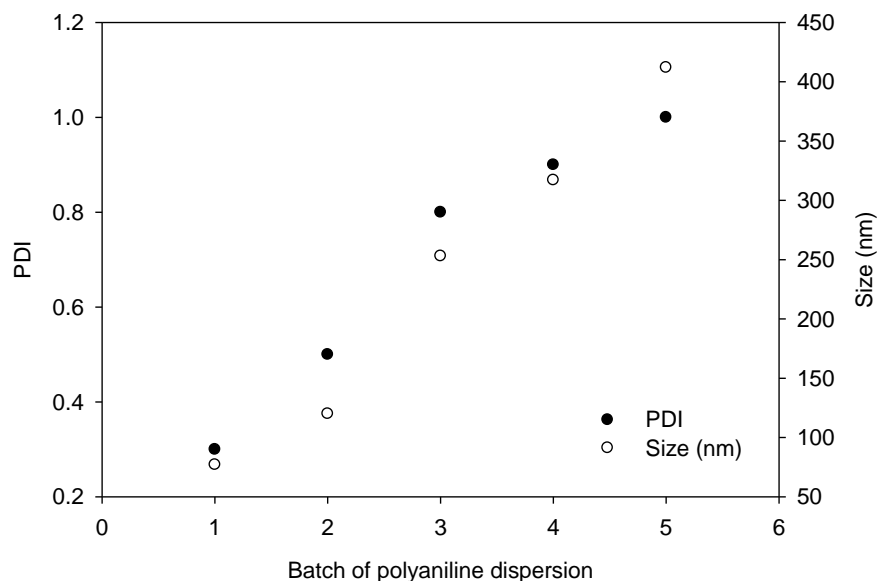


Figure 3.10. The relationship between polyaniline nanoparticle size (nm) and polydispersity of five synthesised batches of polyaniline nanoparticles.

It has been shown that inkjet-printed polyaniline nanoparticles form a homogenous semi-conductive film (Morrin *et al.*, 2008). This happens during the process of inkjet printing. As the printer ejects pL volumes of polyaniline nanodispersions onto the electrode, the micellar structure of the individual nanoparticles are disturbed. They coalesce to form a homogeneous film, which may be reinforced when the sensors are rinsed and cured. It can be concluded that impedance is independent of nanoparticle size as the particles lose all shape and merge into one homogeneous film.

3.2.5. Impact of the synthesis method on zeta-potential and its effect on sensor impedance

As discussed in Chapter 1, Section 1.2.2, polyaniline in the emeraldine salt form is doped to incorporate more protons, producing a positive surface charge (de Medeiros *et al.*, 2003). In 2002, when the micellar emulsion synthesis method was developed, it employed APS as an initiator and DBSA as a surfactant which produced micelles around which aniline was polymerised (Han *et al.*, 2002). The synthesised polyaniline acquired a negative charge which corresponds to the formation of the DBSA micelle (Kirby and Hasselbrink, 2004). This negative charge interacts with the dispersion, which aids in the maintenance of the particles in suspension. The distribution of charge between the particle surface and the solution

is known as the ζ -potential, and is described for nanoparticles in suspension as the electrostatic surface potential of the particles. It is highly dependent on the nature of the solvent in which they are suspended (Doane *et al.*, 2012). The ζ -potential value of a particular dispersion will also relate to how stable the dispersion is likely to be. A ζ -potential value of ± 30 mV and above is associated with a stable colloidal suspension, while any value below this is considered unstable (Malvern Instruments Ltd., 2016, Müller, 1996). This value will vary depending on the dispersion used (Vallar *et al.*, 1999). For the eleven batches of polyaniline nanoparticles synthesised during this study, ζ -potential varied greatly (Table 3.1).

Table 3.1. ζ -potential values for polyaniline nanoparticle dispersions.

Batch number	1	2	3	4	5	6	7	8	9	10	11
ζ-potential (mV)	-48	-1	-40	-45	-2	-2	-6	-1	-7	-33	-9

To date the effect of the ζ -potential of the polyaniline nanodispersions on the impedimetric performance of the sensors has not been investigated. It has been shown that changes in ζ -potential may occur by altering pH, salt and surfactant concentrations (Micheau *et al.*, 2013). SDS is an anionic surfactant which is able to disperse organic materials by adsorption in high concentrations of aqueous solutions (White *et al.*, 2007). Anionic surfactants impart a negative charge, creating repulsion between surfactant molecules which further stabilises the dispersion. SDS was used during the synthesis process of polyaniline nanoparticles, dispersions were dialysed against 0.05 M SDS for 48 hr. Thus, rather than being a simple monodispersion of DBSA-polyaniline nanoparticle in water, it is a more complex co-colloidal suspension of DBSA-polyaniline and SDS micelles. Therefore, it is not immediately possible to measure a ζ -potential of the DBSA-polyaniline alone, or in a manner that reflects the actual ink formulation. To observe the impact SDS had on DBSA-polyaniline, dispersions were dialysed against 0.01, 0.05 and 0.1 M SDS and the resulting impact on ζ -potential and conductivity was assessed (Fig. 3.11). Increasing SDS concentration caused an increase in negative ζ -potential from -1.56 to -5.59 mV

for 0.01 to 0.1 M SDS. The conductivity of the dispersion increased with increasing SDS concentration from 0.005 to 0.016 mS cm⁻¹ for 0.01 to 0.1 M SDS.

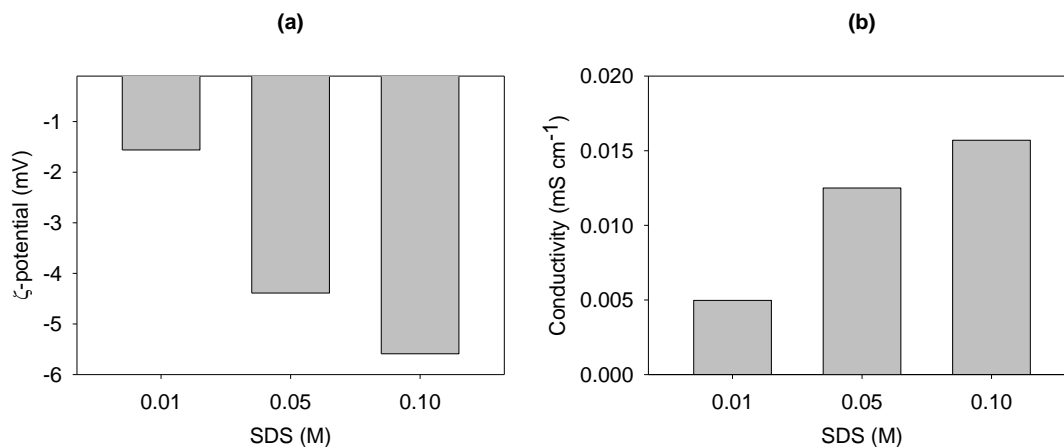


Figure 3.11. Relationship between (a) ζ -potential and (b) conductivity with increasing SDS concentration.

In order for a conclusion to be reached in relation to SDS concentrations, further analysis is required on numerous batches of polyaniline nanoparticles. To assess the relationship between ζ -potential and the impedimetric properties of the polyaniline sensors, batches of polyaniline nanoparticles with different ζ -potentials were impedimetrically measured at 1 kHz in air. Fig. 3.12 shows the relationship between ζ -potential and $|Z|$ of the sensors associated with five batches of polyaniline. The $|Z|$ for these five batches decreased from 660 to 320 Ω with decreasing ζ -potential. While the use of ζ -potential can be an excellent predictor of the stability of colloidal suspensions, its value and usefulness here is not clear. While we have seen large variation in ζ -potential values, this has been in dilute aqueous solutions which do not reflect the actual character of the ink. Significant experience has demonstrated good stability of the SDS co-colloidal suspensions, and so, in this form, the measurement of ζ -potential may be ineffective and irrelevant.

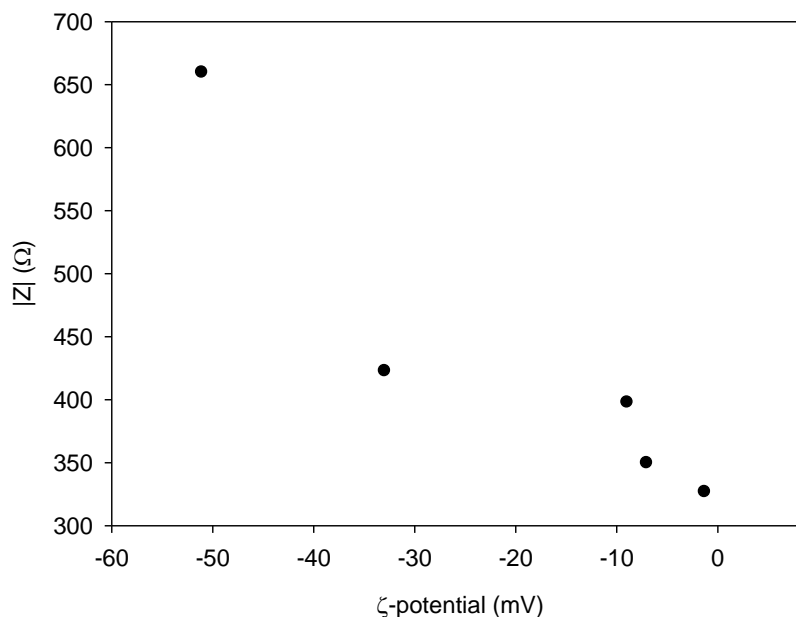


Figure 3.12. The relationship between zeta (ζ)-potential and absolute sensor impedance $|Z|$ of four batches of polyaniline.

3.2.6. Characterisation of the ammonia sensor in response to liquid samples

The development of a blood ammonia sensor system that could detect gaseous ammonia produced from a liquid sample, such as blood was a technical challenge. Ammonia has been measured amperometrically using polyaniline-based sensors (Trojanowicz *et al.*, 1997, Crowley *et al.*, 2008b, Basak *et al.*, 2013). However, this results in current transients which require regeneration of the sensor in buffer, making it unsuitable for direct and continuous contact measurement. Conductivity measurements have been used for continuous monitoring of ammonia using polyaniline sensors (Crowley *et al.*, 2008a, Sutar *et al.*, 2007, Matsuguchi and Asahi, 2011, Stamenov *et al.*, 2012, Wongchoosuk *et al.*, 2012). Conductimetry cannot be performed in direct contact with liquid samples. Although POC testing is not typically continuous, the sample is typically applied directly onto the sensor system. In addition, direct current conductimetry requires the application of a potential which may result in unwanted redox processes and oxidative degradation. While d.c. conductimetry requires the application of a bias potential, ac impedance methods apply a very small a.c. waveform which maintains the material at an average zero potential (Rheume and Pisano, 2011). Impedance has been used to measure the interaction between polyaniline and ammonia (Hibbard *et al.*, 2013a, Subramanian *et al.*, 2013, Basak *et al.*, 2013).

3.2.6.1. The use of a hydrophobic membrane for ammonia gas measurement from a liquid sample

Hydrophobic separation membranes have been used for a long time for the determination of ammonia amongst ammonium ions in solution (Willason and Johnson, 1986). PTFE is a hydrophobic membrane which is impermeable to water but which is permeable to gas (Tarsiche *et al.*, 1997). It is widely used in many applications due to its excellent chemical stability (90-95%) and high melting point of 327°C (Wikol *et al.*, 2007). A SEM of a PTFE membrane with pore size of 0.2 µm can be seen in Fig.3.13.

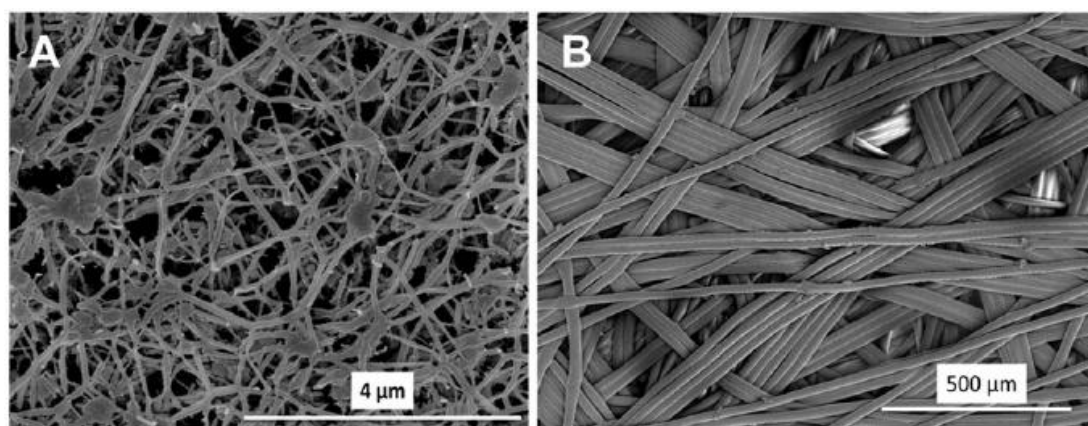


Figure 3.13. Scanning electron micrograph of a Whatman® PTFE membrane filter, (A) 0.2 µm pore size of PTFE active layer (B) support polypropylene layer. Reproduced with permission from Elsevier (Fard *et al.*, 2015).

Ammonia has a high diffusion coefficient of $0.2 \text{ cm}^2 \text{ s}^{-1}$ at room temperature (Massman, 1998) and therefore is expected to pass through the PTFE membrane at a very fast rate. A PTFE membrane has previously been employed by Subramanian *et al.* (2013) for the determination of ammonia in an aqueous secondary refrigerant system. The determination was carried out using polyaniline-modified IDEs in combination with impedance spectroscopy which could not be in direct contact with a liquid. Aqueous measurements were achieved using a PTFE membrane which also allowed gaseous ammonia diffusion whilst preventing liquid from passing through and affecting the analysis. In this way, the membrane serves as a physical support for the liquid-gas interface and does not allow one phase to enter another (Chiam and Sarbatly, 2013). The three phase system works on the basis that ammonia in solution ($\text{NH}_4^+_{(\text{aq})}$) and ($\text{NH}_{3(\text{aq})}$) establishes equilibrium with ammonia in the gas phase

($\text{NH}_3(\text{g})$) and which in turn establishes equilibrium of ammonia in the conducting polymer film.



In this way, direct and continuous measurements of a liquid sample could be made using the change in conductance of the polymer film in response to ammonia. A similar set-up was developed here to assess the polyaniline sensor in response to ammonia. This set-up comprised of the polyaniline sensor upon which a PTFE membrane was suspended 1.78 mm above using a rubber o-ring. Ammonia as ammonium chloride in PBS pH 7.4 was placed on the PTFE membrane and a lid fixed on top creating a sample chamber in which 52 μL of sample was analysed.

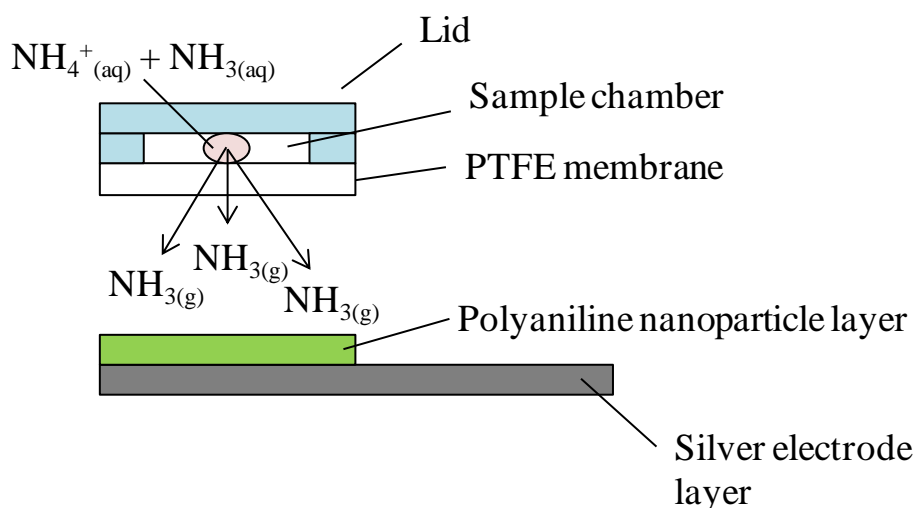


Figure 3.14. Schematic of the aqueous ammonia set-up. Gaseous ammonia ($\text{NH}_3(\text{g})$) from an aqueous sample ($\text{NH}_4^+(\text{aq})$ and $\text{NH}_3(\text{aq})$) diffuses through a PTFE membrane and interacts with the polyaniline sensor.

The ammonia probe developed by Subramanian *et al.* (2013) had a headspace distance of 6 mm and a volume of 1.134 cm^3 . The volume of the refrigerant test system was 220 mL and was under circulation. In the current work, the device was being developed for measurement of ammonia in a drop of blood (52 μL). In comparison to Subramanian *et al.* (2013), the analyte mass transport and mass characteristics of the current work were much less favourable, representing an available analyte mass of only 1/5,000th that available to Subramanian *et al.* (2013), while also being under static fluidic conditions.

3.2.6.2. Ammonia sensor reproducibility and drift

Sensor reproducibility and drift were investigated prior to ammonia measurements. This was carried out using time-based impedimetric experiments on 15 screen printed electrodes modified with ten layers of inkjet-printed polyaniline at 18 V. Sensors were examined at 1 kHz at 5 mV amplitude and a 1 s sampling rate over a period of 160 s ($n = 15$) in air. The recorded impedances consisted of 160 data points and were analysed for inter and intra-sensor differences (Fig. 3.15). Although all 15 sensors were printed in a single batch and measured consecutively, they exhibited variations in $|Z|$. Inter-sensor $|Z|$ ranged from 354 to 466 Ω . This corresponds to an inter-sensor baseline mean, standard deviation and RSD of 390.5 Ω , 26.9 Ω and 6.9% respectively. All 15 sensors displayed stable responses in air for the duration of the baseline measurements. The intra-sensor mean drift for all 15 sensors was 0.4 Ω , the SD and RSD was 0.1 Ω and 25%, respectively. The complete data set for the 15 sensors is listed in Appendix I.

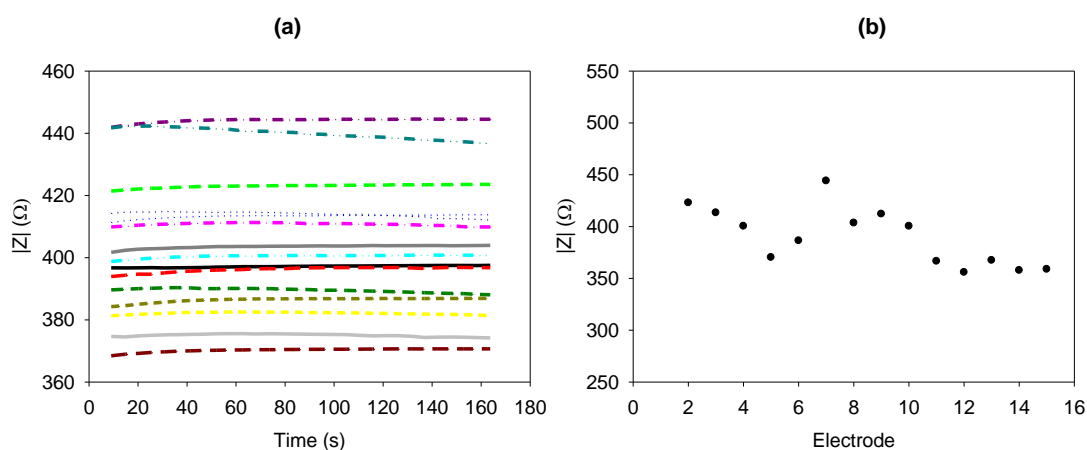


Figure 3.15. (a) Baseline absolute impedance of polyaniline sensors ($n = 15$) at 1 kHz and amplitude of 5 mV for 160 s. (b) Variation in average baseline of 15 inkjet-printed polyaniline layered sensors at 1 kHz frequency, ranging from to 354 to 466 Ω , 6.9% RSD.

Variability in sensor impedance may be due to the variations in the inkjet printing process. For example, material in-homogeneity and/or nozzle blockages during deposition of the ten print layers may result in the observed variations. Inkjet-printed polyaniline ammonia sensors have been fabricated previously with 33% RSD (Hibbard *et al.*, 2013b). This value is 4.8 fold higher than that reported in this work (6.9%). For comparison, commercial companies typically have a RSD of 3 to 5%

(DropSens, 2015a). To compensate for variation in baseline impedances of printed sensors, a ratiometric method has been employed by Hibbard *et al.* (2013b). This method was established based on initial sensor baseline in air (Z_{air}) and the response of the sensor to ammonia (Z). Each individual sensor response was normalised (Z/Z_{air}) with respect to its initial baseline (Z_{air}) and its response to ammonia (Z). It was found that the sensors maintained a constant sensitivity to ammonia when measured in this manner. This method was also adopted throughout this work to compensate for changes in initial sensor (baseline) impedance.

3.2.6.3. Investigation of the polyaniline nanoparticle inkjet printing process on the characterisation and performance of the ammonia sensor

To investigate the effect of the mass of polyaniline deposited during inkjet printing on the characteristics of the sensor, the inkjet printing process was examined. Studies were carried out to determine the optimum printing nozzle voltage and number of inkjet-printed polyaniline layers for ammonia measurement. The process of ink deposition via piezoelectric inkjet printing may be controlled using nozzle voltage. When a drop is ejected from a cartridge nozzle, it leaves with a trailing ligament attached. This ligament is reduced when the nozzle voltage is decreased as the drop falls in its entirety from the cartridge and onto the substrate (Fujifilm Dimatix, 2010). The voltage felt across the drop affects the velocity and mass (Tekin *et al.*, 2008, Saunders *et al.*, 2008). When choosing a drop volume and print number it is important to consider drop splashing and fingering which may occur as a drop with a particular velocity lands on a substrate (Magdassi, 2010).

The Fujifilm Dimatix Inkjet printer has a patterning and firing mode that may be used to deposit materials (Fujifilm Dimatix, 2010). The patterning mode permits printing based on a pre-defined, customized pattern. Herein this case, the material can be deposited layer-by-layer. The firing mode consists of ejecting material at a fixed position. Although this mode does not allow pattern formation, it does allow volume calculations. It may be used to calculate the drop volume, simply by weighing the substrate before and after the deposition of a certain amount of drops and approximating the material density to that of water (1 g ml^{-1}). It is known that nozzle voltage alters the volume of ink deposited. Therefore, nozzle voltage may have an impact on the behaviour of the sensors to the measurement of ammonia. In

order to investigate this, polyaniline nanoparticles were inkjet-printed onto pre-weighed substrates for 60 s at 5 kHz frequency using a range of nozzle voltages. From the literature polyaniline nanoparticles have been inkjet-printed at 16 V (Crowley *et al.*, 2008b, Suman *et al.*, 2011) and 26 V (Hibbard *et al.*, 2013b). Consequently, a nozzle voltage range of 14 to 30 V was studied. The number of drops was estimated to be 1.2×10^6 by multiplying the ejection time (t_e) by the frequency (f) and by the number of working nozzles which was 4, according to Eq. 3.4 (Fujifilm Dimatix, 2010). The drop mass was then calculated by dividing the mass of solution ejected by the number of drops, according to Eq. 3.5 (Fujifilm Dimatix, 2010).

$$N^{\circ} \text{drops} = t_e f N^{\circ} \text{nozzles} \quad \text{Eq. 3.4}$$

$$m = \frac{m_i - m_f}{N^{\circ} \text{drops}} \quad \text{Eq. 3.5}$$

For the 14 mm inkjet pattern using a 20 μm drop spacing there were an estimated 4.9×10^5 drops being ejected at 18 V which was calculated as 2.24×10^{-7} L in one print layer. The results for drops mass and volume of polyaniline deposited for a range of nozzle voltages (14, 18, 22, 26, 30 V) are shown in Table 3.2.

Table 3.2. Inkjet-printed drop mass calculated for a range of nozzle voltages.

Nozzle voltage (V)	Mass of polyaniline (g)	Drop mass (g)	Volume (L) for 10 print layers
14	4.0×10^{-4}	3.33×10^{-10}	1.63×10^{-6}
18	5.0×10^{-4}	4.58×10^{-10}	2.24×10^{-6}
22	8.0×10^{-4}	6.67×10^{-10}	3.27×10^{-6}
26	1.1×10^{-3}	6.67×10^{-10}	3.27×10^{-6}
30	1.0×10^{-3}	7.92×10^{-10}	3.88×10^{-6}

The plot of drop mass versus nozzle voltage for the inkjet printing process is illustrated in Fig. 3.16. Drop mass was seen to increase with nozzle voltage in a linear fashion. Increased nozzle voltages generated polyaniline inkjet drops of a larger mass and velocity. These results were in agreement with those produced by

the manufacturer's technical notes (Fujifilm Dimatix, 2010). For example, the drop mass of polyaniline obtained by applying 30 V for 60 s at 5 kHz using 4 nozzles was 7.92×10^{-10} g, which was nearly two-fold higher than that achieved applying 14 V which was 3.33×10^{-10} g.

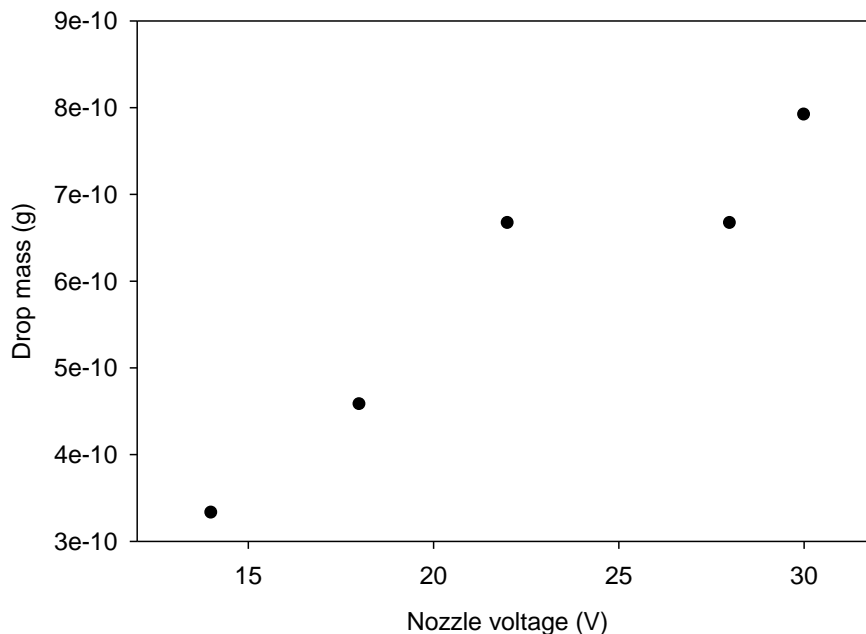


Figure 3.16. Drop mass versus nozzle voltage applied during the inkjet printing process of polyaniline nanodispersions. Ink ejection was carried out using 4 working nozzles for 60 s at 5 kHz frequency.

Fig. 3.16 shows the relationship between nozzle voltage and mass of ink deposited. The relationship between mass deposited (as nozzle voltage) and sensor response to ammonia was also studied. This was conducted using ten inkjet-print layer polyaniline sensors. Fig. 3.17 illustrates the effect of varied nozzle voltage on the 1 mM ammonia ratiometric response of polyaniline sensors ($n = 2$). There was a non-linear relationship between nozzle voltage and impedimetric sensor response to ammonia. However, increased sensitivity to ammonia was observed with decreasing nozzle voltage. This decreased up to the application of 22 V where a saturation point was seen and the sensors possess invariable response ammonia at higher nozzle voltages (and therefore higher deposited mass of polyaniline). This can be seen in the normalised plot but also in the separated absolute impedance data for polyaniline sensors in air and upon exposure to ammonia (Fig 3.17 insert). While at 14 V, the impedance in air was significantly higher than at higher nozzle voltages (and deposition volume), the response to ammonia was proportionately greater than at the

higher voltages. While 14 V gave the highest response to ammonia, reproducibility was 7.9% RSD, while at 18V it was 0.9%. While thinner films deposited at lower voltages appear to have greater sensitivity, they may be more variable in their conductivity as they are at the borderline of confluence, while at 18 V, films are sufficiently confluent to ensure reproducible behaviour (Morrin *et al.*, 2008). It can be seen that 18 V gave the highest and most reproducible response (RSD = 0.9%) to 1 mM ammonia, although 14 V did give a better response it was less reproducible (RSD = 7.9%).

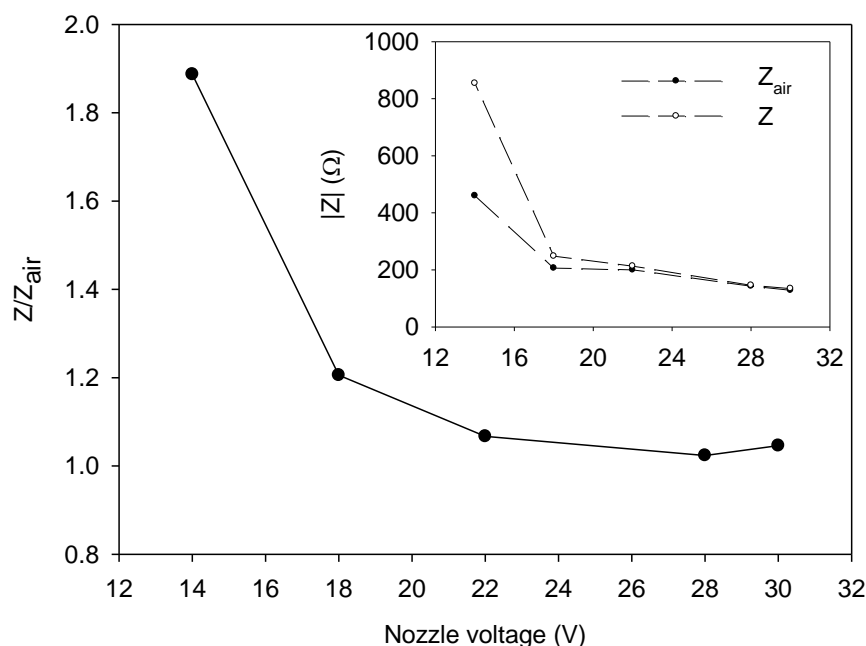


Figure 3.17. Mean impedimetric response of ten inkjet-print polyaniline layered modified electrodes with varying voltages in response to 1 mM ammonia exposure to at a frequency of 1 kHz ($n = 2$). The insertion plots the separated ratiometric data as initial electrode baselines in air (Z_{air}) and after ammonia exposure (Z).

In conclusion, for lower inkjet printer nozzle voltage and therefore for thinner polymer films, the response of the sensors to ammonia was higher. This may be due to the relationship between gas diffusion characteristics through the film and the thickness of the electrical field layer of the IDEs. Thinner films of polyaniline allow more effective diffusion of ammonia to layers of polyaniline which are within the electrical field. However, thin films may not produce continuous, confluent film

which explains the increase in variability between sensors. Baseline impedance is also higher for thinner films which may also be due to this lack of confluence.

An inkjet printer nozzle voltage of 18 V was used throughout the rest of the study as it deposited an appropriate drop volume creating a film with the best balance between sensitivity and reproducibility. Ten inkjet-print layers was used to study nozzle voltages, as it was used in recent published work by our group for the determination of ammonia in breath (Hibbard *et al.*, 2013a). However, there are reports in the literature which utilise a single inkjet-print layer of polyaniline nanodispersion for the determination of urea in serum (Suman *et al.*, 2011). Eight inkjet-print layers have also been reported for use in an aqueous ammonia sensing system (Crowley *et al.*, 2008b). In order to validate the choice in number of layers, a range of layers were deposited and studied for their response to aqueous ammonia. Using nozzle voltages of 18 V, sensors with a range of printed layers (0, 5, 10, 20 and 40 layers) were fabricated and exposed to 1 mM ammonia and assessed using impedance spectroscopy at 1 kHz. It can be seen from Fig. 3.18 that 40 print layers which corresponded to a polyaniline volume of 8.96×10^{-6} L, displayed reproducible responses to 1 mM ammonia with a RSD of 1.9%. A single inkjet-print polyaniline layer, which is the equivalent of 2.24×10^{-7} L, showed the greatest ratiometric impedance response. However, it was not reproducible with a RSD of 38.8%. The impedimetric baseline of the devices (Z_{air}) did decrease with increased polyaniline mass (Fig. 3.18 insert). The major contribution to the overall sensitivity of the device was observed subsequent to ammonia exposure (Z) which also decreased with increased polyaniline mass. There was little difference in the RSD between 5 and 10 (10.1 and 8.7% respectively) inkjet-print layers. Ten inkjet-printed layers (2.24×10^{-6} L), was chosen as the most favourable number of layers for sensor fabrication as it exhibited marginally better reproducibility. Detailed statistical information is provided in Appendix II.

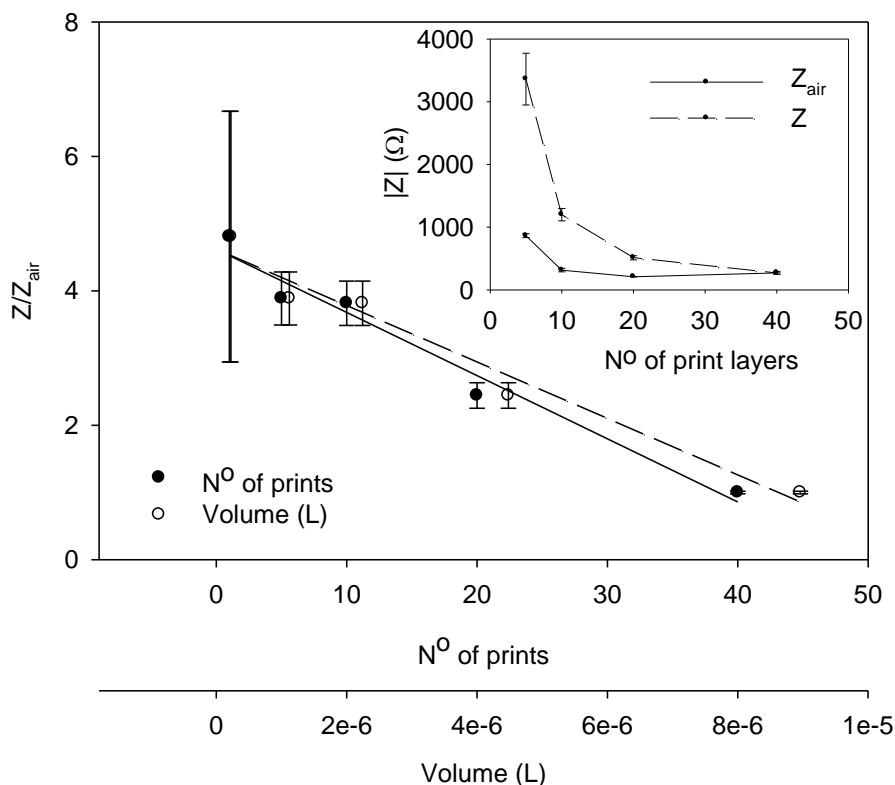


Figure 3.18. Impedimetric response of inkjet-printed polyaniline sensors ($n = 3$) with varying number of prints (1 to 40 layers) to 1 mM ammonia exposure at 1 kHz. The insertion plots the separated ratiometric data as initial electrode baselines in air (Z_{air}) and after ammonia exposure (Z).

Low volumes of material inkjet-printed onto the electrodes resulted in higher ratiometric responses to ammonia, which was consistent with the previous findings. Again, this response was not reproducible which is most likely due to the lack of confluence of the polyaniline film resulting in increased and variable film resistance. This is comparable with the work carried out by Morrin *et al.* (2008), who observed film heterogeneity and lack of confluence at low numbers of prints. The kinetic parameters of a sensor are affected by the diffusion of the gas molecules into the polyaniline film. Thus, decreasing the polyaniline film thickness is known to increase sensitivity of the sensor (Kukla *et al.*, 1996). Diffusion of ammonia through the polyaniline film is restricted by large layering of material deposited on the electrode. Ten layers were considered an appropriate balance between achieving sensor reproducibility, while maximising sensitivity.

In conclusion, it was decided that a nozzle voltage of 18 V and a print number of 10 inkjet layers was optimum for further ammonia sensor production. The volume of material deposited and the time constraints for manufacturing a mass producible sensor were also considered in the selection of these parameters.

3.2.7. Electrochemical characterisation of inkjet-printed polyaniline films

The optimised inkjet-printed polyaniline films were also studied using cyclic voltammetry (CV). This was carried out to corroborate the impedimetric characterisation of the polyaniline nanodispersion. Initially CVs were performed on polyaniline films obtained by drop casting 7 μL of the polymer dispersion onto GCEs (as inkjet printing onto GCEs was not possible) and cycled in 1 M HCl at a scan rate of 0.1 V s^{-1} vs. Ag/AgCl. The CV in Fig. 3.17 shows typical polyaniline redox electrochemistry obtained using the DBSA-polyaniline nanodispersion (Wallace *et al.*, 2002). On the oxidative sweep, the peaks correspond to the transformation of leucoemeraldine base to emeraldine salt at approximately 0.23 V and from emeraldine salt to pernigraniline at approximately 0.78 V. On the reduction scan the peaks correspond to the conversion of pernigraniline to emeraldine salt at 0.75 V and from emeraldine salt to leucoemeraldine at 0.08 V. The peaks in between are associated with the transformation of *p*-benzoquinone and hydroquinone as side products upon cycling to high oxidative potentials necessary to observe the transition (Mirmohseni and Wallace, 2003).

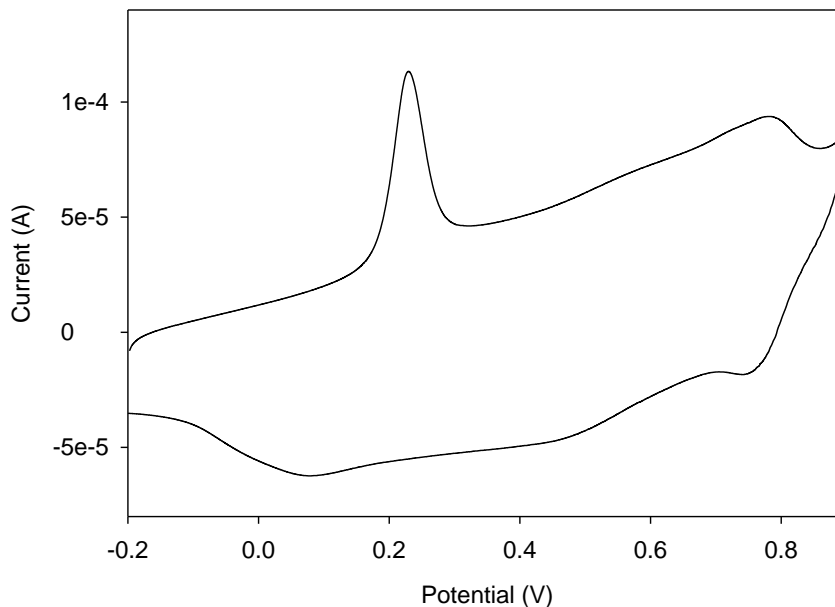


Figure 3.19. Cyclic voltammogram of a polyaniline nanodispersion drop cast onto a glassy carbon electrode and cycled in 1 M HCl at a scan rate of 0.1 V s^{-1} from -0.2 to $0.9 \text{ V vs. Ag/AgCl}$.

The CV observed in this study was very similar to that obtained by Ngamna *et al.* (2007) for a polyaniline nanodispersion cast on GCE and cycled at a scan rate of 0.1 V s^{-1} . They observed peak potentials in the same region. However, peak currents in that study were ten-fold greater than those observed here (Ngamna *et al.*, 2007) and may relate to the amount of material deposited.

In order to characterise inkjet-printed polyaniline films, polyaniline nanodispersions were deposited onto carbon screen printed electrodes supplied by DropSens, Spain. The DropSens electrodes were obtained because they were reproducible enough to ensure no interference relating to the screen print production was observed on the cyclic voltammograms. These electrodes had a 4 mm diameter carbon working electrode, carbon counter electrode and silver reference electrode (DropSens, 2015c). A number of polyaniline layers (0, 1, 5, 10, 15, 20, 30, 40) were inkjet-printed onto the DropSens electrodes and were cycled in 1 M HCl at a scan rate of 0.1 V s^{-1} from -0.2 to $0.9 \text{ V vs. Ag/AgCl}$. The peak which can be seen at approximately 0.2 V in Fig. 3.20 (a) is typical of the emeraldine salt form of polyaniline as seen when polyaniline was drop cast onto GCEs in Fig. 3.19. The emeraldine salt peak is clearly defined at approximately 0.2 V in both instances.

Peak current was then plotted against inkjet-print layer; see Fig. 3.20 (b). A near linear relationship was observed between the peak current and the number of prints deposited onto the electrode. Comparing this data to that of Fig. 3.19 where the polymer was drop-cast onto GCE which is the equivalent of 31 inkjet-printed polyaniline layers as per the drop calculation (Table 3.2). This produced a current of 1×10^{-4} A. This is comparable when 35 layers were inkjet-printed onto DropSens screen printed electrodes which also produced a current of 1×10^{-4} A.

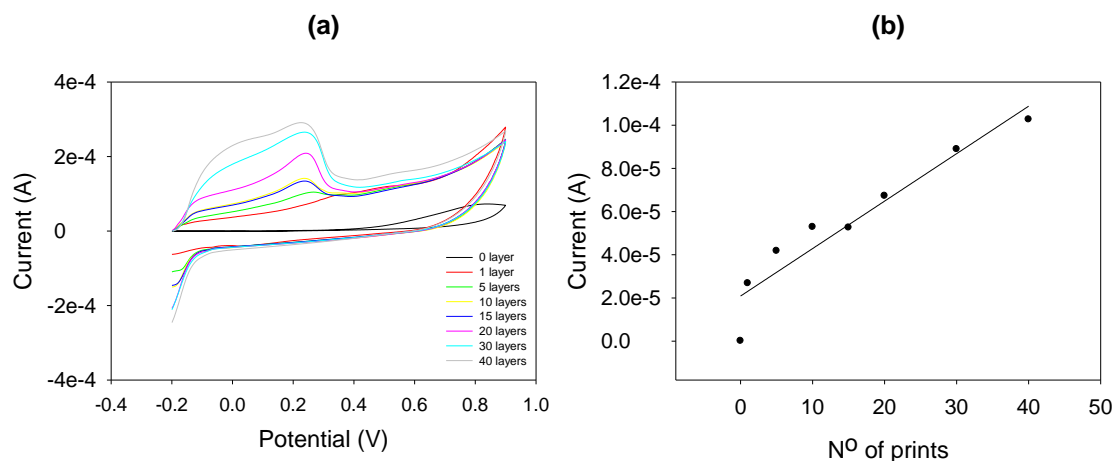


Figure 3.20. Cyclic voltammogram of 0 to 40 layers inkjet-printed polyaniline modified DropSens screen printed carbon electrodes in 1 M HCl at a scan rate of 0.1 V s^{-1} from -0.2 to 0.9 V vs. Ag/AgCl. The voltammetric peak current at 0.2 V was then plotted against increasing inkjet-printed polyaniline layers.

The data gathered here is comparable with the manufacturers technical note in which DropSens available carbon screen printed electrodes modified with polyaniline (DropSens, 2015b) were assessed. The peak voltage appear in the same region (approximately 0.3 V), however the peak currents in the technical note were lower (1.1×10^{-5} A) than those obtained during this study (2.2×10^{-4} A).

It has been seen by Morrin *et al.* (2008) that increasing the number of layers (and therefore thickness) varies the charge held within the film. Layer thickness was also studied using SEM. Fig. 3.21 (a) shows the typical morphology of a bare silver electrode being a grainy, coarse bright surface imaged using the backscattered electron detector (BSE). Fig. 3.21 (b), (c), (d) and (e) show 5, 10, 20 and 40 layers respectively of the polyaniline on silver electrodes which were gold sputtered. Increasing number of polyaniline layers was seen to build up on the surface, filling

in the bright grainy surface resulting in a smoother, darker morphology. Polyaniline coverage for five inkjet-print layers was sparse. At 10 inkjet-print layering, polyaniline covered the silver surface which remained visible from beneath the smooth dark polyaniline deposit. The homogeneous polyaniline layers begin to become visible after 20 layers have been inkjet-printed. It has been seen in the literature that 30 layers was required for homogenous film formation to be observed (Morrin *et al.*, 2008). However, the inkjet-print parameters were not comparable.

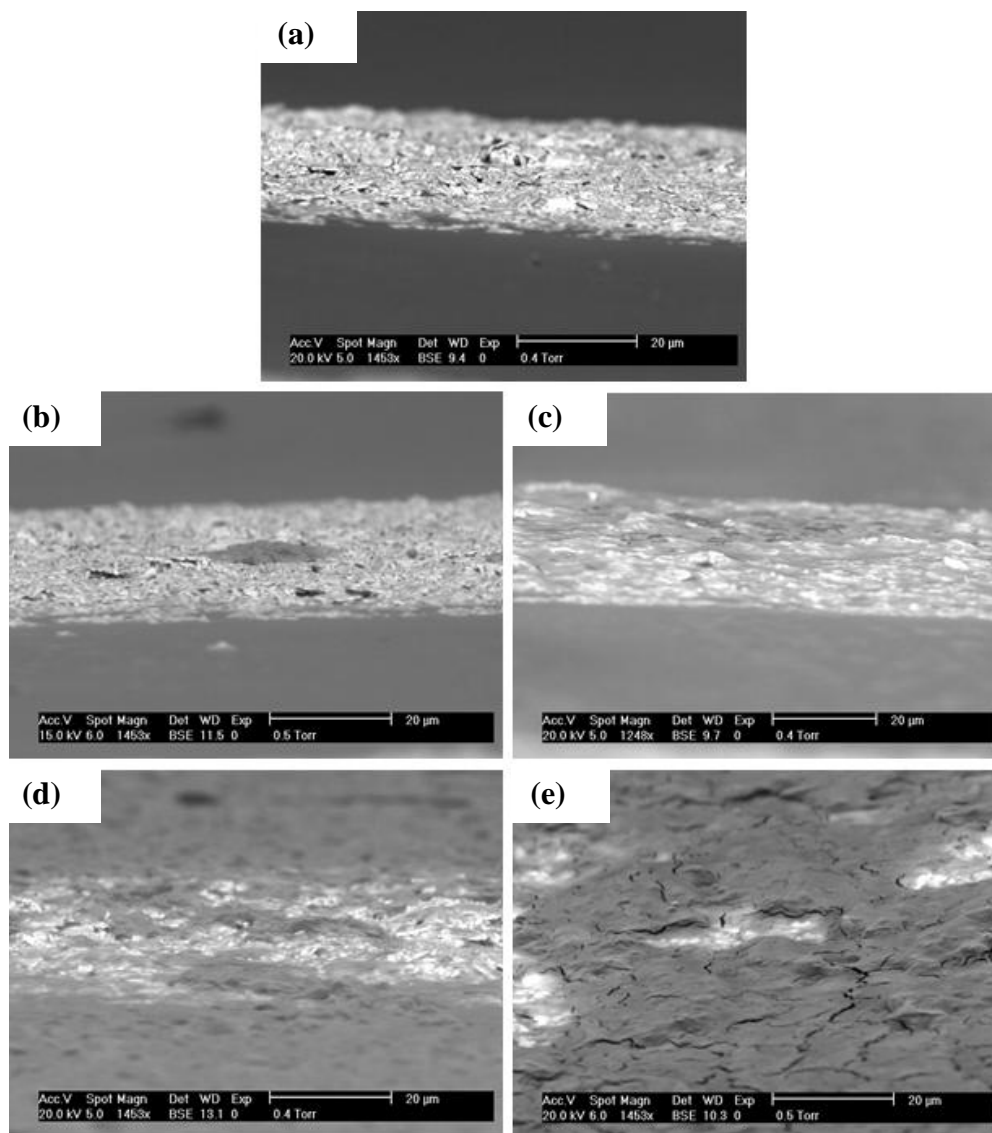


Figure 3.21. Scanning electron micrographs were taken using the backscattered electron detector of gold sputtered (a) bare screen printed silver electrode and (b) 5, (c) 10, (d) 20 and (e) 40 layers of polyaniline inkjet-printed onto the silver electrode at 20 kV and 1453 × magnification.

Individual polyaniline nanoparticles cannot be seen as they appear to coalesce forming a continuous film. This is a phenomenon seen in previous work (Morrin *et al.*, 2008). Nano-structuring was thought to be lost upon inkjet printing, where nanoparticles combine to form a continuous polymer film. The continuous film described is evident in Fig. 3.21 (d). The polymer film can be seen to cover most of the electrode. The cracks seen in the polyaniline film (Fig. 3.21 (e)) may be drying artefacts during the vacuum process of SEM or gold sputtering.

3.3. CONCLUSIONS

Polyaniline nanoparticles were synthesised utilising micellar polymerisation of aniline to produce an aqueous printable ink. This ink was characterised using UV-visible spectroscopy, TEM and DLS. The ink was then deposited via inkjet printing onto silver screen printed IDEs to fabricate polyaniline sensors for ammonia determination. In order to measure gaseous ammonia from a liquid sample, the sensors were combined with an o-ring and a gas-permeable membrane. This set-up was used along with established impedance measurement protocols to optimise inkjet printing parameters. Ammonia sensors were fabricated using 10 inkjet-printed layers of polyaniline at a nozzle voltage of 18 V. Chapter 4 continues on to develop a device capable of detecting aqueous ammonia concentrations in water and buffer at the clinically relevant range (11 to 50 μM) for blood ammonia testing.

3.4. REFERENCES

Basak, S.P., Kanjilal, B., Sarkar, P. and Turner, A.P.F. (2013) Application of electrical impedance spectroscopy and amperometry in polyaniline modified ammonia gas sensor. *Synthetic Metals*. 175 pp.127-133.

Chiam, C. and Sarbatly, R. (2013) Vacuum membrane distillation processes for aqueous solution treatment-A review. *Chemical Engineering and Processing*. 74 pp.27-54.

Crowley, K., Morrin, A., Hernandez, A., O'Malley, E., Whitten, P.G., Wallace, G.G., Smyth, M.R. and Killard, A.J. (2008a) Fabrication of an ammonia gas sensor using inkjet-printed polyaniline nanoparticles. *Talanta*. 77 (2), pp.710-717.

Crowley, K., O'Malley, E., Morrin, A., Smyth, M.R. and Killard, A.J. (2008b) An aqueous ammonia sensor based on an inkjet-printed polyaniline nanoparticle-modified electrode. *Analyst*. 133 (3), pp.391-399.

de la Rica, R., Fernandez-Sanchez, C. and Baldi, A. (2006) Polysilicon interdigitated electrodes as impedimetric sensors. *Electrochemistry Communications*. 8 (8), pp.1239-1244.

de Medeiros, D.W.O., dos Santos, D.S., Dantas, T.N.C., Pereira, M.R., Giacometti, A. and Fonseca, J.L.C. (2003) Zeta potential and doping in polyaniline dispersions. *Materials Science-Poland*. 21 (2), pp.251-257.

Detsri, E. and Popanyasak, J. (2015) Fabrication of silver nanoparticles/polyaniline composite thin films using Layer-by-Layer self-assembly technique for ammonia sensing. *Colloids and Surfaces A-Physicochemical and Engineering Aspects*. 467 pp.57-65.

Doane, T.L., Chuang, C., Hill, R.J. and Burda, C. (2012) Nanoparticle zeta-Potentials. *Accounts of Chemical Research*. 45 (3), pp.317-326.

DropSens (2015a) *Innovative Technology for Miniturised Electrochemistry*. Available from: <http://www.dropsens.com/en/home.html>.

DropSens (2015b) *Polyaniline Modified Screen-Printed Carbon Electrode*. Available from: http://www.dropsens.com/en/pdfs_productos/new_brochures/110pani-c1110pani.pdf.

DropSens (2015c) *Screen-Printed Carbon Electrodes*. Available from: http://www.dropsens.com/en/pdfs_productos/new_brochures/110-c110.pdf.

Dubas, S.T. and Pimpan, V. (2008) Green synthesis of silver nanoparticles for ammonia sensing. *Talanta*. 76 (1), pp.29-33.

Fard, A.K., Manawi, Y.M., Rhadfi, T., Mahmoud, K.A., Khraisheh, M. and Benyahia, F. (2015) Synoptic analysis of direct contact membrane distillation performance in Qatar: A case study. *Desalination*. 360 pp.97-107.

Fernandez-Sanchez, C., McNeil, C.J. and Rawson, K. (2005) Electrochemical impedance spectroscopy studies of polymer degradation: application to biosensor development. *Trac-Trends in Analytical Chemistry*. 24 (1), pp.37-48.

Fujifilm Dimatix (2010) Dimatix Materials Printer DMP-2800 series User Manual. .

Guajardo, C., Ngamchana, S. and Surareungchai, W. (2013) Mathematical modeling of interdigitated electrode arrays in finite electrochemical cells. *Journal of Electroanalytical Chemistry*. 705 pp.19-29.

Guo, H. and Tao, S. (2007) Silver nanoparticles doped silica nanocomposites coated on an optical fiber for ammonia sensing. *Sensors and Actuators B-Chemical*. 123 (1), pp.578-582.

Han, M.G., Cho, S.K., Oh, S.G. and Im, S.S. (2002) Preparation and characterization of polyaniline nanoparticles synthesized from DBSA micellar solution. *Synthetic Metals*. 126 (1), pp.53-60.

Hibbard, T., Crowley, K., Kelly, F., Ward, F., Holian, J., Watson, A. and Killard, A.J. (2013a) Point of Care Monitoring of Hemodialysis Patients with a Breath Ammonia Measurement Device Based on Printed Polyaniline Nanoparticle Sensors. *Analytical Chemistry*. 85 (24), pp.12158-12165.

Hibbard, T., Crowley, K. and Killard, A.J. (2013b) Direct measurement of ammonia in simulated human breath using an inkjet-printed polyaniline nanoparticle sensor. *Analytica Chimica Acta*. 779 pp.56-63.

Kalaji, M. and Peter, L.M. (1991) Optical and Electrical Ac Response of Polyaniline Films. *Journal of the Chemical Society-Faraday Transactions*. 87 (6), pp.853-860.

Karmakar, N.S., Kothari, D.C. and Bhat, N.V. (2013) Ammonia Sensing Properties of Silver Nanocomposite with Polypyrrole. *Solid State Physics, Vol 57*. 1512 pp.294-295.

Kavinkumar, T. and Manivannan, S. (2016) Uniform decoration of silver nanoparticle on exfoliated graphene oxide sheets and its ammonia gas detection. *Ceramics International*. 42 (1), pp.1769-1776.

Kim, B.J., Oh, S.G., Han, M.G. and Im, S.S. (2001) Synthesis and characterization of polyaniline nanoparticles in SDS micellar solutions. *Synthetic Metals*. 122 (2), pp.297-304.

Kirby, B. and Hasselbrink, E. (2004) Zeta potential of microfluidic substrates: 1. Theory, experimental techniques, and effects on separations. *Electrophoresis*. 25 (2), pp.187-202.

Kukla, A.L., Shirshov, Y.M. and Piletsky, S.A. (1996) Ammonia sensors based on sensitive polyaniline films. *Sensors and Actuators B-Chemical*. 37 (3), pp.135-140.

Li, G.F., Martinez, C. and Semancik, S. (2005) Controlled electrophoretic patterning of polyaniline from a colloidal suspension. *Journal of the American Chemical Society*. 127 (13), pp.4903-4909.

Macdonald, J.R. (1992) Impedance Spectroscopy. *Annals of Biomedical Engineering*. 20 (3), pp.289-305.

Magdassi, S. (2010) *The Chemistry of Inkjet Inks*. Singapore: World Scientific.

Magdassi, S. and Ben Moshe, M. (2003) Patterning of organic nanoparticles by ink-jet printing of microemulsions. *Langmuir*. 19 (3), pp.939-942.

Malvern Instruments Ltd. (2016) Zeta Potential and Electrokinetic Phenomena. *Zetasizer Nano Course*.

Mamishv, A.V., Sundara-Rajan, K., Yang, F., Du, Y.Q. and Zahn, M. (2004) Interdigital sensors and transducers. *Proceedings of the IEEE*. 92 (5), pp.808-845.

Massman, W.J. (1998) A review of the molecular diffusivities of H₂O, CO₂, CH₄, CO, O₃, SO₂, NH₃, N₂O, NO, AND NO₂ in air, O₂ AND N₂ near STP. *Atmospheric Environment*. 32 (6), pp.1111-1127.

Matsuguchi, M. and Asahi, T. (2011) Properties and stability of polyaniline nanofiber ammonia sensors fabricated by novel on-substrate method. *Sensors and Actuators B-Chemical*. 160 (1), pp.999-1004.

Micheau, C., Bauduin, P., Diat, O. and Faure, S. (2013) Specific Salt and pH Effects on Foam Film of a pH Sensitive Surfactant. *Langmuir*. 29 (27), pp.8472-8481.

Mirmohseni, A. and Wallace, G.G. (2003) Preparation and characterization of processable electroactive polyaniline–polyvinyl alcohol composite. *Polymer*. 44 (12), pp.3523-3528.

Morrin, A., Ngamna, O., O'Malley, E., Kent, N., Moulton, S.E., Wallace, G.G., Smyth, M.R. and Killard, A.J. (2008) The fabrication and characterization of inkjet-printed polyaniline nanoparticle films. *Electrochimica Acta*. 53 (16), pp.5092-5099.

Moulton, S.E., Innis, P.C., Kane-Maguire, L.A.P., Ngamna, O. and Wallace, G.G. (2004) Polymerisation and characterisation of conducting polyaniline nanoparticle dispersions. *Current Applied Physics*. 4 (2-4), pp.402-406.

Müller, R.H. (1996) *Zeta Potential Und Partikeladung in Der Laborpraxis*. Stuttgart: Wissenschaftliche Verlagsgesellschaft mbH.

Ngamna, O., Morrin, A., Killard, A.J., Moulton, S.E., Smyth, M.R. and Wallace, G.G. (2007) Inkjet printable polyaniline nanoformulations. *Langmuir*. 23 (16), pp.8569-8574.

Renedo, O.D., Alonso-Lomillo, M.A. and Martínez, M.J.A. (2007) Recent developments in the field of screen-printed electrodes and their related applications. *Talanta*. 73 (2), pp.202-219.

Rheume, J.M. and Pisano, A.P. (2011) A review of recent progress in sensing of gas concentration by impedance change. *Ionics*. 17 (2), pp.99-108.

Saunders, R.E., Gough, J.E. and Derby, B. (2008) Delivery of human fibroblast cells by piezoelectric drop-on-demand inkjet printing. *Biomaterials*. 29 (2), pp.193-203.

Sheppard, N.F., Tucker, R.C. and Wu, C. (1993) Electrical-Conductivity Measurements using Microfabricated Interdigitated Electrodes. *Analytical Chemistry*. 65 (9), pp.1199-1202.

Snook, G.A., Kao, P. and Best, A.S. (2011) Conducting-polymer-based supercapacitor devices and electrodes. *Journal of Power Sources*. 196 (1), pp.1-12.

Stamenov, P., Madathil, R. and Coey, J.M.D. (2012) Dynamic response of ammonia sensors constructed from polyaniline nanofibre films with varying morphology. *Sensors and Actuators B-Chemical*. 161 (1), pp.989-999.

Subramanian, R., Crowley, K., Morrin, A. and Killard, A.J. (2013) A sensor probe for the continuous in situ monitoring of ammonia leakage in secondary refrigerant systems. *Anal. Methods*. 5 (1), pp.134-140.

Suman, O'Reilly, E., Kelly, M., Morrin, A., Smyth, M.R. and Killard, A.J. (2011) Chronocoulometric determination of urea in human serum using an inkjet printed biosensor. *Analytica Chimica Acta*. 697 (1-2), pp.98-102.

Sutar, D.S., Padma, N., Aswal, D.K., Deshpande, S.K., Gupta, S.K. and Yakhmi, J.V. (2007) Preparation of nanofibrous polyaniline films and their application as ammonia gas sensor. *Sensors and Actuators B-Chemical*. 128 (1), pp.286-292.

Tarsiche, I., Hopirtean, E. and Ciurchea, D. (1997) Least-squares analysis of ammonia diffusion through PTFE membranes. *Measurement Science & Technology*. 8 (11), pp.1367-1371.

Tekin, E., Smith, P.J. and Schubert, U.S. (2008) Inkjet printing as a deposition and patterning tool for polymers and inorganic particles. *Soft Matter*. 4 (4), pp.703-713.

Trojanowicz, M., Krawczyk, T.K.V., Zmorzynska, M. and Campanella, L. (1997) Amperometric sensing of ammonia in aqueous solutions using a polyaniline-modified electrode in flow injection systems. *Electroanalysis*. 9 (14), pp.1062-1066.

Vallar, S., Houivet, D., El Fallah, J., Kervadec, D. and Haussonne, J.-. (1999) Oxide slurries stability and powders dispersion: optimization with zeta potential and rheological measurements. *Journal of the European Ceramic Society*. 19 (6-7), pp.1017-1021.

Chapter 3

Vieville, J., Tanty, M. and Delsuc, M. (2011) Polydispersity index of polymers revealed by DOSY NMR. *Journal of Magnetic Resonance*. 212 (1), pp.169-173.

Wallace, G.G., Spinks, G.M., Kane-Maguire, L.A.P. and Teasdale, P.R. (2002) *Conductive Electroactive Polymers: Intelligent Polymer Systems*. 3rd ed. Boca Raton, FL: CRC Press.

Wang, J. (1994) Decentralized Electrochemical Monitoring of Trace-Metals - from Disposable Strips to Remote Electrodes - Plenary Lecture. *Analyst*. 119 (5), pp.763-766.

Weng, B., Shepherd, R.L., Crowley, K., Killard, A.J. and Wallace, G.G. (2010) Printing conducting polymers. *Analyst*. 135 (11), pp.2779-2789.

White, B., Banerjee, S., O'Brien, S., Turro, N.J. and Herman, I.P. (2007) Zeta-potential measurements of surfactant-wrapped individual single-walled carbon nanotubes. *Journal of Physical Chemistry C*. 111 (37), pp.13684-13690.

Wikol, M., Bailey, C., Lange, K., Sutsko, M. and Tronto, K. (2007) Expanded Polytetrafluoroethylene Membranes and their Applications. In: Meltzer, T.H.J., M.W., ed. (2007) *Filtration and Purification in the Biopharmaceutical Industry*. USA: CRC Press, pp.619-640.

Willason, S.W. and Johnson, K.S. (1986) A Rapid, Highly Sensitive Technique for the Determination of Ammonia in Seawater. *Marine Biology*. 91 (2), pp.285-290.

Wongchoosuk, C., Jangtawee, P., Lokavee, S., Udomrat, S., Sudkeaw, P. and Kerdcharoen, T. (2012) Novel Flexible NH₃ Gas Sensor Prepared By Ink-Jet Printing Technique. *Biomaterials and Applications*. 506 pp.39-42.

Zaretsky, M.C., Mouayad, L. and Melcher, J.R. (1988) Continuum Properties from Interdigital Electrode Dielectrometry. *Ieee Transactions on Electrical Insulation*. 23 (6), pp.897-917.

CHAPTER 4

DESIGN AND TESTING OF THE AQUEOUS AMMONIA DEVICE

4.1. INTRODUCTION

Gaseous ammonia determination has attempted using a wide range of sensors. During this time a wide range of sensors have been developed including catalytic, conducting polymers, metal oxides and optical sensors (Timmer *et al.*, 2005). Determining gaseous ammonia in an aqueous environment has proven more of a challenge. In previous work, ammonia in liquid has been determined using inkjet-printed polyaniline nanoparticle-based sensors. Measurements have taken place in a continuous flow system amongst PBS (Crowley *et al.*, 2008) and brine (Subramanian *et al.*, 2013) in the range of 0.02 to 10 mM and 0.28 to 5.6 mM, respectively. The work carried out by Crowley *et al.* (2008) utilised an amperometric three-electrode set-up in direct contact with PBS at pH 7.5. Ammonium ion (NH_4^+) as a representative of aqueous ammonia concentrations was determined. The ammonia sensing probe developed by Subramanian *et al.* (2013) utilised a polyaniline sensor in conjunction with a gas-permeable membrane for the impedimetric sensing of gaseous ammonia in brine. This work demonstrated the ability of ammonia gas to permeate through PTFE and be determined by a polyaniline sensor. Permeation, P , of gaseous ammonia through the PTFE membrane can be thought of as:

$$P = DS \quad \text{Eq. 4.1}$$

Where D is the diffusion coefficient and S is the solubility coefficient (Yampolskii, 2012). The solubility of a particular gas may be given by Henry's Law (Budd and McKeown, 2010).

$$S = kHc \quad \text{Eq. 4.2}$$

Where c is the concentration of the gas in solution and kH is the Henry's Law constant (Atkins and de Paula, 2009). The Henry's Law constant relates the partial pressure of ammonia in the gas phase to its concentration in solution. The Henry's Law constants for ammonia in water (+4 to -15°C) are in the range of 172.77 to 511.88 mol kg⁻¹ bar⁻¹ (National Institute of Standards and Technology, 2011). Dissolved species such as salts may alter water availability and complicate this equilibrium (Sing *et al.*, 1999).

The work presented in Chapter 3 focussed on the optimisation of the fabrication process of the polyaniline nanoparticle-based sensor for the measurement of aqueous ammonia. Optimisation of the sensor utilised a PTFE gas-permeable membrane in conjunction with an o-ring, which generated a gas headspace for ammonia gas to diffuse into. This chapter focuses on the integration of the polyaniline sensor into a preliminary device capable of measuring ammonia in a static liquid sample at relevant minimum ammonia concentrations of 11 to 50 μM (Barsotti, 2001). This was done by encapsulating the polyaniline sensors, o-ring and gas-permeable membrane using pressure sensitive adhesive (PSA). Testing was carried out on this preliminary device in water and electrolyte matrices at the clinically relevant range for blood ammonia testing. This device was further adapted into a prototype device for the eventual testing of ammonia in blood. This preliminary device was fabricated in a manner that would be consistent with the requirements of a POC patient test i.e. inexpensively mass produced, simple to use, disposable and self-contained integrated devices.

4.2. RESULTS AND DISCUSSION

4.2.1. Impedance spectroscopic characterisation of the prototype ammonia measurement device

The sensor set-up utilised in Chapter 3 was modified in this Chapter to establish a prototype ammonia measurement device. The initial configuration included a PTFE membrane and an o-ring to create a gas headspace bonded together by adhesive PSA layers. PSA transformed the sensor set-up into an air tight, durable device.

To assess the device for ammonia determination, detailed impedance spectroscopic characterisation in air, aqueous media (PBS buffer) and in the presence of ammonia was performed. Impedance spectroscopic characterisation took place across a frequency range of 0.1 Hz to 100 kHz at amplitude of 5 mV rms. The impact of the device upon exposure to air, 52 μL of PBS and PBS containing ammonia was assessed (Fig. 4.1).

The impedimetric spectra of all three systems (air, PBS and ammonia in PBS) exhibited that of a resistor and capacitor in series. As discussed in Chapter 3,

Section 3.2.3, printed polyaniline sensors in air behave as bulk resistance in series with capacitance. This is typically observed on the Nyquist plot as an arching vertical line, and as a horizontal line on the Bode modulus and phase plots at low frequency values (Fernandez-Sanchez *et al.*, 2005). It is clear from the Nyquist plot of the device in air shown in Fig. 4.1 (a), that while some change in $-Z''$ appears to be present, indicating a capacitance, this is insignificant in comparison to the magnitude of Z' which indicates resistance, as seen in the isotropic insert. This suggests that the device appears to exhibit the characteristics of a resistor and capacitor in series in which the capacitance is negligible. This is supported by the Bode modulus and phase diagrams (b and c) which show negligible frequency-dependent changes in absolute impedance ($|Z|$) or phase (ϕ), which is typically associated with that of a resistor.

Upon exposure of the device to PBS, a decreased response was observed for $|Z|$ and ϕ across all frequencies. This is most evident in the Bode modulus plot, Fig. 4.1 (b). At lower frequencies a decrease in $|Z|$ of $50\ \Omega$ was observed which increased to $200\ \Omega$ at higher frequencies. The decrease in impedance in PBS when compared to air, suggests that species from PBS (water vapour) are able to diffuse across the membrane and are affecting the impedance of the sensor. While it was observed that, in the presence of PBS, there was an overall decrease in impedance (largely due to resistance), PBS containing 1 mM ammonia exhibited a significant overall increase in impedance. This is most evident in Fig. 4.1 (b) where $|Z|$ can be seen to increase by approximately $1\ \text{k}\Omega$ compared to the device in air.

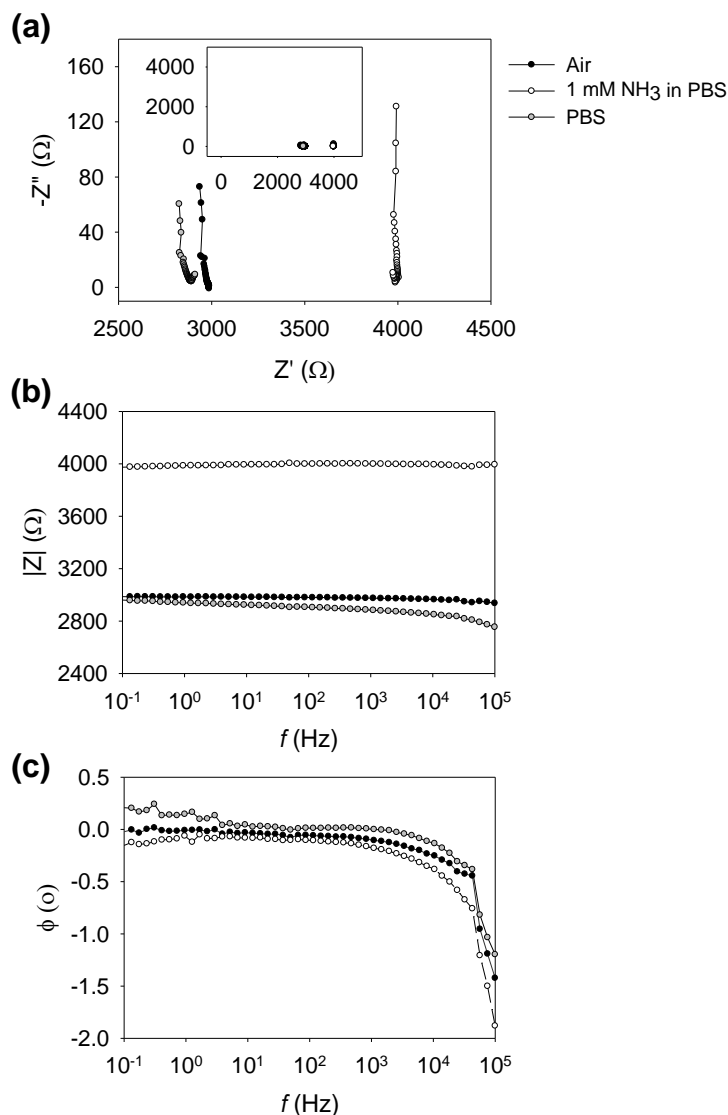


Figure 4.1. Impedance spectra of the device in air, PBS and 1 mM ammonia in PBS. (a) Nyquist, (b) Bode modulus and (c) phase plots across a frequency range of 0.1 Hz to 100 kHz.

While species from the PBS buffer were seen to contribute to a decrease in impedance of the device when compared to the device measured in air, ammonia in buffer was seen to contribute to an opposing increase in impedance. Water vapour is known to cause a decrease in the resistance of polyaniline films when in direct contact (Crowley *et al.*, 2008, Wu *et al.*, 2000, Hibbard *et al.*, 2013a). While the use of a hydrophobic PTFE membrane prevents diffusion of liquid water, it would appear that it does not prevent water vapour. This is well known in the fabrics industry with the production of Gore-Tex® which is made from PTFE. It repels liquid water while allowing water vapour to pass through. It has been seen that water

vapour may permeate the PTFE membrane if pressure, humidity, or temperature varies across the membrane (Wikol *et al.*, 2007). This has been seen to correspond to a decrease in resistance, as water vapour is conductive (Wu *et al.*, 2000). The work by Subramanian *et al.* (2013) using an analogous system did not make this observation. This may have been due to the large volumes and high ammonia concentrations used in the system which lead to large magnitude of resistance. Thus, water vapour capacitance was observed as background signal. However, this study is attempting to measure extremely low concentrations of ammonia in very small samples and so water vapour interference may be more significant under these conditions.

In order to assess ammonia determination in the presence of water vapour preliminary devices were exposed to deionised water, PBS and ammonia in PBS as described in detail in Chapter 3, Section 3.2.6.2. It can be seen from Fig. 4.2 that deionised water caused a consistent decrease in $|Z|$ with frequency range. The decrease was observed at a Z/Z_{air} value of 0.95 which was approximately 320 Ω below its baseline in air (Appendix III). The decrease in resistance for PBS was also steady throughout the range of frequencies. However, it displayed a larger Z/Z_{air} decrease of 0.98, corresponding to 1180 Ω below its baseline. Upon comparison of the water and PBS results, it was speculated that something other than water was traversing the membrane. It is widely known that small molecules such as helium, oxygen and carbon dioxide can permeate through PTFE membrane via micro-porous gaps in the polymer structure. It can be seen from Fig. 4.2 that high concentrations of ammonia such as 1 and 5 mM in PBS exhibited a ratiometric increase of 1.0 and 1.2, respectively (943 and 14,787 Ω). However, 0.1 mM had a Z/Z_{air} less than 1 (0.97), which indicated the response to low concentration ammonia was lower than its baseline in air. In this case the water vapour signal was effectively a negative interferent i.e. the magnitude of impedimetric decrease was so substantial that any increase associated with ammonia was obscured. Full impedimetric spectra are available in Appendix IV.

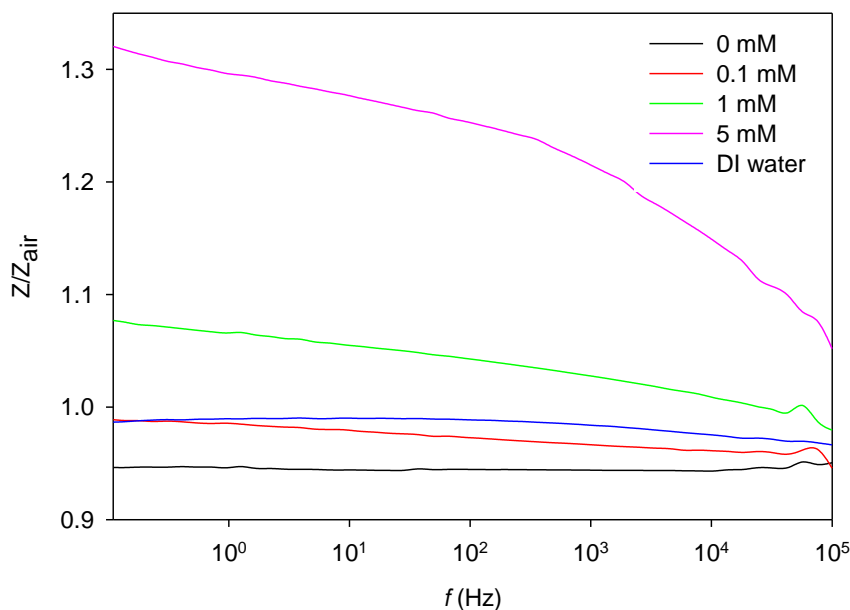


Figure 4.2. Ratiometric impedance spectrum of the device upon exposure to deionised water, 0, 0.1, 1 and 5 mM ammonia in PBS. Frequency range 0.1 Hz to 100 kHz.

From the literature it has been observed that as the concentration of ammonia increases the rate of deprotonation of the polyaniline film is heightened which is proportional to the increased resistance of the film (Subramanian *et al.*, 2013, Wu *et al.*, 2000, Hibbard *et al.*, 2013a). This increased resistance caused by ammonia is also associated with a corresponding decrease in resistance due to the PBS matrix. Unfortunately, at the concentrations of ammonia found in blood (between 11 - 50 μM), the decrease in impedance brought about by the matrix was greater than the increase in impedance due to the presence of ammonia, which would render the sensor unsuitable for measurement in blood at the required concentrations. While the response to the aqueous medium may be constant, it was necessary to be able to differentiate it from the ammonia signal. The impact on the quantitative measurement of ammonia in the presence of the opposing response exhibited by the aqueous medium was further investigated.

4.2.2. Strategies to eliminate solvent interferences

4.2.2.1. Investigation of the effect of membrane composition

Upon contemplation of the solvent interferences, the possibility of preventing water vapour permeation through the PTFE membrane was explored. The addition of

compounds to reinforce the PTFE membrane was considered. It was seen from the literature that ethyl cellulose (EC) and Brij® S10 have been employed to support hydrophobic membrane during the development of an aqueous ammonia test (Dobler *et al.*, 2006) and also to control water breakthrough (Malinowska and Meyerhoff, 1998, Munkholm, 2000). It was decided to combine these compounds with the PTFE membrane. The concentrations used were taken from studies by Malinowska and Meyerhoff (1998) and Munkholm (2000). A 10% EC solution was dissolved in 80:20 ratio of toluene to ethanol. The 30% Brij® solution was made up in deionised water and heated to 50°C to encourage homogeneity. The Whatman® PTFE membrane filter used in the device had a polypropylene support material on one side on which Brij® was deposited using a paint brush. EC was deposited onto the PTFE side of the membrane filter in the same way. The modified membrane was incorporated into the device and exposed to ammonia at a concentration range of 0 to 30 mM in buffer and measured impedimetrically.

It can be seen from Fig. 4.3 for all ammonia concentrations used that their Z/Z_{air} values were approximately 1. Thus, the use of EC and Brij® in combination with the PTFE membrane prevented a decrease in impedance associated with water vapour. However, this also compromised ammonia permeation as no increase upon a Z/Z_{air} was observed.

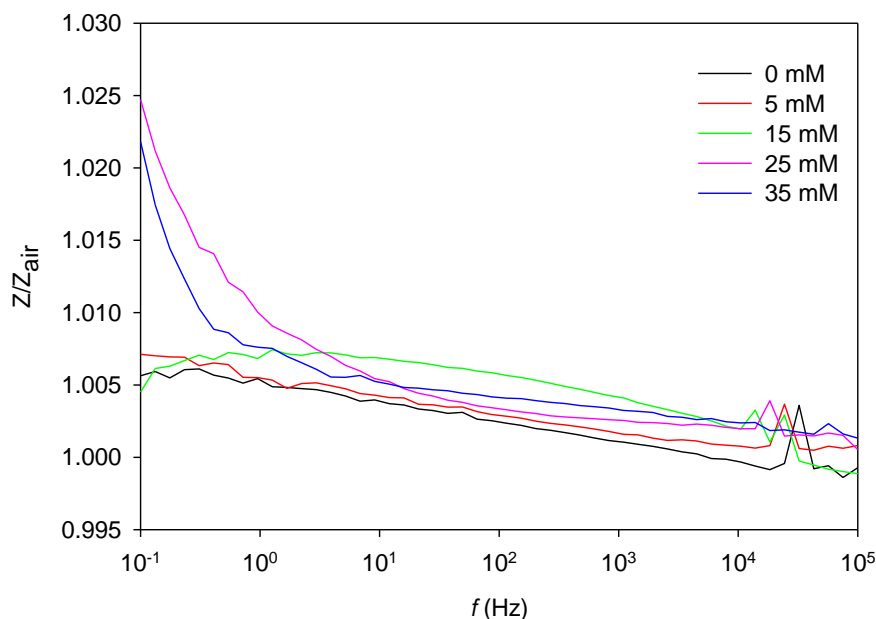


Figure 4.3. Ratiometric impedance data of the device incorporating a modified PTFE membrane coated with 10% EC and 30% Brij® S10 on either side. The device was exposed to 0, 5, 15, 25 and 35 mM ammonia in PBS.

This modified PTFE membrane completely prevented permeation. This was an unexpected result as Brij® is known to transport ammonia through hydrophobic membranes (Kapoor *et al.*, 2013) in combination with EC this was not the case here. Brij® and EC were extremely viscous and therefore difficult to manipulate and deposit onto the membrane homogenously. It was also evident from the data gathered in Fig. 4.3 that they were completely prevented all permeation through the membrane i.e. water vapour and also gaseous ammonia. It was for this reason another direction was employed to manage the effect of water vapour on the preliminary device.

4.2.2.2. Ammonia sensor recovery

Limiting the effect of water vapour interference by prevention did not appear to be successful. It was decided to explore the possibility of eliminating the effect of water vapour after it permeated through the membrane. It can be seen in the literature that polyaniline sensors for ammonia determination have been recovered to their initial baselines upon exposure to air (Wu *et al.*, 2000, Hibbard *et al.*, 2013a, Wang *et al.*, 2004, Blighe *et al.*, 2012, Wongchoosuk *et al.*, 2012, Prasad *et al.*, 2005). As discussed in Chapter 1, Section 1.2.3 polyaniline films donate protons

from their positively charged local centres upon exposure to NH_3 forming energetically favourable NH_4^+ . This causes an increase in resistance as valence electrons can no longer easily hop from one positively charged centre to another. When the polyaniline film is in contact with air, NH_4^+ decomposes into NH_3 and protons. The protons are integrated once again into the local centres restoring initial levels of conductivity (Wu *et al.*, 2000, Blighe *et al.*, 2012, Chabukswar *et al.*, 2001). Conversely, upon exposure of the polyaniline films to humidity, adsorption occurs and water molecules are held within the charged centres via weak hydrogen bonding. This bond is readily broken by moderate heating (Lubentsov *et al.*, 1991) and exposure to air. The movement of air across the film breaks the weak hydrogen bonds and dissipates the water vapour. Thus, the rate of association of ammonia with polyaniline is very high and its dissociation is very slow. However, both the rate of association and dissociation of water with polyaniline are rapid (Kukla *et al.*, 1996). This is due to the binding that occurs during interaction with ammonia a strong chemisorption interaction is observed.

Analyses of the literature lead to the conclusion that in order to displace water vapour from the device, they may be exposed to air and/or heat. Three methods were trialled for this purpose subsequent to PBS exposure. Devices were either (a) heated to 30°C in a dry heat oven for 30 min, (b) desiccated for 30 min or (c) the air from the device headspace was removed by pulling the air out using a 10 mL syringe. It can be seen from Fig. 4.4 that heating the devices to 30°C produced the lowest Z/Z_{air} value (0.78) of the three methods trialled. Devices that were desiccated produced a ratiometric value of 0.92. It was expected that dehydrating the devices from residual water vapour would also recover the devices to their initial baselines. Devices that were desiccated produced a ratiometric value of 0.92. However, this was not the case. Devices that had the headspace gas displaced by withdrawing it had the highest ratiometric value (0.96) of the three methods trialled. All three methods trialled resulted in ratiometric values below 1, meaning sensors displayed a decrease in resistance with respect to their baseline in air. Thus, had the devices been exposed to ammonia, any related increases would be concealed by the decrease associated with water vapour.

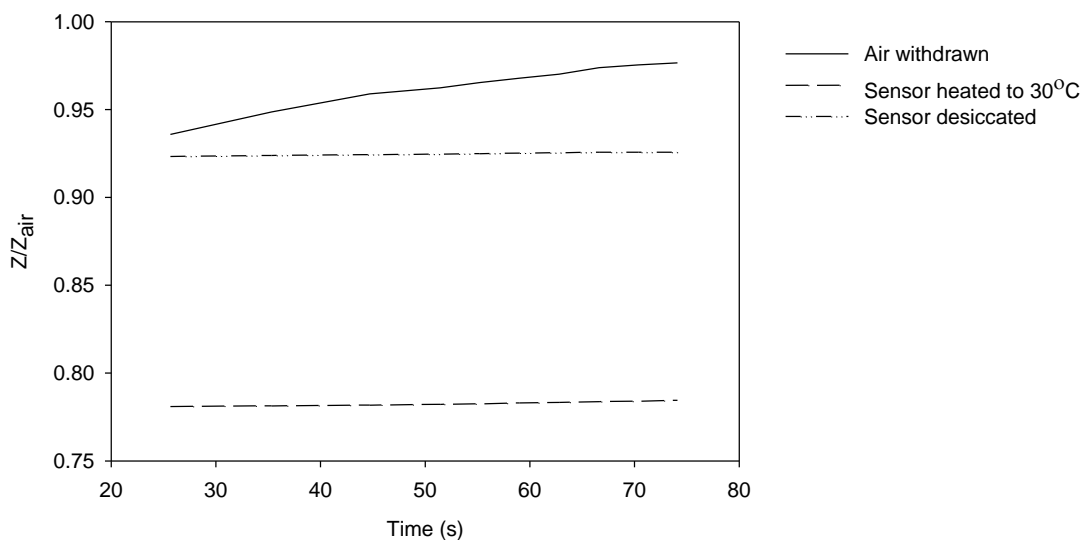


Figure 4.4. Ammonia device recovery subsequent to PBS exposure at $n = 2$, by (a) heating to 30°C for 30 min, (b) desiccating for 30 min, (c) removing headspace gas. Impedance analysis took place at a frequency of 1 kHz.

The relationship between humidity and temperature are obviously linked. They have been seen to decrease the resistance of the polyaniline sensors (Wu *et al.*, 2000, Yoshikawa *et al.*, 2006). As with increased temperature in dry heat oven, the humidity decreased. The decrease in resistance associated with temperature is suggested to be due to an irreversible loss of water molecules from the hydrated polyaniline film (Mondal and Munichandraiah, 2006). In the work of Mondal and Munichandraiah (2006), polyaniline could be recovered to its initial baseline in air if left at atmospheric conditions to rehydrate, achieving equilibrium with the atmospheric conditions. The reduced vapour pressure of water vapour in the gas phase above the sensor would be much lower than the vapour pressure on the sensor surface, causing the water vapour on the sensor to diffuse into the headspace in an attempt to re-equilibrate the vapour pressure. This hypothesis together with literature studies showing that air has been widely used to regenerate polyaniline sensor baselines was further explored.

The method of withdrawing gas from the device headspace proved difficult as it was too vigorous and damaged the device. This was caused by the rate of air flow being removed with a 10 mL syringe from the 247 mm³ headspace. Instead of withdrawing the gas in the device headspace it was decided to purge the device headspace with 5 psi of compressed air. This was hypothesised to displace water

vapour from the device headspace and allow those that were on the sensor surface to equilibrate with the regenerated gas in the headspace. In order to do this the o-ring component of the device was pierced with needles on either side. Fig. 4.5 presents the modified device. The top view can be seen on the left and the underside on the right. This modification allowed the headspace to be easily filled with air via one needle and exited through the needle on the opposite side of the o-ring.

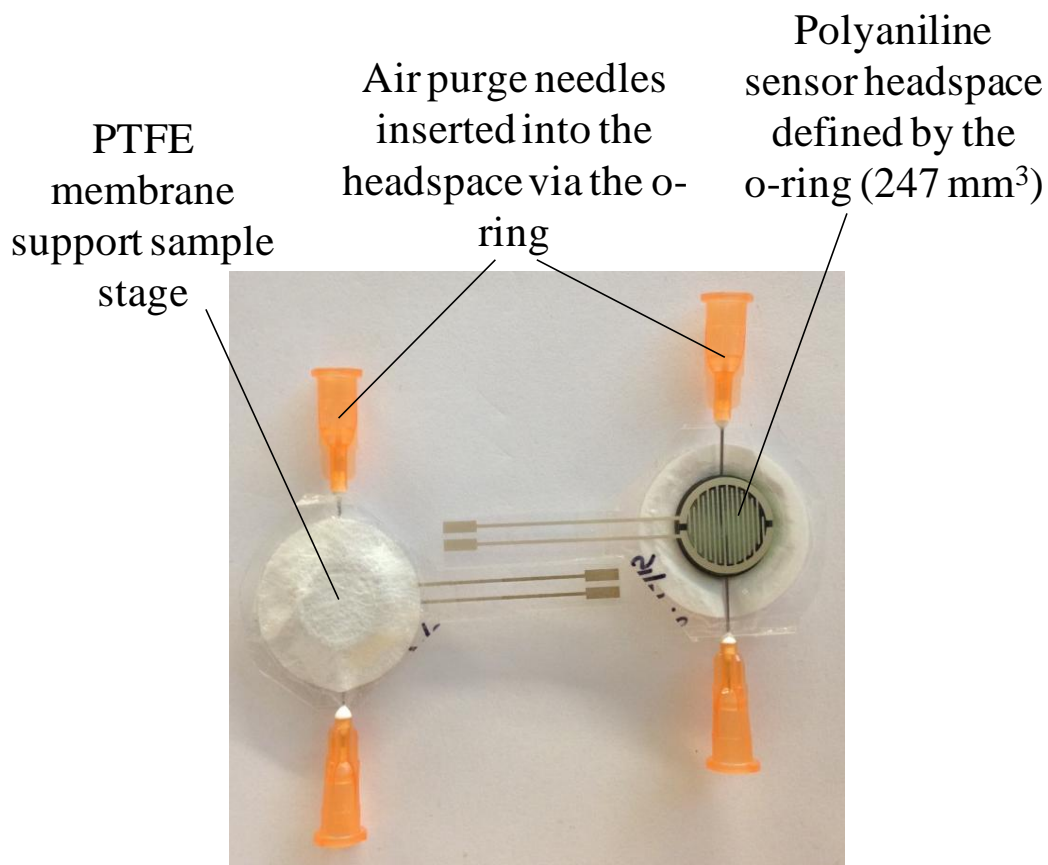


Figure 4.5. Photograph of the ammonia device. Depicted are two needles inserted into the 247 mm³ headspace via the o-ring. This allows the air purge to pass over the polyaniline sensor, by entering through one needle and leaving via the other on this opposite side. Left shows the top view, while the right shows the view from the underside.

The configuration shown in Fig 4.5 was used to examine the recovery of the device to initial baselines in air using an air purge subsequent to water vapour exposure. An initial impedimetric baseline reading was taken across a frequency range of 0.1 Hz to 100 kHz. The sensor was then exposed to PBS for 15 min before being removed. Subsequently, the sensor headspace was then purged with 5 psi air

for 1 min and a final absolute impedimetric reading was taken after. It was observed from Fig. 4.6 that at 1 kHz a device with an initial baseline $|Z|$ of 528 Ω , upon exposure to PBS the devices decreased by 68 Ω in impedance to a $|Z|$ of 460 Ω (this decrease corresponds to a Z/Z_{air} of 0.87). Low frequencies (<1 kHz) typically correspond to the resistive properties of the device in which there is a significant decrease due to water vapour associated with PBS. The subsequent air purge recovered the initial baseline to 528 Ω (corresponding to a $|Z|$ of 1.0).

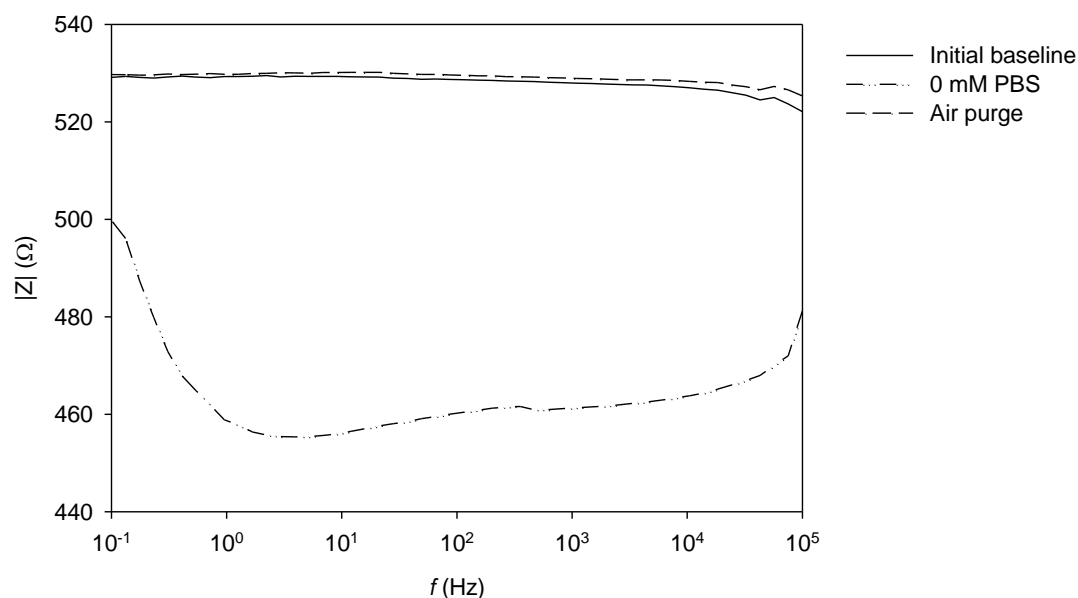


Figure 4.6. Device recovery upon being purged with compressed air for 1 min after the exposure of PBS for 15 min.

In conclusion, the air purge successfully recovered the aqueous ammonia device upon exposure of PBS. Device recovery was considered a critical aspect in attaining the LOD required for blood ammonia analysis. Returning the device to its initial baseline allowed increases in resistance associated with physiological levels of ammonia to be observed without being concealed by matrix interference. The photograph in Fig. 4.5 therefore illustrates the optimised prototype device which was used for further studies and assessed for the potential of blood ammonia determination.

4.2.2.3. Investigation of sample exposure time in the sampling chamber

Ideally, a blood ammonia device should reach the minimum physiological level of blood ammonia testing which is approximately 11 - 50 μM . Testing was

carried out to find the LOD of the developed prototype device. It was accepted that the 1 min air purge at 5 psi of the device headspace returned the devices to their initial baselines across all frequencies. Thus, single point ratiometric impedance (Z/Z_{air}) data of the device were analysed at 1 kHz for increased time intervals (2, 4, 8, 16 and 32 min) and prior to each reading an air purge took place. It was hypothesised that increased ammonia exposure time may lead to an increase in the resistance of the polymer film, allowing the capacity for lower concentration ammonia to be determined. Fig. 4.7 depicts the ratiometric values of the device in response to varied ammonia concentrations (100 to 1,000 μM) versus time. The ratiometric resistance of the devices increased over time for each concentration studied. This suggests that the polyaniline and NH_3 interaction continues over time. For 250 μM ammonia, Z/Z_{air} increased by a factor of 1.1 over the period of 2 to 32 min, whereas 1,000 μM increased by a factor of 1.3. The prototype device was capable of analysing ammonia concentrations down to 250 μM , beyond that the sensor suffered sensitivity limitations, as 100 μM produced a higher Z/Z_{air} response than 250 μM . It may be assumed impedance response would eventually saturate due to the limited number of NH_3 molecules available to deprotonate the polyaniline film.

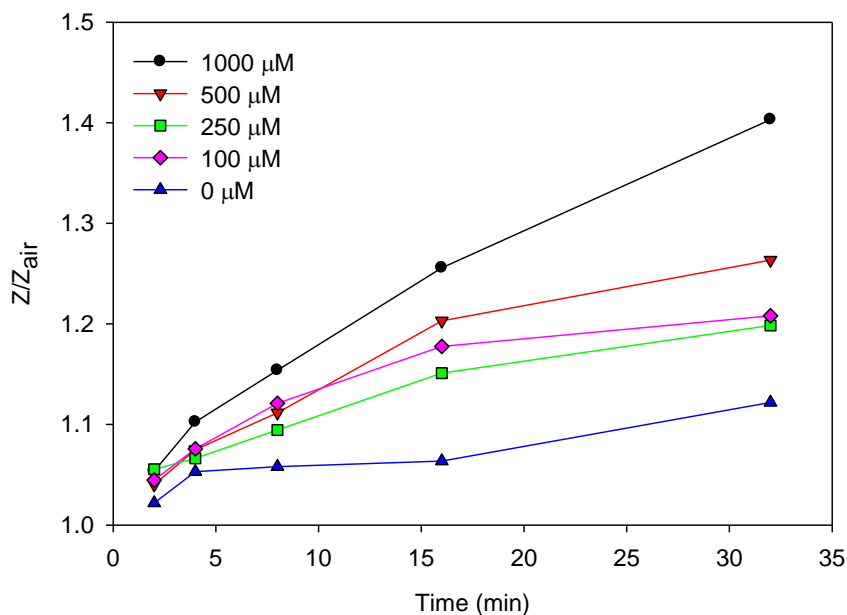


Figure 4.7. Change in the ratiometric impedance of the devices in response to concentrations of ammonia (0, 100, 250, 500, and 1000 μM) over time. Impedimetric data was gathered at a frequency of 1 kHz subsequent to a 1 min 5 psi air purge.

While increased exposure time was observed to increase the ratiometric impedance of the devices in response to ammonia, it was important to keep in mind the POC application of the device. Thus, a balance between acceptable POC exposure time and increased response needed to be reached. It seemed that 15 min exposure time was the best choice because it gave a greater Z/Z_{air} than earlier times. It was also considered a reasonable time for a POC test and was therefore used for further device testing. Sample exposure time of 15 min in combination with the air purge method improved the impedimetric response of the device to ammonia somewhat. However, further improvements needed to be made in order to reach the relevant minimum level of blood ammonia testing of 11 to 50 μM .

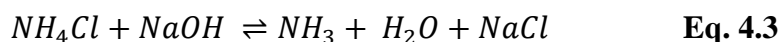
4.2.2.4. Investigation of the effect of sample pH

The previous section optimised sample exposure time in order to improve the sensitivity of the prototype device. However, the LOD of the device was still not adequate. In 52 μL of 25 μM ammonia in PBS at pH 7.4 there are 7.83×10^{14} molecules of ammonia compared to that of Subramanian *et al.* (2013) in which a 220 mL continuous flow system was used to expose polyaniline electrodes to ammonia

in brine. The lowest concentration of ammonia reached by this system was 0.28 mM (5 ppm) which equates to 3.71×10^{21} molecules of ammonia. The impedimetric increase associated with ammonia was observed by Subramanian *et al.* (2013) amongst the water vapour decreases due to high concentrations of ammonia at high volumes. The relevant minimum level of blood ammonia is between 11 and 50 μM , so it can be concluded that detection of ammonia at these concentrations is unreasonable using the current set-up (i.e. low volumes).

This section outlines the investigations undertaken to further improve the sensitivity of the device and its measurement of ammonia. Ammonia has a pKa of 9 meaning that in aqueous solution NH_3 and NH_4^+ are in equal abundance at this pH. When the pH of the solution is neutral (that is, two units below the pKa) 99% of ammonia is in the NH_4^+ form. Reciprocally, at pH 11 (two units above the pKa), 99% of ammonia will exist as NH_3 (Atkins and de Paula, 2009). In the context of the prototype blood ammonia device which operates at neutral pH, only some 1% of ammonia is available in the gaseous form to diffuse from solution through the PTFE membrane into the device headspace, to be measured by the polyaniline sensor. Thus, by altering the pH of the solution to shift the balance towards $\text{NH}_{3(\text{g})}$, this may result in more ammonia molecules being available to diffuse through the membrane and thus be measured. This approach has been incorporated into commercial ammonia test kits (Vitros® and PocketChem™). It may be performed *in situ* by impregnating an absorbent layer with an alkaline reagent, so when the ammonia sample is in direct contact with the buffer it causes a shift in the pH generating more NH_3 (Dobler *et al.*, 2006). However, for initial studies the alteration of pH was investigated in this study by changing the pH of the sampling solution *ex situ*. This was done with the aim of integrating an alkaline reagent into the sensing device if proven to be successful.

$\text{NaOH}_{(\text{aq})}$ is a strong base with a pKa of approximately 14. When in solution it donates a hydroxide to hydrogen in solution forming water, to make the solution more basic. In this work ammonia was typically prepared as ammonium chloride in PBS pH 7.4. When sodium hydroxide is in solution with ammonium chloride it produces ammonia along with salt and water, see Eq. 4.3.



The addition of NaOH was employed to produce more NH_3 molecules with the aim of increasing the impedimetric response of the device. The PBS pH 7.4 buffer was adjusted to pH 11.0 by adding 2 μL of 5 M NaOH to 50 μL of the ammonia sample (ratio of 1:25 PBS to 5 M NaOH) in an Eppendorf tube. Subsequent to the sample pH change, 52 μL of the sample from the Eppendorf tube was introduced to the device sampling chamber and impedance measurements were performed over 32 min. Prior to measurement, the device chamber was purged with air, creating an accumulative ammonia response. This was then compared to PBS pH 11.0 and ammonia in PBS pH 7.4 using the same parameters. NaOH in PBS at pH 11.0 did not cause an increase in impedance of the film (Fig. 4.8). Ammonia contributed to the increased impedance. Increasing the proportion of NH_3 in solution by increasing pH of the sample from 7.4 to 11.0 resulted in approximately five-fold increase in Z/Z_{air} for 1 mM ammonia in PBS. Over time, the ratiometric impedance of the sample at pH 7.4 was consistent with little variance (0.019). The response of the sample at pH 11.0 increased gradually over time up to 15 min, whereupon it decreased slightly. This suggests that for a higher number of NH_3 molecules in pH 11.0 there is a saturation point beyond 15 min, due to the limited number of NH_3 molecules in solution.

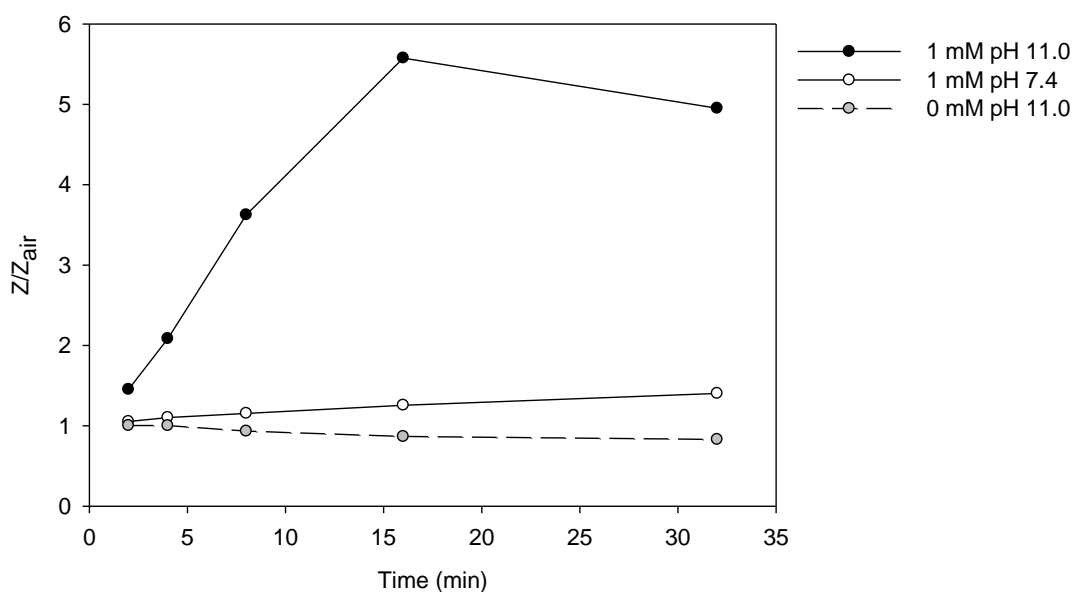


Figure 4.8. The effect of sample pH on ratiometric impedance response over time of the prototype device to 1 mM ammonia. The devices were purged with air prior to impedimetric measurements taken at frequency of 1 kHz.

Increasing the pH of the sample did appear to increase the response of the devices to ammonia in solution. This can be considered to increase the number of NH_3 molecules available to interact with polyaniline. This ammonia-polyaniline association continues over time, up to a saturation point of 15 min.

In order to increase the number of NH_3 molecules in solution via pH change, optimisation of the interaction kinetics was studied. Previously the change in pH was conducted *ex situ* in an Eppendorf tube and introduced to the device immediately. It was hypothesised that allowing time for this process to occur would increase the number of NH_3 molecules. To study the kinetics of the pH change and its effect on the device, the 1 mM ammonia sample was held in the Eppendorf tube for 1, 5 and 10 min of pre-incubation before being introduced to the device sample chamber for measurement. The reaction was carried out as described previously using a 1:25 ratio of 5 M NaOH to sample solution. The samples were kept on ice during pre-incubation, in line with clinical protocols which would be used in further studies with serum and plasma (Huizenga *et al.*, 1994). The devices were then impedimetrically measured, subsequent to an air purge at various time intervals up to 32 min. It can be seen from Fig. 4.9 that the ammonia response continued to increase with time. Pre-incubation may have had some effect between 1 and 5 min. However, the rates were consistent after this. 10 min was little improved over 5 min.

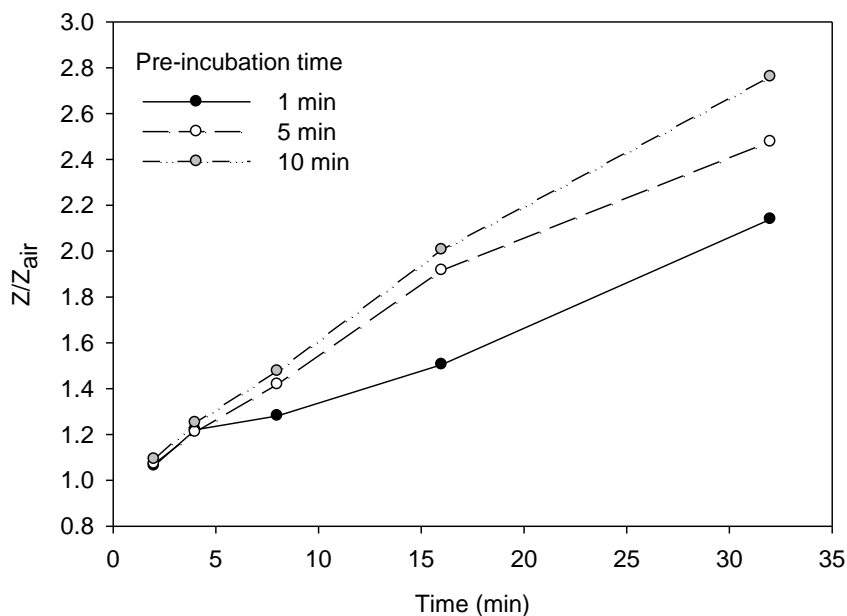


Figure 4.9. Kinetic study of the 1 mM ammonia pH sample change from 7.4 to 11.0 using 5 M NaOH. The devices were purged with air for 1 min at 5 psi prior to impedimetric measurements taken at a time intervals up to 32 min at a frequency of 1 kHz.

The pre-incubation step resulted in near linear response of the devices to ammonia. This should be compared to when the sample was not incubated and placed directly on the device which after 15 min a saturation point was reached (Fig. 4.8). It appears that NH_3 may be accumulating during pre-incubation and diffusing from the sample in larger quantities which increased the impedimetric response of the device. It is possible a saturation point beyond 10 min of pre-incubation may be reached, however this was not covered in the scope of this study. An incubation time of 10 min is typical of the ion exchange process used in a similar study which allowed 20 min for pre-incubation time using sodium acetate and ammonium chloride (Ayyub *et al.*, 2015). It was concluded, from the data gathered and previous literature that 10 min of pre-incubation time was used for further studies.

To summarise, the methodology developed and used throughout further studies. Initial device baseline in air was measured impedimetrically at 1 kHz, this is denoted Z_{air} . Ammonia as ammonium chloride was dissolved in PBS pH 7.4. The pH of this sample was adjusted to pH 11.0 by adding 2 μL of 5 M NaOH to 50 μL of the ammonia sample (ratio of 1:25 PBS to 5 M NaOH) in an Eppendorf tube which was

left to pre-incubate for 10 min. Subsequently, 52 μL of the sample from the Eppendorf tube was introduced to the prototype device sampling chamber and exposed for 15 min, upon which the sample was removed and a 1 min at 5 psi air purge was introduced to the device headspace. A final impedimetric measurement was taken which was denoted Z . This final impedimetric measurement (Z) was divided by the initial baseline measurement (Z_{air}) to give the ratiometric response (Z/Z_{air}) of the device to ammonia.

4.2.3. Time course analysis of the ammonia measurement process

It has been established in the previous sections that water vapour effects on device impedance were eliminated when the device headspace was purged with air. Increased exposure time and a change in pH of the sample increased the scope for low ammonia concentrations to be determined. The majority of these developments were made upon analysis of ratiometric data (Z/Z_{air}) of the devices with respect to their initial baselines in air i.e. measurements took place after all exposure. It was important to gain a comprehensive understanding of the 15 min sample exposure process. This would allow the study of the NH_3 effects on polyaniline sensor as part of the developed device. In order to do this the ratiometric impedance at 1 kHz was monitored over time (Fig. 4.10). The procedure was as follows, ammonia samples were incubated with 5 M NaOH for 10 min prior to device exposure. Approximately 200 s of baseline device readings in air were recorded impedimetrically. The pre-incubated ammonia sample was then introduced to the sample chamber for 15 min exposure, the sample was then removed and the device headspace was purged with air for 1 min. It can be seen from Fig. 4.10 that the ratiometric impedance value for the devices baseline in air was 1, which was expected. Upon exposure to the 52 μL sample solution an initial impedimetric increase was seen in proportion for all ammonia concentrations with respect to the baseline readings. Cross over between ammonia concentrations was observed during the 15 min sample exposure and it was corrected when the electrode was purged with air at 1,100 s. This crossover may be due to matrix effects.

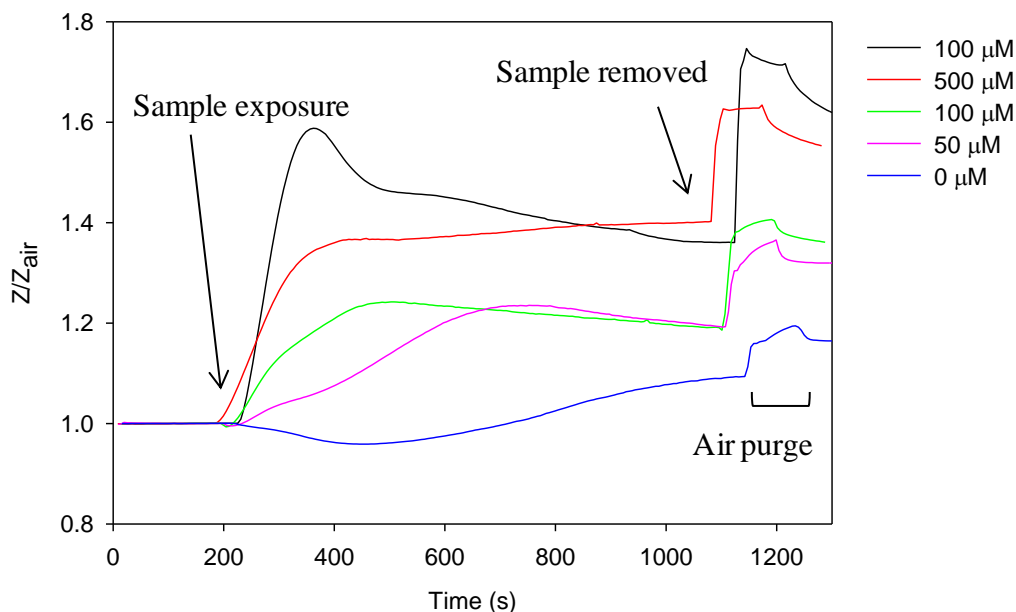


Figure 4.10. Continuous ratiometric impedance monitored at 1 kHz over time upon exposure of ammonia in solution at pH 11.0 to prototype devices.

It is evident from this real time experiment that there was an initial decrease in ammonia measurement due to the matrix effect of PBS. The initial decrease was expected upon consideration of previous experimentation, discussion and theory around water vapour and matrix effects on the device. However, it remains unknown why a gradual increase in impedance was observed. The 1 min air purge has been seen to remove water vapour from the device headspace leaving residual ammonia to be measured. Higher concentration of ammonia means that there was a higher proportion of deprotonation resulting in higher impedance. In the literature, polyaniline gas sensors have had response times of approximately 2 min (Kukla *et al.*, 1996, Jin *et al.*, 2001, Sutar *et al.*, 2007), and fast recovery times of 1 - 5 min (Sutar *et al.*, 2007). This was useful information going forward for complete device recovery. It was assumed if the devices were left for a longer period of time they would return to baseline levels. However, this was an issue as the final impedimetric measurement was taken immediately after the air purge because it has been seen in the literature that recovery times vary with concentration (Prasad *et al.*, 2005). It is important to note that variations in device response to ammonia were thought to be linked to the reproducibility of the devices produced. This issue needed to be solved if accurate blood ammonia determinations were to be carried out.

4.2.4. Sensor pre-calibration

Sensor reproducibility is a critical parameter in solving sensitivity issues. Pre-calibration is a method carried out to validate the eventual measurements of the devices in this case. This approach has been seen to improve sensor reproducibility (Moser and Jobst, 2013). To test the pre-calibration approach, three devices were pre-calibrated using a known concentration of ammonia (1 mM) prior to a range of calibration standards 5 days later. For the three devices tested the impedimetric response to ammonia was improved upon re-exposure from an average Z/Z_{air} of 3.8 to 4.2. Conversely, the statistical information available in Table 4.1 shows the deterioration of the baseline on day 5 compared with baseline impedance on day 1. It worsened from an average and relative standard deviation of 315 to 406 Ω and 9.0 to 10.2%, respectively.

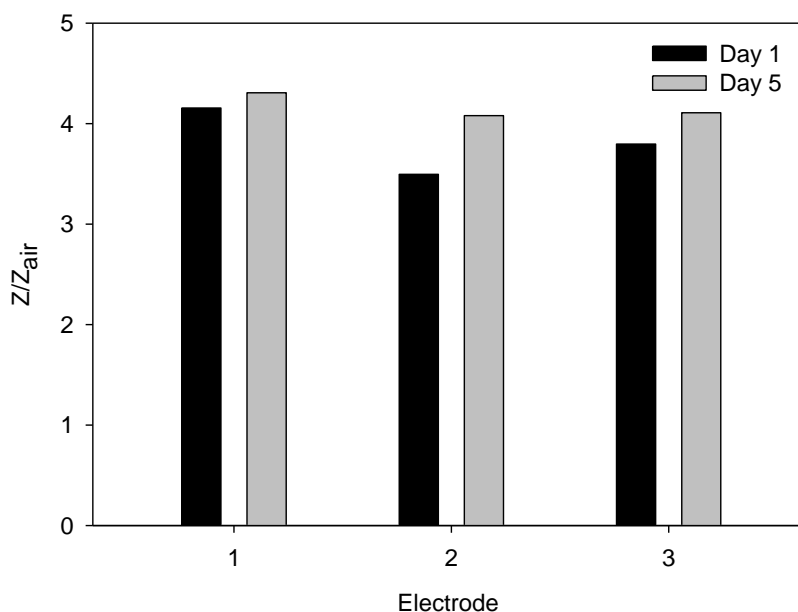


Figure 4.11. Impedance responses of 3 ammonia sensors to 1 mM ammonia in PBS pH 11.0 on day 1 and re-exposure of 1 mM ammonia on day 5.

Table 4.1. Statistical table of impedimetric results from ammonia sensors response to the effect of 1 mM ammonia re-exposure after 5 days.

Aqueous NH ₃ device	Z/Z_{air} Day 1	Z/Z_{air} Day 5	Z_{air} Day 1	Z_{air} Day 5
1	4.15	4.31	311	398
2	3.50	4.08	345	451
3	3.80	4.11	289	369
Average	3.82	4.16	315	406
SD	0.33	0.12	28.21	41.58
%RSD	8.65	2.98	8.96	10.24

This pre-calibration study allowed the reversible process of ammonia and polyaniline using atmospheric air to be studied. It was seen that leaving the electrodes for 5 days before re-exposing to ammonia them improved the impedimetric reproducibility of the response. It is not fully understood why the reproducibility of ammonia response of the devices is accompanied with an increase in baseline impedimetric variance after 5 days. It has been seen in the literature that the polyaniline interaction with ammonia is a reversible one that improves the reproducibility of the response over time. Reports of polyaniline coated multiwall carbon nanotubes showed good reproducibility and stability when repeatedly exposed to 75 ppm ammonia (He *et al.*, 2009). However, these reports of reversibility (Wu *et al.*, 2013, Hibbard *et al.*, 2013b) are contradicted by many researchers (Blighe *et al.*, 2012, Jin *et al.*, 2001, Sutar *et al.*, 2007). Prasad *et al.* (2005) observed some irreversibility at high concentrations of ammonia (150 ppm = 8.4 mM) and suggests this may be due to increased amount of chemisorbed ammonia which in turn enhances desorption rates and recovery. These issues are irrelevant for biomedical applications as these concentrations are not required.

It was evident from Fig. 4.11 that pre-calibration of the devices improved the reproducibility of the device response to ammonia. The time between pre-calibration and exposure was then optimised. To do this, devices were first exposed to 0.5 mM ammonia in PBS pH 11.0 and subsequently measured at two day intervals upon 0.5 mM ammonia re-exposure. The results are depicted in Fig. 4.12. They demonstrate

that device sensitivity to ammonia initially increased with re-exposure time until a decrease was observed for an interval of day 5 and beyond. Re-exposure of 0.5 mM ammonia on day 3 gave the best response to ammonia ($Z/Z_{air} = 3.4$), however resulted in one of the worst RSD values of 11.0%. Day 5 resulted in the best RSD (0.9%), see statistical information of Table 4.2.

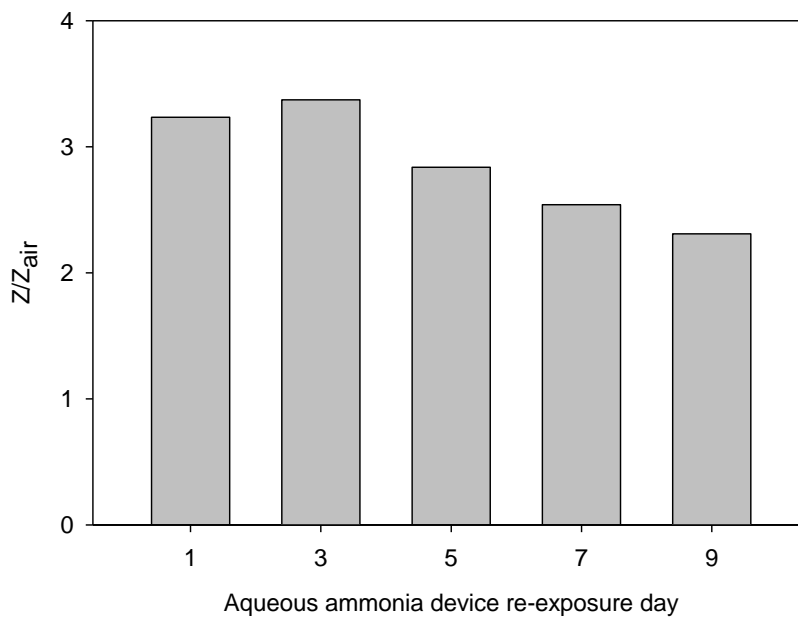


Figure 4.12. Ammonia sensors are pre-calibrated with, and re-exposed to 0.5 mM ammonia in PBS pH 11.0 on 2 day intervals ($n = 2$).

Table 4.2. Statistical data for increased re-exposure day of 0.5 mM ammonia in PBS pH 11.0 to ammonia sensors.

Re-exposure day	1	3	5	7	9
Average	3.23	3.37	2.84	2.54	2.31
SD	0.57	0.37	0.02	0.11	0.10
%RSD	17.78	10.96	0.86	4.50	4.29

The aim of this study was to find the optimal time between pre-calibration and re-exposure which would result in high ratiometric response but also good reproducibility. This study has shown an increase of Z/Z_{air} for re-exposure up to day 3, beyond this a decline is seen. Interestingly beyond this point, reproducibility improves. It could be thought that the response to ammonia would eventually

saturate with time. However, there are studies that quote the response lifetime of a polyaniline sensor as less than 7 hours (Blighe *et al.*, 2012). Contrastly, work carried out by Wu *et al.* (2000) demonstrated polyaniline film sensitivity to ammonia remained consistent over time up to 80 days. Combining knowledge from the pre-calibration study carried out it was decided for laboratory convenience pre-calibration of the sensors was carried out 7 days prior to subsequent exposure using 0.5 mM ammonia in PBS pH 11.0.

The optimised polyaniline modified sensing devices were then used to impedimetrically determine ammonia at the clinically relevant range of blood ammonia in a matrix of PBS pH 11.0. Ammonia pre-calibration was carried out using the optimised conditions as detailed above. In brief, the 0.5 mM ammonia as ammonium chloride was incubated with 5 M NaOH for 10 min on ice prior to 52 μL of sample volume being exposed to the sensing device for 15 min. The sample was removed from the device and 5 psi of air was passed through the headspace for 1 min before the sensor was impedimetrically assessed. This procedure was repeated 7 days later with the calibration concentrations (0, 25, 50, 100 and 200 μM) of ammonia. The relationship between ratiometric impedance (Z/Z_{air}) and ammonia concentration produced excellent linearity across the clinically relevant range. Data points including error bars are clearly distinguished, with an R^2 of 0.9868, a slope of 0.0043 and an intercept of 0.9562, statistical data is available in Appendix V. Physiological ammonia reference levels are between 11 and 50 μM . This demonstrated that the device was suitable for measurement of physiological concentrations of ammonia in a liquid sample.

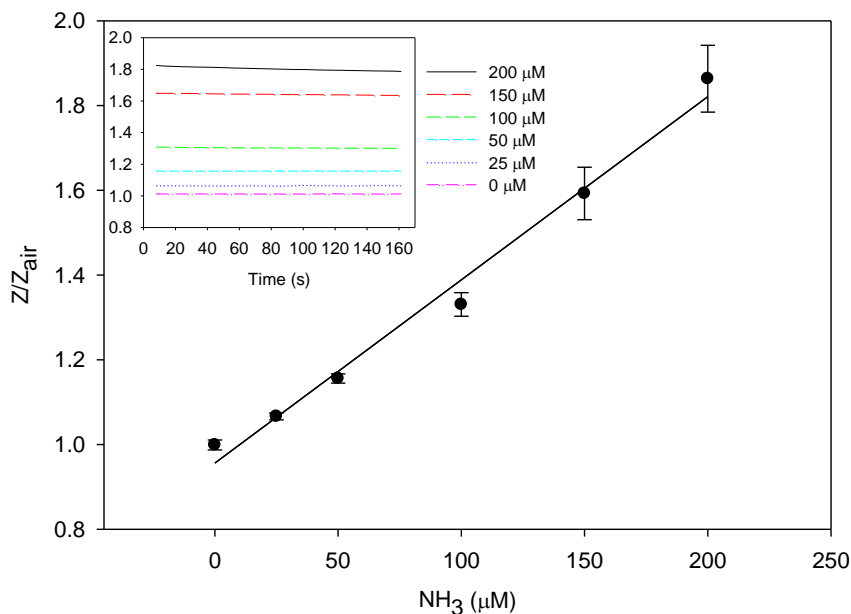


Figure 4.13. Measurement of ammonia in PBS pH 11.0 from 25 to 200 μM ($R^2 = 0.9868$, slope = 0.0043 and intercept = 0.9562 at $n = 3$) at 1 kHz.

4.3. CONCLUSION

The development and optimisation of a miniaturised aqueous ammonia device composed of inkjet-printed polyaniline nanoparticles was demonstrated. An aqueous dispersion of polyaniline was deposited over a silver IDE array using piezoelectric inkjet printing technique. These sensors in combination with a hydrophobic PTFE membrane created a platform for ammonia sensing in liquid sample. The developed device solved problems relating to the measurement of ammonia in physiological buffers. The device employs a pH change and an air purge. The pH change increased the availability of NH_3 while the air purge displaced solvent interferences from the gas headspace, leaving behind the residual ammonia response. This resulted in the final selective and sensitive measurement of ammonia.

The device was found to perform well in response to ammonia across the clinically relevant range with calibration plots obtained for 25 to 200 μM . Pre-calibration of the sensors was shown to improve the reproducibility of the response to ammonia. This work illustrated a low-cost, mass production method for ammonia devices with the potential of blood ammonia POC testing. Thus, the goal was then to isolate the impedimetric signal specific to ammonia from the common physiological interferences in blood. By combination of polyaniline-based silver electrodes and

Chapter 4

a.c. impedance, isolation and quantification of an ammonia signal in the necessary range is shown to be among the matrix of human blood.

4.4. REFERENCES

Atkins, P. and de Paula, J. (2009) *Physical Chemistry*. 9th ed. UK: Oxford University Press.

Ayyub, O.B., Behrens, A.M., Heligman, B.T., Natoli, M.E., Ayoub, J.J., Cunningham, G., Summar, M. and Kofinas, P. (2015) Simple and inexpensive quantification of ammonia in whole blood. *Molecular Genetics and Metabolism*. 115 (2-3), pp.95-100.

Barsotti, R. (2001) Measurement of ammonia in blood. *Journal of Pediatrics*. 138 (1), pp.S11-S19.

Blighe, F.M., Diamond, D., Coleman, J.N. and Lahiff, E. (2012) Increased response/recovery lifetimes and reinforcement of polyaniline nanofiber films using carbon nanotubes. *Carbon*. 50 (4), pp.1447-1454.

Budd, P.M. and McKeown, N.B. (2010) Highly permeable polymers for gas separation membranes. *Polymer Chemistry*. 1 (1), pp.63-68.

Chabukswar, V.V., Pethkar, S. and Athawale, A.A. (2001) Acrylic acid doped polyaniline as an ammonia sensor. *Sensors and Actuators B-Chemical*. 77 (3), pp.657-663.

Corrosion Resistant Products Ltd. (2016) *Permeation through Fluoropolymers*. Available from: <http://www.crp.co.uk/technical.aspx?page=199> .

Crowley, K., O'Malley, E., Morrin, A., Smyth, M.R. and Killard, A.J. (2008) An aqueous ammonia sensor based on an inkjet-printed polyaniline nanoparticle-modified electrode. *Analyst*. 133 (3), pp.391-399.

Dobler, L.J., Gibbons, J.M. and Evtodienko, V.Y. (2006) *Quick Acting Toxic Ammonia Test for Aqueous Samples* Hach Company US7033839 B1.

Fernandez-Sanchez, C., McNeil, C.J. and Rawson, K. (2005) Electrochemical impedance spectroscopy studies of polymer degradation: application to biosensor development. *Trac-Trends in Analytical Chemistry*. 24 (1), pp.37-48.

He, L., Jia, Y., Meng, F., Li, M. and Liu, J. (2009) Gas sensors for ammonia detection based on polyaniline-coated multi-wall carbon nanotubes. *Materials Science and Engineering B-Advanced Functional Solid-State Materials*. 163 (2), pp.76-81.

Hibbard, T., Crowley, K., Kelly, F., Ward, F., Holian, J., Watson, A. and Killard, A.J. (2013a) Point of Care Monitoring of Hemodialysis Patients with a Breath Ammonia Measurement Device Based on Printed Polyaniline Nanoparticle Sensors. *Analytical Chemistry*. 85 (24), pp.12158-12165.

- Hibbard, T., Crowley, K. and Killard, A.J. (2013b) Direct measurement of ammonia in simulated human breath using an inkjet-printed polyaniline nanoparticle sensor. *Analytica Chimica Acta*. 779 pp.56-63.
- Huizenga, J.R., Tangerman, A. and Gips, C.H. (1994) Determination of Ammonia in Biological-Fluids. *Annals of Clinical Biochemistry*. 31 pp.529-543.
- Jin, Z., Su, Y.X. and Duan, Y.X. (2001) Development of a polyaniline-based optical ammonia sensor. *Sensors and Actuators B-Chemical*. 72 (1), pp.75-79.
- Kapoor, Y., Bengani, L.C., Tan, G., John, V. and Chauhan, A. (2013) Aggregation and transport of Brij surfactants in hydroxyethyl methacrylate hydrogels. *Journal of Colloid and Interface Science*. 407 pp.390-396.
- Kukla, A.L., Shirshov, Y.M. and Piletsky, S.A. (1996) Ammonia sensors based on sensitive polyaniline films. *Sensors and Actuators B-Chemical*. 37 (3), pp.135-140.
- Li, X., Ju, M. and Li, X. (2004) Chlorine ion sensor based on polyaniline film electrode. *Sensors and Actuators B-Chemical*. 97 (1), pp.146-149.
- Lubentsov, B.Z., Timofeeva, O.N. and Khidekel, M.L. (1991) Conducting Polymer Interaction with Gaseous Substances .2. Pani-H₂o, Pani-Nh₃. *Synthetic Metals*. 45 (2), pp.235-240.
- Malinowska, E. and Meyerhoff, M.E. (1998) Influence of nonionic surfactants on the potentiometric response of ion selective polymeric membrane electrodes designed for blood electrolyte measurements. *Analytical Chemistry*. 70 (8), pp.1477-1488.
- Mondal, S.K. and Munichandraiah, N. (2006) The effect of low temperature treatment on electrochemical activity of polyaniline. *Journal of Electroanalytical Chemistry*. 595 (1), pp.78-86.
- Moser, I. and Jobst, G. (2013) Pre-Calibrated Biosensors for Single-Use Applications. *Chemie Ingenieur Technik*. 85 (1-2), pp.172-178.
- Munkholm, C. (2000) *Hydrophobic Fluorescent Polymer Membrane for the Detection of Ammonia*, Bayer Corporation.
- National Institute of Standards and Technology (2011) *Henry's Law Data for Ammonia*. Available from: <http://webbook.nist.gov/cgi/cbook.cgi?ID=C7664417&Mask=10> .
- Prasad, G.K., Radhakrishnan, T.P., Kumar, D.S. and Krishna, M.G. (2005) Ammonia sensing characteristics of thin film based on polyelectrolyte templated polyaniline. *Sensors and Actuators B-Chemical*. 106 (2), pp.626-631.
- Sing, R., Rumpf, B. and Maurer, G. (1999) Solubility of ammonia in aqueous solutions of single electrolytes sodium chloride, sodium nitrate, sodium acetate, and sodium hydroxide. *Industrial & Engineering Chemistry Research*. 38 (5), pp.2098-2109.

Subramanian, R., Crowley, K., Morrin, A. and Killard, A.J. (2013) A sensor probe for the continuous in situ monitoring of ammonia leakage in secondary refrigerant systems. *Anal. Methods*. 5 (1), pp.134-140.

Sutar, D.S., Padma, N., Aswal, D.K., Deshpande, S.K., Gupta, S.K. and Yakhmi, J.V. (2007) Preparation of nanofibrous polyaniline films and their application as ammonia gas sensor. *Sensors and Actuators B-Chemical*. 128 (1), pp.286-292.

Timmer, B., Olthuis, W. and van den Berg, A. (2005) Ammonia sensors and their applications - a review. *Sensors and Actuators B-Chemical*. 107 (2), pp.666-667.

Wang, J., Chan, S., Carlson, R.R., Luo, Y., Ge, G.L., Ries, R.S., Heath, J.R. and Tseng, H.R. (2004) Electrochemically fabricated polyaniline nanoframework electrode junctions that function as resistive sensors. *Nano Letters*. 4 (9), pp.1693-1697.

Wikol, M., Bailey, C., Lange, K., Sutsko, M. and Tronto, K. (2007) Expanded Polytetrafluoroethylene Membranes and their Applications. In: Meltzer, T.H.J., M.W., ed. (2007) *Filtration and Purification in the Biopharmaceutical Industry*. USA: CRC Press, pp.619-640.

Wongchoosuk, C., Jangtawee, P., Lokavee, S., Udomrat, S., Sudkeaw, P. and Kerdcharoen, T. (2012) Novel Flexible NH₃ Gas Sensor Prepared By Ink-Jet Printing Technique. *Biomaterials and Applications*. 506 pp.39-42.

Wu, S., Zeng, F., Li, F. and Zhu, Y. (2000) Ammonia sensitivity of polyaniline films via emulsion polymerization. *European Polymer Journal*. 36 (4), pp.679-683.

Wu, Z., Chen, X., Zhu, S., Zhou, Z., Yao, Y., Quan, W. and Liu, B. (2013) Enhanced sensitivity of ammonia sensor using graphene/polyaniline nanocomposite. *Sensors and Actuators B-Chemical*. 178 pp.485-493.

Yampolskii, Y. (2012) Polymeric Gas Separation Membranes. *Macromolecules*. 45 (8), pp.3298-3311.

Yoshikawa, H., Hino, T. and Kuramoto, N. (2006) Effect of temperature and moisture on electrical conductivity in polyaniline/polyurethane (PANI/PU) blends. *Synthetic Metals*. 156 (18-20), pp.1187-1193.

CHAPTER 5

CHARACTERISATION AND VALIDATION OF THE BLOOD AMMONIA SENSOR DEVICE

5.1. INTRODUCTION

There has been an increase in research efforts around electrochemical sensors for healthcare use. This increase is a result of population longevity demand and higher global mortality rates (Turner, 2013). Electrochemical sensing has demonstrated the capability of POC testing by providing accurate and rapid measurement in complex matrices such as blood. Together with mass producible fabrication techniques they are used to deliver inexpensive, disposable, single use sensors (Wang, 2006).

Earlier work in this thesis focused on the production of a printed polyaniline sensor. This sensor was then incorporated into a device capable of measuring ammonia in liquid samples. The work detailed in this chapter utilises the platform for ammonia measurements in buffer and applies it to serum. The developed device was also validated against a commercially available assay kit. Validation of any analytical method is a key requirement in ensuring reliability, traceability and compatibility of results (Isabel Lopez *et al.*, 2015).

5.1.1. Blood buffering capacity

The developed device incorporated a pH change of the PBS – a buffer which is designed to mimic the pH, ionic strength and buffering characteristics of physiological buffers in blood. Biological buffering systems strictly regulate blood pH at 7.4 (Good *et al.*, 1966). They each possess a characteristic buffering range. The buffering capacity of a system, β , is the ratio of incremental amount of acid or base added relative to the responding change in pH (Voet and Voet, 2004, Mohan, 2003).

There are numerous buffering systems in the body. The main two are the bicarbonate and phosphate systems. These work by utilising the hydrogen ion (H^+) to regulate systemic pH, which is one of the most tightly regulated systems in human physiology (Kellum, 2000). Proteins also play an important role in buffering systems. They act as proton donors and acceptors via functional groups and are abundant in the blood system (Ellison *et al.*, 1958). The buffering capacity of blood was a critical parameter to investigate with respect to the development of the blood ammonia device. During the evolution of the device sodium hydroxide was utilised

to induce a pH change (to pH 11.0). This was necessary to facilitate low level ammonia determinations. This pH change was developed in a phosphate buffered system which has three pKa values 2.12, 7.21, 12.31 (Mohan, 2003). This buffering system was capable of maintaining an alkaline pH. However, this is not the case for biological based systems which are strictly regulated around pH 7.4. The significant increase in pH may precipitate or degrade blood components.

A blood ammonia test does not have the capacity to identify an acid-base imbalance. It exclusively quantifies ammonia levels. The device developed in the study will act as a prompt for further investigations such as urinalysis, urine pH and blood gas analysis which would then indicate alkalosis.

5.1.2. Consideration of sample interferences

Moving from measurements in buffers to blood samples it was expected that the sample may contain additional interferences. Clinical laboratory analyses of blood samples are often affected by interferents. These interfering substances may arise from endogenous (e.g., haemoglobin, bilirubin, lipids, and proteins) and exogenous sources (e.g., drugs prescribed for the patient). Lipids are known to interfere with spectrophotometric analysis by turbidity, light scattering and volume displacement. Volume displacement caused by lipids may also affect analytical methods by displacing water, thereby giving rise to problems such as pseudo-hyponatremia (Kroll and Elin, 1994). Hyperlipidaemia is a condition in which there are elevated levels of lipids in the blood (Beaumont *et al.*, 1970). Lipoproteins typically range in size from 6 to 1,000 nm depending on the category (Nikolac, 2014). Hyperlipidaemia has been known to interfere with the determination of glucose, phosphorous, total bilirubin, uric acid and total protein (Kroll and Elin, 1994).

5.2. RESULTS AND DISCUSSION

5.2.1. Spectrophotometric analysis of ammonia in solution using the Berthelot reaction

A number of commercial ammonia quantification kits were considered for the purpose of validating the developed device, including Abcam®, PocketChem™, Sekisui, Sigma Aldrich® and Vitros® ammonia tests. The Abcam® Ammonia Assay Kit which utilises the Berthelot spectrophotometric reaction was chosen to validate the ammonia device because it is an enzyme-free method. This method was also specific and sensitive enough to reach the critically relevant range of blood ammonia testing. For further information on the Berthelot reaction, see Chapter 1, Section 1.2.

The Abcam® Ammonia Assay Kit was used in line with protocol instructions provided by the manufacturer. This is fully described in Chapter 2, Section 2.4.9. In brief, 100 µL of ammonia standards were prepared in 0.1 M PBS using the provided 1 mM ammonium chloride calibrator stock. To this, 80 µL of Assay Reagent 1 (nitroferricyanide, 2-phenylphenol) and 40 µL of Assay Reagent 2 (sodium hypochlorite) were added. The resulting blue colouration was measured spectrophotometrically at 650 nm after 30 min incubation at room temperature. A standard calibration curve was prepared for 25 to 200 µM ammonia at $n = 4$. This can be seen in Fig. 5.1, showing excellent reproducibility and linearity with a correlation of determination of 0.9989, a slope of 0.0038, intercept of 0.2628 and a RSD of 3.85%.

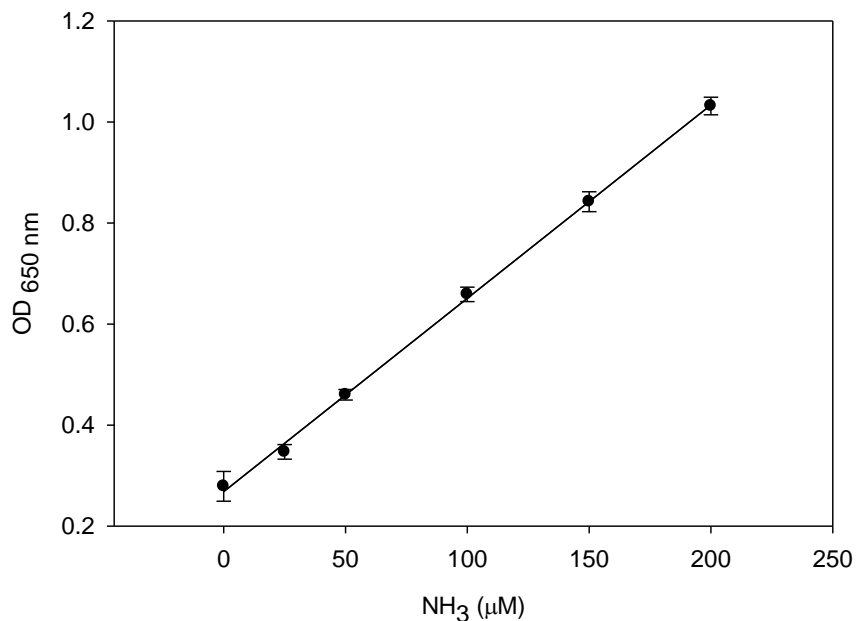


Figure 5.1. Spectrophotometric calibration of ammonia standards in PBS using the Abcam® ammonia assay ($n = 4$). $R^2 = 0.9989$, slope = 0.0038, intercept = 0.2628, RSD = 3.85%.

The Abcam® assay was capable of quantifying ammonia levels across the range of 25 to 200 µM in a buffer such as PBS. The Abcam® assay is an established method reporting a very low LOD (>10 µM) for ammonia determinations which may be conducted in complex matrices such as urine, serum, plasma and blood. This extremely reproducible result confirmed the assay as a credible validation method for the developed device.

5.2.2. Validation of the device using the Abcam® spectrophotometric assay

To assess the possibility of using the Abcam® assay to validate the device, both methods were exposed to a set of calibration standards (0 to 200 µM, ammonia in PBS at $n = 2$). The calibration standards were prepared using the 1 mM calibrator stock provided in the assay kit and were simultaneously exposed to both measurement methods. The correlation of both methods can be seen in Fig 5.2. This data shows excellent correlation of the two methods with a correlation coefficient of 0.9747, intercept of 0.6654 and slope of 1.1526, $p < 0.0001$.

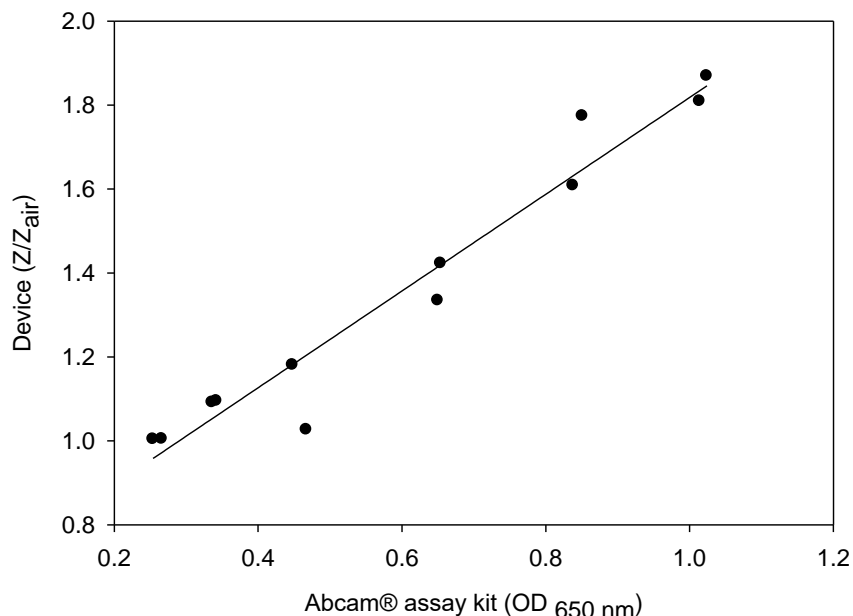


Fig.5.2. Correlation of the spectrophotometric and impedimetric responses of the ammonia calibration standards (sample size 6 at $n = 2$), $R = 0.9747$, intercept = 0.6654 and slope = 1.1526, $p < 0.0001$.

There was a good linear relationship between the device and the assay. The low p -value (< 0.0001) indicated there was little difference between both methods. This data established the Abcam® assay as a viable validation method. In order to assess the accuracy and precision of the developed device it was compared to the assay.

A set of calibration standards (0 to 200 μM , ammonia in PBS) were prepared using the 1 mM calibrator stock provided in the assay kit. Test samples (0 to 200 μM , ammonia in PBS) were also prepared in-house using ammonium chloride. The calibration standards and the test samples were analysed at $n = 2$ using the assay and the device. The spectrophotometric assay results are plotted in Fig. 5.3. A calibration curve with calculated 95% confidence intervals can be seen for the calibration standards. This is presented alongside the test sample measurements. The calibration curve for the calibrator standards demonstrated excellent correlation with a coefficient of determination of 0.9988, a slope of 0.0039 and an intercept of 0.2579. All data points lay within the 95% confidence intervals. The test samples also exhibited a linear tendency. However, they all lay outside the confidence intervals governed by the calibration standards. All test sample data lay above the upper

confidence interval. The test sample deviation from the calibration curve increased with concentration. This data shows there was a discrepancy between the calibrators and the test samples. The interpretation of this discrepancy is discussed below.

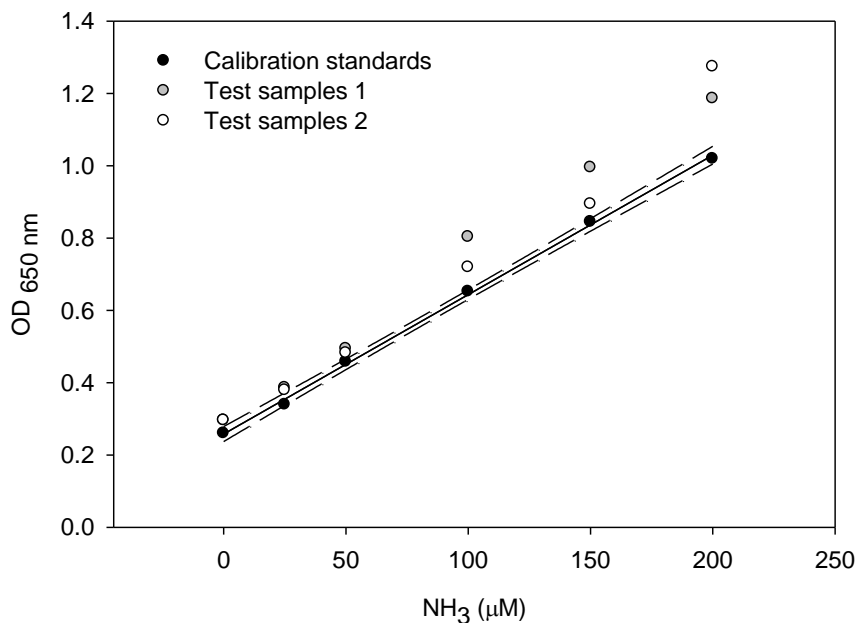


Figure 5.3. Comparison of 0 to 200 μM ammonia calibrator standards and test samples ($n = 2$) in PBS with spectrophotometric response using Abcam® assay measured at 650 nm. $R^2 = 0.9988$, slope = 0.0039, intercept = 0.2579 and 95% confidence intervals for calibration standards.

The same calibration standards and test samples used in the spectrophotometric assay were also measured impedimetrically using the device at approximately the same time. Ratiometric impedance (Z/Z_{air}) measurements were taken at 1 kHz and 5 mV amplitude. The results can be seen in Fig. 5.4 including the best fit line for the calibrators. A similar linear response with concentration as observed spectrophotometrically with the assay was seen impedimetrically using the device. The coefficient of determination was 0.9901 with a slope and intercept of 0.0044 and 0.9833, respectively. The ratiometric impedance responses of the test samples ($n = 2$) measured were also plotted on Fig. 5.4. The ratiometric response of the device exposed to the test samples increased linearly with concentration. Test samples deviated from the calibration curve with increasing concentrations. This tendency was also observed spectrophotometrically.

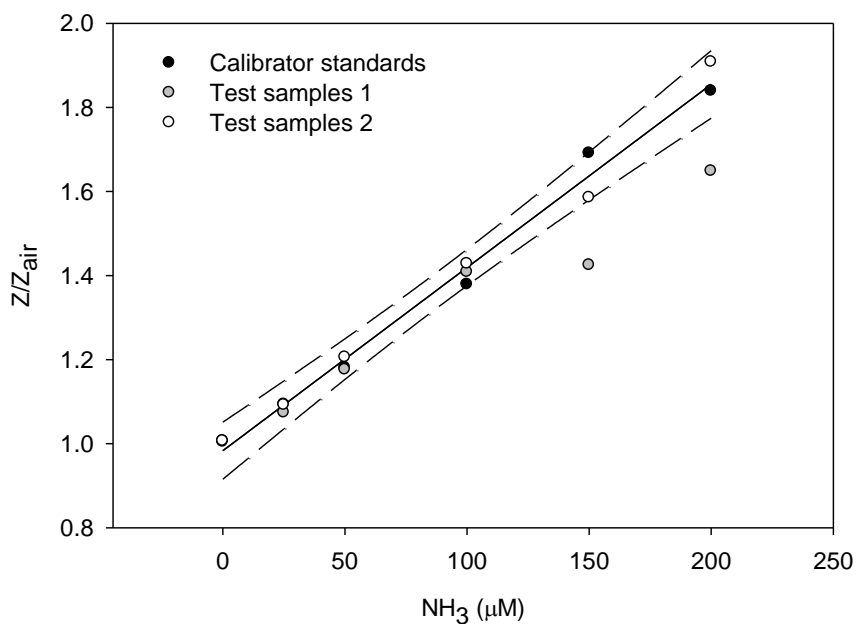


Figure 5.4. Ratiometric impedance responses of 25 to 200 μM ammonia of the calibrator standards and test samples ($n = 2$) in PBS measured at 1 kHz. $R^2 = 0.9901$, slope = 0.0044 and intercept = 0.9833 with 95% confidence intervals for calibrator standards.

Interestingly, the device tended to underestimate high ammonia concentrations, while the assay kit tended to overestimate at high concentrations. The response error associated with the device was larger compared to the assay kit. For the device, 83% of the test samples lay within the 95% confidence intervals as governed by the calibration standards. This can be compared with 0% for the assay, although the response errors for the calibrators were lower. As can be seen, there were significant differences in the behaviour of the calibrators and the test samples. Therefore, it may have been unfair to compare both standards as the errors observed may have been caused by them and not by the measurements. The 1 mM ammonia Abcam® calibrators were prepared in water, whereas the test samples made in-house were prepared in PBS pH 7.4. It was suspected that the calibrators contained stabilisers, but this was confirmed not to be the case by the manufacturer. This is surprising considering the expiry date was one year upon the date of purchase and it is well known that ammonia is volatile in solution.

In order to validate the device, the data from both methods were combined to statistically assess their correlation and agreement. The standard calibrations at $n = 2$ were used to investigate the true experimental concentration of the test samples. The relationship between the true experimental concentration values for each method can be seen in Fig. 5.5 as represented by (a) correlation and (b) Bland-Altman plots. A good correlative relationship was observed in Fig. 5.5 (a) for a test sample size of 6 at $n = 2$ with a correlation coefficient of 0.9679 and p -value of 0.0088. This correlation declined at higher concentrations with three data points outside the 95% confidence intervals. This was expected as both methods exhibited imprecision and inaccuracy for higher concentrations of ammonia. The slope and the intercept were 0.7017 and 3.4302, respectively. The Bland-Altman plot shown in Fig. 5.5 (b) presents the level of agreement between these two methods in measuring ammonia. Bland-Altman analysis also demonstrates a close agreement from 0 to 100 μM , but increasing lack of agreement and imprecision at higher concentrations.

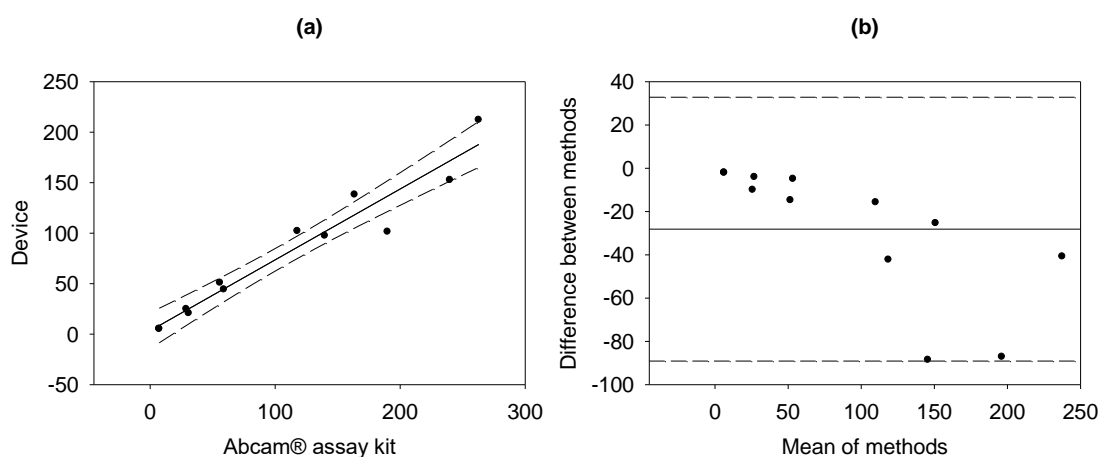


Figure 5.5. Statistical correlation and agreement of the test samples (sample size 6 at $n = 2$, with respect to the calibration plots generated using the calibration standards) between the Abcam® assay and the device as represented by (a) correlation plot with an $R = 0.9679$, slope = 0.7017, intercept = 3.4302, $p < 0.0088$ and (b) Bland-Altman plot at 95% confidence intervals.

The test samples used in these studies were prepared in-house. Calculated concentrations of the test samples (sample size 5 at $n = 2$) were compared to the experimentally determined values (as calculated from the calibration standards). This information is presented in Table 5.1 for both methods, along with their percentage difference. The largest difference of the device was $\sim 20\%$, while the largest

difference of the Abcam® assay was ~29%. The least difference was <1% for the device and was ~15% for the assay kit. Mean difference for the device was ~9% and 21% for the Abcam® assay.

Table 5.1. Percentage mean difference for $n = 2$ of the Abcam® assay kit and the developed device for the measurement of ammonia in PBS.

Calculated (μM)	Abcam®			Device		
	Found 1 μM	Found 2 μM	$M_{\text{Difference}}$ (%)	Found 1 μM	Found 2 μM	$M_{\text{Difference}}$ (%)
200	239.82	262.82	25.66	152.67	212.19	8.78
150	189.91	163.52	17.81	101.38	138.15	20.15
100	139.74	117.79	28.77	97.50	102.07	0.21
50	59.00	55.87	14.87	44.23	50.95	4.82
25	30.78	28.95	19.46	20.79	24.90	8.60
Mean			21.31			8.71

The device was more accurate in the determination of ammonia test samples (8.71). However, for $n = 2$ the spread of data was larger (as seen by the larger \pm values) than the assay measurements. The device measured ammonia as good as the reputable, commercially available Abcam® assay kit. The assay consistency overestimated the ammonia test sample concentrations, while the device consistently underestimated them (relative to the Abcam® calibrator standards). However, in general the underestimation of the device was far lower than the overestimation by the assay.

In conclusion, there was excellent correlation between the two methods using Abcam® calibrators. The statistical correlation and agreement between the methods for test samples (relative to the calibrators) was good. This affirmed the Abcam® assay as a validation method for the quantification of ammonia using the developed ammonia device. The assay results provided the knowledge of acceptable measurement errors for a commercial ammonia measurement kit. In comparison with these standards the device was seen to be more reproducible than the assay.

5.2.3. Interference study

The ammonia device showed potential for blood ammonia testing, having demonstrated acceptable accuracy and reproducibility in buffer test samples in comparison to the Abcam® assay. However, before the quantification of ammonia could be conducted in serum, the response of the device to a number of common potential electrochemical interferents was evaluated (Park, 2013, Mundaca-Uribe *et al.*, 2014, Nuttall *et al.*, 2003, Sutariya *et al.*, 2016, Liang *et al.*, 2015). Electroactive interferents including acetaminophen (600 μM) and ascorbic acid (100 μM) were assessed, along with ammonia-associated compounds such as creatinine (45 μM), glutamic acid (100 μM) and uric acid (500 μM) (Table 5.2). These interferents were introduced to the device and assessed across 0.1 Hz to 100 kHz frequency range in the manner previously described in Chapter 2, Section 2.4.8. The impedimetric responses of ammonia and the potential interferents can be seen in Fig. 5.6. The responses of interferents were comparable to background matrix effects of PBS which is typically found at ratiometric value (Z/Z_{air}) of 1. No distinguishable difference in response was observed between the electroactive species and ammonia-associated compounds. This was expected as these compounds are volatile. The results from this study suggested that the ammonia device was suitable for the selective determination of ammonia in the presence of potential interferents commonly found in blood and serum.

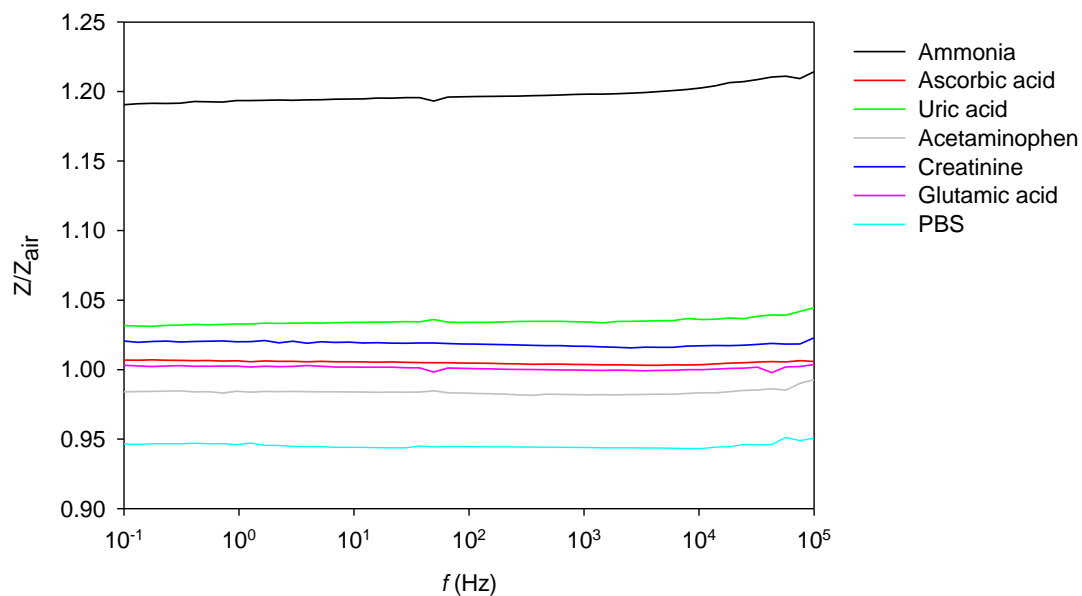
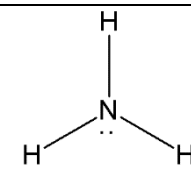
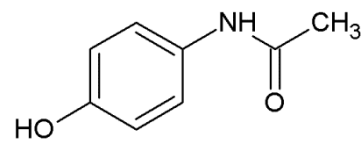
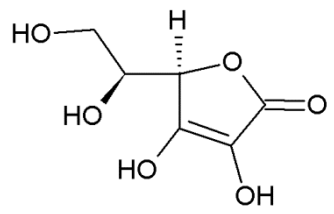
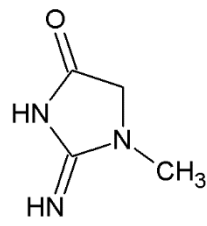
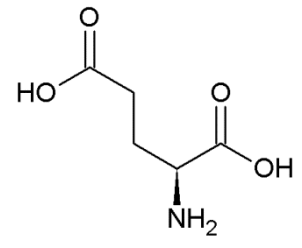
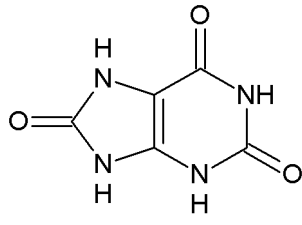


Figure 5.6. Selectivity of the device to ammonia (30 μM) in the presence of 1 M PBS and electroactive species such as acetaminophen (600 μM) and ascorbic acid (100 μM) as well as potential ammonia associated compounds such as creatinine (45 μM), glutamic acid (100 μM) and uric acid (500 μM) across a frequency range of 0.1 Hz to 100 kHz.

Table 5.2. Ammonia and the list of potential interferents analysed using the device, along with their ratiometric impedance (Z/Z_{air}) values.

Compound	μM	Z/Z_{air}	Structure
Ammonia	30	1.197	
Acetaminophen	600	0.983	
Ascorbic acid	100	1.005	
Creatinine	45	1.018	
Glutamic acid	100	1.001	
Uric acid	500	1.033	

The electroactive species trialled in this study may not have interfered due to the neutral bias potential of the polyaniline film being applied throughout all electrochemical impedance spectroscopic measurements. The measurement of electroactive species and ammonia associated compounds require the application of a voltage potential because they are redox active (Erden *et al.*, 2015, Yadav *et al.*,

2011, Barberis *et al.*, 2015, Girousi *et al.*, 2001, Zheng *et al.*, 2011). Polyaniline has been used to determine creatinine levels in urine in the presence of the enzyme creatinine deiminase (Shih and Huang, 1999). Glutamate has also been determined by utilising the glutamate dehydrogenase enzymatic reaction in combination with polyaniline/polypyrrole nanoparticles modified gold electrode in food produce (Batra *et al.*, 2014). This was not covered in the scope of this work, as it was considered to have been extensive, complex and costly at the stage of the device development. Compounds such as conjugated bilirubin (684 μM), unconjugated bilirubin (684 μM), plasma pyruvate (0.75 mM), plasma lactate (22.2 mM), intralipid (6.8 mM) may also be assessed as they have the potential to vary blood ammonia levels. The enzymes associated with the metabolism of these compounds, were not present in the PBS matrix and may not be present in blood as they are typically found in organs such as the liver.

5.2.4. Characterisation of sample matrix effects on ammonia measurement

5.2.4.1. Determination of ammonia in a protein sample matrix

Proteins may be anabolised (Sprinson and Rittenberg, 1949) or catabolised (Huizenga *et al.*, 1996) to utilise or release ammonia. Potentially, the presence of protein in a serum matrix may interfere with ammonia measurements. In order to investigate this, serum albumin (as BSA) was evaluated for its effect on the impedimetric measurement of ammonia. Albumin is a soluble monomeric protein that makes up half of the blood serum protein content (Voet and Voet, 2004). Albumin is only synthesised in the liver. It is important in transportation and has the capacity to bind to ammonia (Butterworth, 2003, Richards *et al.*, 1975).

In order to assess the effect of a protein matrix on the impedimetric determination of ammonia BSA was employed. BSA was prepared in PBS as per typical concentrations found in human blood (50 mg mL⁻¹) (Norde and Gage, 2004). This matrix was then spiked with 25 to 200 μM ammonia. Impedance measurements were then conducted using the device as described in Chapter 2, Section 2.4.8. Results can be seen in Fig. 5.7. A non-linear response was observed for ammonia determination in a protein matrix. The error associated with the protein measurement (0.08, $n = 3$) was more significant than those in PBS (0.03, $n = 2$) (Fig. 5.4). There were significant differences between the data generated for ammonia in protein and

the data generated in PBS. For example, there was an increased background signal (Z/Z_{air}) from 1.00 in PBS to 1.69 in protein. The statistical data for Fig. 5.7 is provided in Appendix VI. The slope of the line for ammonia in PBS was 0.0044, whereas, the slope of the curve for points 25 and 150 μM was 0.0058 and 0.0020, respectively. The slope was higher at lower concentrations and decreased with concentration. This was due to the production of ammonia in the protein sample, which if this trend was to progress would saturate the response.

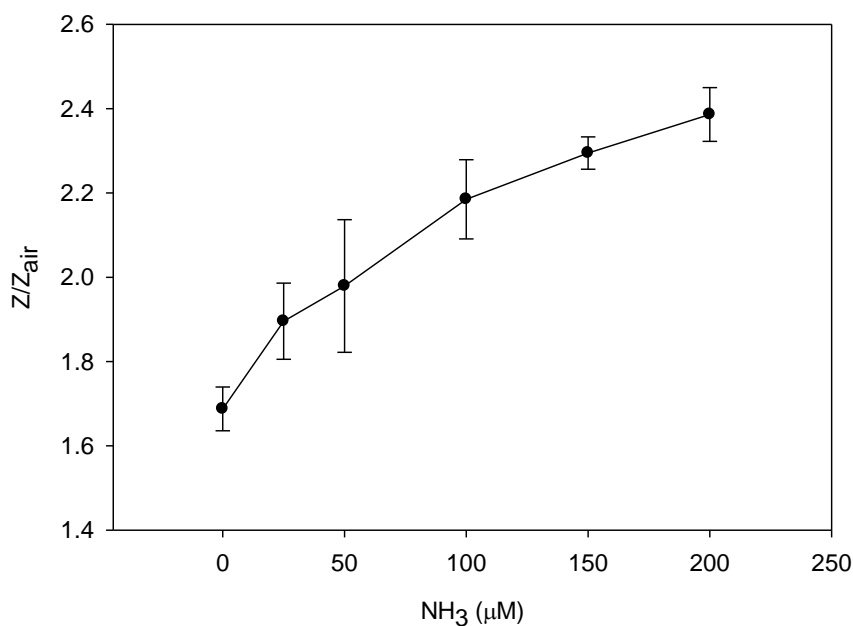


Figure 5.7. Impedimetric response of the device to 0 to 200 μM ammonia in BSA (50 mg mL^{-1} in PBS), slope = 0.0058 and 0.0020 for 25 and 150 μM ammonia at $n = 3$.

The increase in background signal observed for the measurement of ammonia in a protein matrix is believed to be caused by the disintegration of proteins into smaller molecules due to the alkaline environment of the experiments (Svedberg and Sjögren, 1930). Serum albumin is stable between pH 4 and 9. Outside of these regions, proteins may undergo irreversible and drastic conformational changes (Baler *et al.*, 2014). Alkaline conditions are known to cause decomposition of proteins, especially peptide bond cleavage and disulphide degradation (Manabe and Jin, 2005). The breakdown of proteins in the presence of NaOH is known as alkaline hydrolysis (Fountoulakis and Lahm, 1998). Upon hydrolysis an amide converts into a carboxylic acid and an amine or ammonia group. Protein associated ammonia may

then pass from the sample into the device to be measured. This was observed by an increased the background signal.

This data demonstrated that while there were increased challenges of reproducibility and non-linearity, the device did have the capacity to quantitatively measure ammonia in a protein matrix. In order to fully evaluate and understand the processes in a biological matrix that may alter the device response to ammonia, measurements were assessed in serum.

5.2.4.2. Ammonia analysis in serum

Serum is often used as a sample matrix for analytical measurements. It is studied in order to understand the matrix effect of blood when developing a POC device. It is obtained from coagulated blood, by inducing a fibrin clot to form along with blood cells. Coagulation factors are then separated by centrifugation from the remaining serum (Yu *et al.*, 2011). The remaining serum is a non-cellular fluid containing components such as proteins, electrolytes, lipids, and immune factors. The principal components of serum do not vary significantly between mammalian species (Spahr and Edsall, 1964). In this regard, bovine serum was used as a substitute for human serum for initial investigations of its effect on ammonia measurement.

In order to assess the effect of serum on ammonia measurement, foetal bovine serum (FBS) was spiked with ammonia (25 to 200 μM). The ratiometric response of ammonia in serum is plotted in Fig. 5.8. There was no relationship between ammonia concentration and impedance response. The response range for the concentrations studied in serum was between approximately 2.6 and 3.5 and was inconsistent with concentration. This may be considered as background noise associated with the measurement in a complicated matrix such as serum.

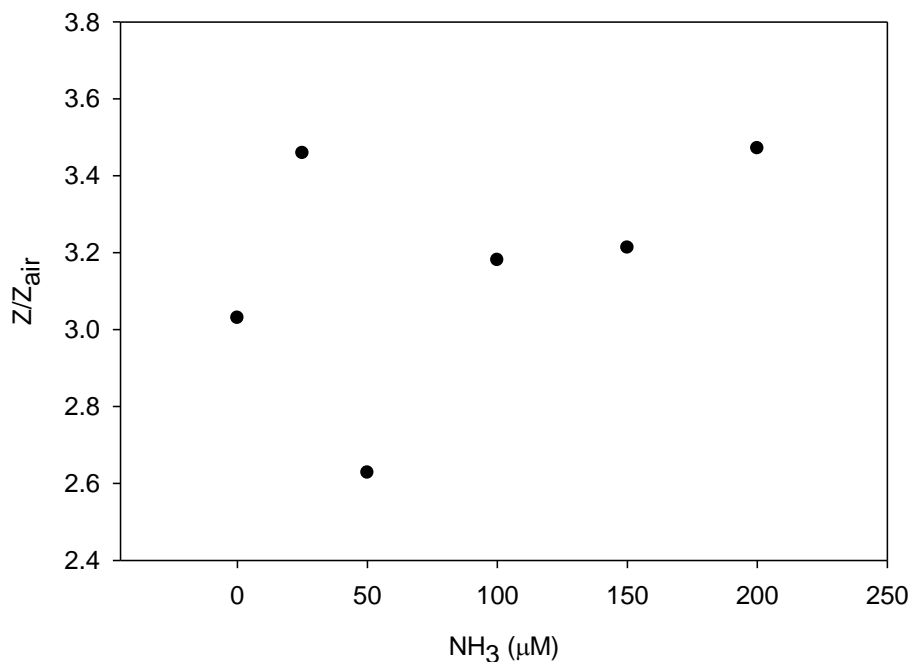


Figure 5.8. Impedimetric response of the ammonia device to ammonia (0 to 200 μM) in foetal bovine serum.

It can be seen for serum the background signal (0 μM ammonia) displayed a significantly high Z/Z_{air} response (3.03) when compared to those attained for ammonia concentrations studied in PBS and BSA (1.00 and 1.69, respectively). As discussed for the ammonia measurements conducted in BSA, there was a significant increase in background signal due to protein associated release of ammonia. This signal was higher for serum as it is a more complicated matrix. The fluctuated impedimetric response of the device with respect to ammonia in serum was not caused by a higher concentration of protein in the serum sample compared with the BSA sample. The protein content in the foetal bovine serum was 37.5 mg mL⁻¹, this was 50 mg mL⁻¹ in BSA.

In an attempt to understand this issue, the effect of the serum sample matrix on the response of the device and the assay was monitored over time. Measurements were made at varied time intervals (0, 5, 10, 15, 30, 60 min). The spectrophotometric and impedimetric response to the serum can be seen in Fig. 5.9. The impedimetric response was seen to increase significantly by a factor of 2.25 (Z/Z_{air} from 1.08 to 2.43) over the 60 min period. Considering the total analysis time of the device was 25 min (which included the time taken for the pH change and incubation time), the

impedimetric response in serum at this time point was 1.50, this increased to 2.43 after 60 min. An impedance response level in the range of 2.6 to 3.5 was observed for experiment conducted on serum which was spiked with 25 to 200 μM ammonia (Fig. 5.8). It is reasonable to conclude that it was ammonia being measured and therefore, being released in the control serum sample. The spectrophotometric data showed no change with respect to time, and responses ranged from 0.3076 to 0.3035 OD at 650 nm. The spectrophotometric data gathered was considered baseline levels for the typical spectrophotometric response of 0 μM ammonia with no ammonia associated colouration for the Berthelot reaction as previously observed in the PBS studies.

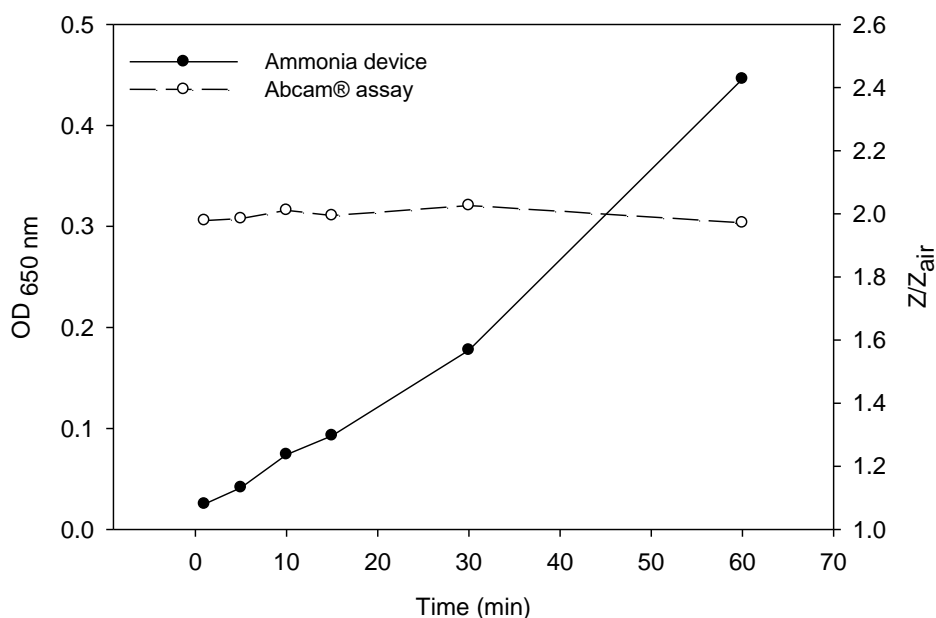


Figure 5.9. The effect of the incubation time of the serum sample matrix on the spectrophotometric response of the assay and the impedimetric response of the device.

The result of this study may be interpreted in two ways. Either the device was more sensitive than the assay to ammonia in serum or it was responding to something other than ammonia. Considering the latter, the PTFE membrane used in the device possessed a pore size of 0.2 μm , through which ammonia or any other constituents would have pass in order to interact with the polyaniline film. However, it is more probable that the device was reacting to ammonia produced during lipoprotein metabolism and/or degradation in the serum caused by the alkaline

measurement environment (Fountoulakis and Lahm, 1998). The spontaneous degradation of the proteins due to the alkaline environment has been discussed above in relation to the measurement of ammonia in a BSA protein matrix.

5.2.4.3. Spectrophotometric assessment of protein and lipid assay interference

Spectrophotometric measurement of ammonia in serum did not display the ammonia associated blue coloration of the Berthelot reaction. Therefore, an experiment was conducted to investigate the inhibition of the assay in serum. It is known that spectrophotometric assays such as the Abcam® assay are prone to protein interference. Abcam® recommends removing protein from biological samples with the use of a 10 kDa spin column when using this assay. Lipids are also known to interfere with spectrophotometric assays (Kroll and Elin, 1994). In the body, fatty acids are known to inhibit the urea cycle utilisation of ammonia. This inhibition is carried out on carbamoyl phosphate synthetase and glutamate dehydrogenase. Thus, the two main ammonia metabolism processes are inhibited by fatty acids contributing to a rise in systemic ammonia (Derr and Zieve, 1976). This rise in ammonia may be unpredictable and may result in false positive results in blood. It is possible that hyperlipidaemia may also interfere with the spectrophotometric measurement of ammonia. During a serum gas analysis study at the Academic Hospital of Verona, Italy, 11% out of a total of 478 serum samples were unsuitable for measurement due to hyperlipidaemia. This study denotes hyperlipidaemia as one of the most common interferences in blood analysis (Salvagno *et al.*, 2012). It has been recommended that hyperlipidaemic serum or plasma samples should be ultra-centrifuged at 100,000 to 200,000 × g before analysis (Nikolac, 2014). However, it has also been shown that a centrifugal force of 10,000 × g was just as efficient at removing lipid layer upon accumulation of large lipid particles (Dimeski and Jones, 2011).

Trichloroethanoic acid (TCA) is known to denature and precipitate proteins (Link and LaBaer, 2011). TCA was therefore employed to precipitate proteins and/or lipids that may be active in serum and potentially affecting ammonia assay measurement in serum. The precipitated protein would be removed via centrifugation using a Vivaspin column with a MWCO of 3 kDa. Scipac Ltd. supplied delipidated human serum which contained virtually no lipids (1 mg dl⁻¹).

TCA was added to both delipidated and lipidated sera at a concentration of 15%. Samples were then centrifuged using the spin filter at 3°C at a speed of $3005 \times g$ for 30 min in order to separate protein from the serum and measured using the assay ($n = 3$). The spectrophotometric results can be seen in Fig. 5.10. It can be seen that the only sample to show the typical Berthelot blue colouration indicating the presence of ammonia was the delipidated serum sample which had been centrifuged without the addition of TCA. The addition of TCA increased the turbidity of the samples which did not dissipate upon centrifugation at $3005 \times g$ using the 3 kDa spin filter column, and perhaps a larger centrifugal force was required to pellet the TCA precipitate. Turbidity caused by TCA may have inhibited the spectrophotometric assay. Both delipidated and lipidated serums without TCA displayed no visible turbidity.

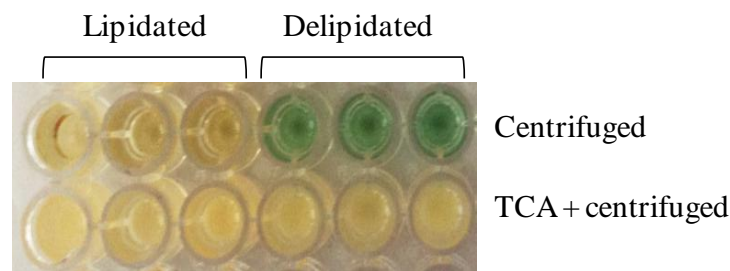


Figure 5.10. Spectrophotometric results of the Abcam® assay for delipidated and lipidated sera which were centrifuged using a 3 kDa spin filter at 3°C at a speed of $3005 \times g$ for 30 min with and without 15% (w/v) TCA ($n = 3$).

The delipidated centrifuged serum sample was treated identically to the lipidated serum. However, only the delipidated serum was spectrophotometrically active. As mentioned previously, lipid content is known to impede spectrophotometric determination of ammonia (Kroll and Elin, 1994). In this case, lipids were shown to not only interfere with, but completely inhibit the Berthelot ammonia response of the Abcam® assay even if the serum was deproteinated. Therefore, delipidated serum was used for further studies.

The centrifugation of delipidated serum was examined to ensure it was proteins that were removed during the process (Fig. 5.10). The Vivaspin column used during centrifugation had a MCWO of 3 kDa. High density lipoproteins and protein albumin have molecular weights of 435 and 69 kDa, respectively (Lodish *et*

al., 2000). Therefore they were retained in the upper phase. In order to investigate this, the presence of proteins along with residual lipids and cell debris were examined. Oil Red O staining for cellular lipids and a Bradford protein assay were carried out on the delipidated serum (a) before, and after centrifugation (the (b) pellet and (c) supernatant). Results from the Oil Red O staining were examined under a light microscope and showed no staining for all three samples. Oil Red O stains cellular lipids and serum is a non-cellular matrix which in this case was also lipid free. After centrifugation, the Bradford protein assay (Fig. 5.11) revealed the supernatant contained no measurable protein. The BSA calibration curve had a coefficient of determination of 0.9601, a slope of 294.2262 and an intercept of 38.0357. The equation of the line was used to calculate the concentration of protein in the delipidated serum (a) before and after ((b) pellet and (c) supernatant) centrifugation. These values were calculated to be (a) 4.17, (b) 4.19 and (c) $-0.18 \mu\text{g} \mu\text{L}^{-1}$, respectively. This demonstrated that the centrifugation step with a 3 kDa cut off filter removed protein in delipidated serum.

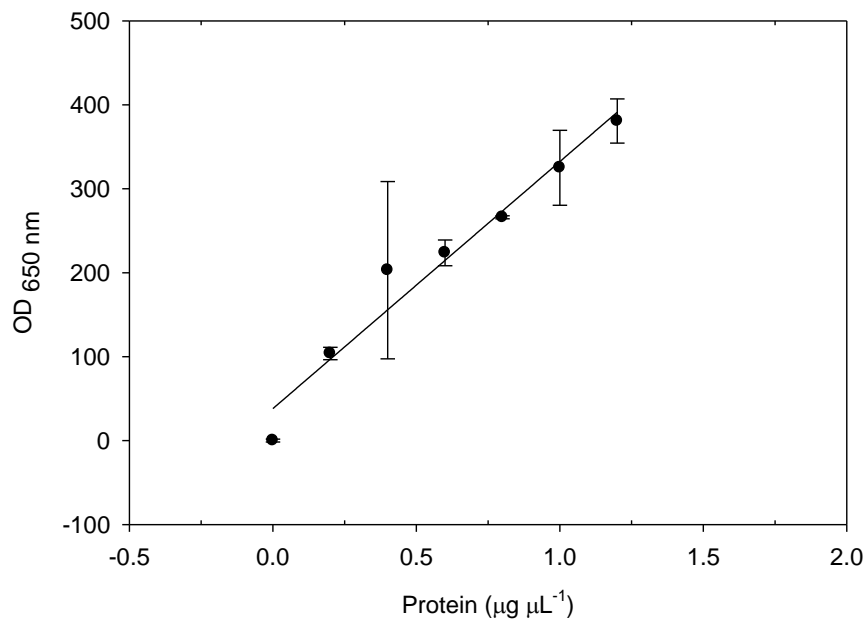


Figure 5.11. Bradford protein assay standard calibration using BSA ($n = 3$).

In conclusion, TCA was unsuccessful at permitting the spectrophotometric measurement of ammonia. Although it may have been successful in removing lipoprotein, the turbidity of the sample prevented the spectrophotometric measurement. Centrifugation of delipidated serum with a spin filter column was

successful in removing protein as confirmed by Bradford protein analysis. Spectrophotometric measurement of ammonia using the Abcam® assay kit was affected by protein and lipids. This can be compared to the ammonia device which was shown to be affected by protein and lipids.

5.2.4.4. Delipidated and deproteinated serum as a matrix for ammonia determination using the ammonia device

Protein appeared to passively affect the device via absorption or blocking diffusion of ammonia. However, measurements in lipids affected the device in a different way. They appeared to actively affect the measurement, changing the response over time caused by protein metabolism and/or degradation. The impact of protein on the device was assessed using delipidated serum. There was no relationship between the impedimetric response of the device and the concentration of ammonia in the delipidated serum, See Appendix VII. This proved that not only were lipids interfering with the device measurement but it was also the increasing number of complex proteins in a serum sample.

Delipidated serum samples were deproteinated by centrifugation at 3°C for 30 min at a speed of $3005 \times g$ with the use of a 3 kDa cut off column. This delipidated protein free serum was then spiked with Abcam® ammonia calibrator stock in order to prepare a set of calibration standards (25 to 200 μM) at $n = 3$. Simultaneously, the same delipidated protein free serum was spiked with ammonia test samples prepared in-house at $n = 3$. These sets of standards were measured impedimetrically using the device and also spectroscopically with the Abcam® assay (Fig. 5.12). Excellent linearity (0.9984) was obtained for the ratiometric impedance response of the calibrator standards (Fig. 5.12 (a)). A slope of 0.0046 and an intercept of 1.1534 were attained. RSD values ranged from 4.03 to 6.61% for 25 - 200 μM ammonia, respectively. The Abcam® calibration curve for the same calibration standards, seen in Fig. 5.12 (b), also showed excellent linearity (0.9780) with a slope and intercept of 0.0031 and 0.4162, respectively. RSD values ranged from 10.26 to 1.84% for 25 to 200 μM ammonia. This demonstrated inherent error across all concentrations of ammonia calibration standards unlike the device which displayed increasing irreproducibility with increasing concentration. Comparing the impedimetric and spectrophotometric calibrations obtained in delipidated serum with

those in PBS under the same conditions (Figs. 5.3 and 5.4), both sets of calibrations were in approximately the same response range ($Z/Z_{air} = 1.0$ to 2.0 and $OD = 0.4$ to 1.0). Full statistical information can be found in Tables 5.4 and 5.5.

Fig. 5.12 (a and b) also show impedimetric and spectroscopic responses of ammonia test samples which were prepared in-house, sample size five at $n = 3$. Both the device and the assay kit overestimated the test samples.

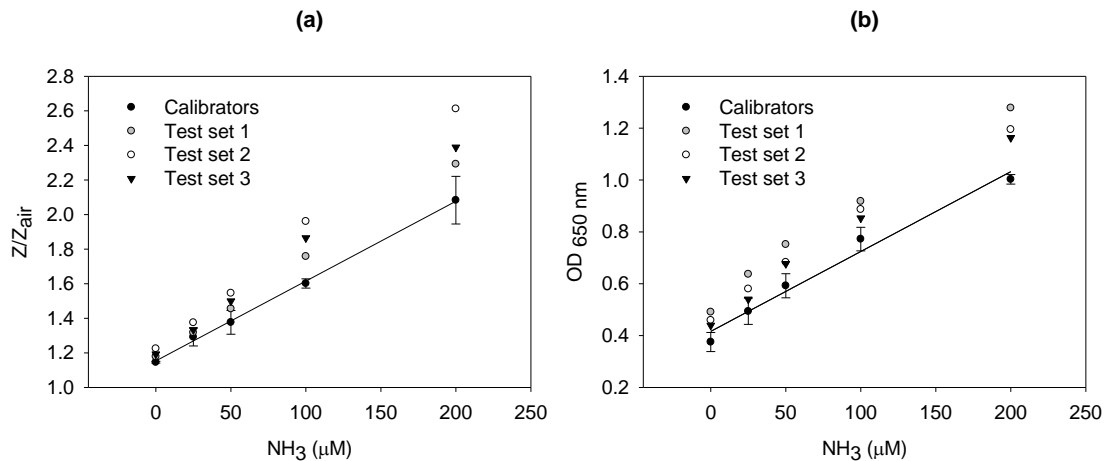


Figure 5.12. (a) Impedimetric and (b) spectrophotometric results of ammonia standards (25 to 200 μM) in delipidated serum calibration curves ($n = 3$) and test samples ($n = 3$). Equation of lines for the calibrations were as follows (a) $R^2 = 0.9984$, slope = 0.0046, intercept = 1.1534 and (b) $R^2 = 0.9780$, slope = 0.0031, intercept = 0.4162.

The correlation of both methods for calibration standards (sample size 5 at $n = 3$) measured is shown in Fig. 5.13. This shows excellent correlation (0.9699 , $p < 0.0001$) between the device and the Abcam® assay, along with a slope and intercept of 0.5631 and 1.4472, respectively. The low p -value (< 0.0001) indicated there was little difference between both methods for measurements in serum.

Table 5.4. Detailed impedimetric analytical data of the device in response to calibrator standards and test samples in delipidated serum.

NH ₃ (μ M)	Calibrator 1	Calibrator 2	Calibrator 3	Calibrator Mean	Calibrator SD	Test 1	Test 2	Test 3	Test Mean	Test SD
200	2.14	2.18	1.93	2.08	0.14	2.29	2.61	2.39	2.43	0.16
100	1.57	1.63	1.60	1.60	0.03	1.76	1.96	1.86	1.86	0.10
50	1.42	1.41	1.30	1.38	0.07	1.46	1.55	1.50	1.50	0.05
25	1.35	1.29	1.24	1.29	0.05	1.32	1.38	1.33	1.34	0.03
0	1.14	1.15	1.14	1.15	5.2×10^{-3}	1.18	1.22	1.19	1.20	0.02

Table 5.5. Detailed spectroscopic analytical data of Abcam® assay in response to calibrator standards and test samples in delipidated serum.

NH ₃ (μ M)	Calibrator 1	Calibrator 2	Calibrator 3	Calibrator Mean	Calibrator SD	Test 1	Test 2	Test 3	Test Mean	Test SD
200	1.02	1.00	0.99	1.00	0.02	1.28	1.20	1.16	1.21	0.06
100	0.82	0.77	0.73	0.77	0.05	0.92	0.89	0.85	0.89	0.04
50	0.64	0.58	0.55	0.59	0.05	0.75	0.68	0.68	0.70	0.04
25	0.54	0.51	0.44	0.49	0.05	0.64	0.58	0.54	0.59	0.05
0	0.38	0.41	0.34	0.38	3.7×10^{-2}	0.49	0.46	0.44	0.46	0.03

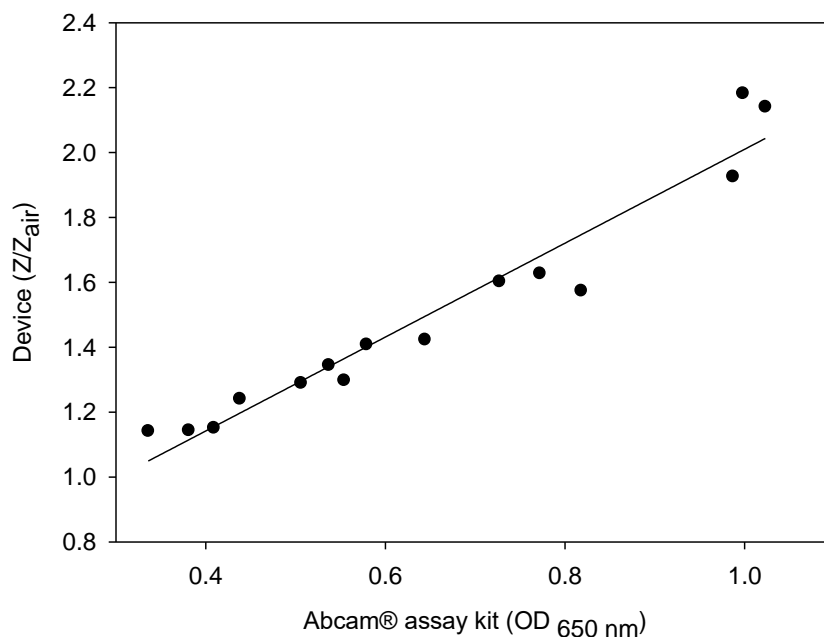


Figure 5.13. Correlation of the spectroscopic and impedimetric responses of ammonia calibration standards (sample size 5 at $n = 3$). $R = 0.9699$, intercept = 0.5631 and slope = 1.4472 , $p < 0.0001$.

Full validation of the ammonia device with the Abcam® assay was then conducted in the same way as previously performed for ammonia in PBS. In brief, the linear regressions obtained from the calibration standards were used to determine ammonia concentrations for the test samples. These calculated concentrations of ammonia for both methods were plotted against each other for comparison with 95% confidence intervals (see Fig. 5.14 (a)). The correlation between both methods was good across the concentration range ($R = 0.9642$, $p < 0.7312$), with a slope and intercept of 1.1031 and -14.1310, respectively. This correlation was lower than that in PBS (0.9679) with five samples lying outside of the 95% confidence intervals. The statistical agreement between the ammonia device and the Abcam® assay in delipidated serum was then analysed using Bland-Altman analysis with 95% confidence intervals (Fig. 5.14 (b)). This shows a strong agreement at lower concentrations of ammonia, with results increasing in a sporadic pattern above 100 μM along with one sample lying outside of the 95% confidence intervals.

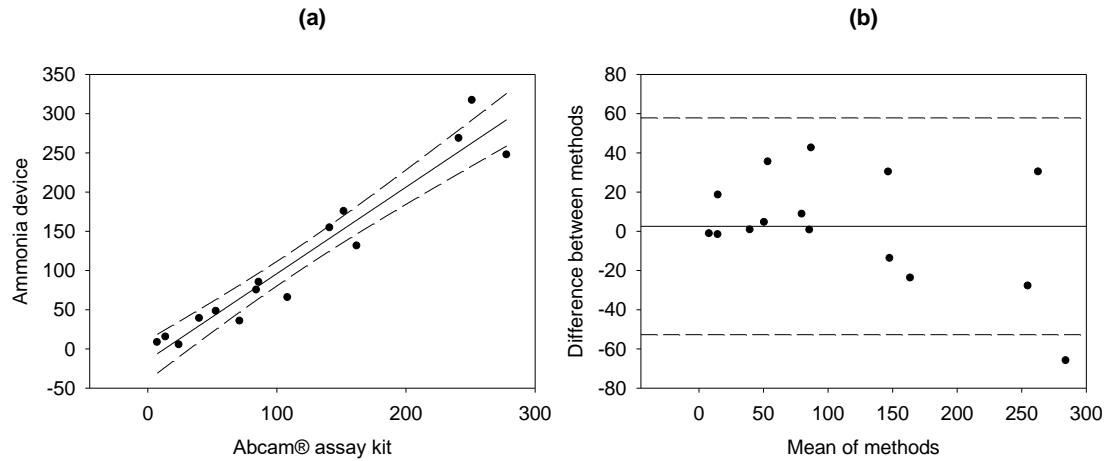


Figure 5.14. Correlative and Bland-Altman analysis of ammonia measurement in the Abcam® assay kit and the device as represented by (a) scatter plot with an R of 0.9642, a slope of 1.1031, an intercept of -14.1310, $p < 0.7312$ and (b) Bland-Altman plot at 95% confidence intervals.

The response of the test samples as determined by both methods was compared with the calculated values of ammonia. The true experimental concentration for the test samples was known as they were prepared in-house and denoted as test samples for the sake of method validation. The difference between the experimental values and the calculated values is shown in Table 5.6 as percentage difference. The biggest difference of the assay was 119%, while the biggest difference for the device was 64%. The least difference for the assay was 28%, while the best for the device was 39%. The mean difference for the assay and the device was 71% and 52%, respectively.

Table 5.6. Percentage difference of ammonia in serum as measured using the Abcam® assay and the developed ammonia device for $n = 3$.

Abcam®		Device				
Calculated (μM)	Found μM		Difference (%)	Found μM	SD	Difference (%)
200	256.68	35.63	28.33	277.80	19.15	38.90
100	151.52	22.06	51.52	153.90	10.49	53.90
50	92.81	9.80	85.61	75.43	13.44	50.87
25	54.63	6.46	118.53	41.00	15.72	64.00
Mean		18.49	71.00		14.70	51.92

The assay was less accurate in the determination of ammonia test samples in serum (71.00 difference) than the device (51.92 difference). For $n = 3$, the spread of data measured with the assay was larger (18.49) than the device measurements (14.70). This data can be compared with Table 5.1 for a similar experiment in PBS. The accuracy and precision of both methods decrease significantly when measuring in serum. This is due to the nature of the serum which is a complex matrix.

The ammonia device was successfully validated in delipidated centrifuged serum using the Abcam® assay. It was evident from the results that the ammonia device when measuring in un-processed serum suffered from poor accuracy and precision. This was overcome by an investigation of the matrix effects and thus, pre-treating the serum sample in a way to prevent interferences. The device developed was just as good as the Abcam® assay at determining serum ammonia concentrations. It also competes with other kits and devices available on the market. Table 5.7 lists the detailed analytical specifications of these kits and devices. It can be seen that the LOD and range of the developed device was comparable with all listed. The sample volume and operating temperature was also comparable. The major limitations of the device were the need for sample preparation and analysis time. The analysis time is comparable to the Abcam® and Sigma Aldrich® kits. This time may be reduced with further studies and optimisations of the device.

Table 5.7. Analytical performance characteristics of a range of commercial kits and devices for ammonia

Product Name	Technique	LOD (μM)	Range (μM)	Analysis Time (min)	Sample Volume (μL)	Operational Temperature ($^{\circ}\text{C}$)	Refs
Device	EIS	12	25-200	25	52	RT	Current work
PocketChem™ BA and ammonia test kit II	Berthelot	Not specified	2-285	~6	20	10-35	(Arkray, 2016)
Vitros® Chemistry Products AMON Slides	Berthelot	Not specified	8.7-500	5	10	37	(Ortho-Clinical Diagnostics Inc., 2015)
Abcam® Ammonia Assay Kit - Modified Berthelot	Berthelot	>10	Not specified	30	100	37	(Abcam Plc., 2016)
Sekisui Ammonia L3K®	Enzymatic	4.1	8.8-1174	Not specified	Not specified	Not specified	(Sekisui Diagnostics (UK) Ltd., 2013)
Sigma Aldrich® Ammonia Assay Kit	Enzymatic	12	12-881	20	10-200	18-35	(Sigma-Aldrich Co. LLC., 2015)

5.2.5. Lifetime study of the blood ammonia device

To assess the lifetime of the device, twelve devices were stored each at (a) under ambient conditions, (b) in a desiccator and (c) in a vacuum desiccator for a five month period. Impedance baselines at 1 kHz in air were recorded every month (Fig. 5.15). It can be seen for devices stored under ambient conditions with an initial average baseline impedance of 826 Ω (RSD = 6.8%, $n = 12$), they remained relatively stable until month three from then on baselines began to increase from approximately 790 to 1300 Ω in month five. This pattern may relate to initial absorption of water vapour, followed by hydrolytic decomposition of the polymer, or as a result of absorption of atmospheric contaminants causing film deprotonation. The desiccator and vacuum desiccator retained devices near to their initial baselines. The total RSD over the five month period for the desiccators and vacuum desiccators was 0.64 and 0.77%, respectively.

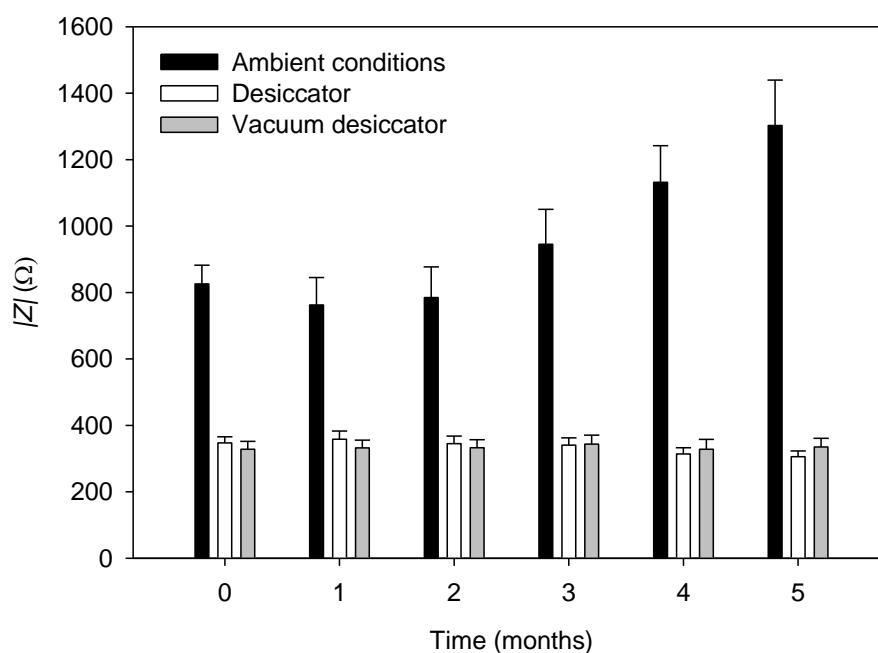


Figure 5.15. Lifetime study of the ammonia devices stored at (a) ambient conditions, in a (b) desiccator and (c) in a vacuum desiccator, each at $n = 12$.

This study shows that moisture followed by oxygen had a significant impact on the device baseline. For storage purposes, the ammonia devices were then kept in vacuumed sealed bags with added desiccant.

To evaluate the impact of storage on the response of the device to ammonia, devices at $n = 3$ were stored in a desiccator and their impedance response to air or ammonia at 1 mM was impedimetrically measured every four days for 21 days at 1 kHz. The response to ammonia grew upon day 0 from Z/Z_{air} 1.04 to an average of 3.33 for days 5 to 21 (Fig. 5.16 (b)). The response above day five was not reproducible with an overall RSD of 10.16%. After storage, the devices shifted to a new level of sensitivity. Beyond this shift there were fluctuations which remained within a range. This may have been a systematic bias due to the measurement procedure on day 0. However, a similar effect was seen during the development of the pre-calibration method chosen for device use (Chapter 4, Section 4.2.4). It may be that aging of the device shifts them to a higher sensitivity. The ratiometric response of PBS remained reproducible over the same time period with an overall RSD of 5.49% (Fig. 5.16 (a)).

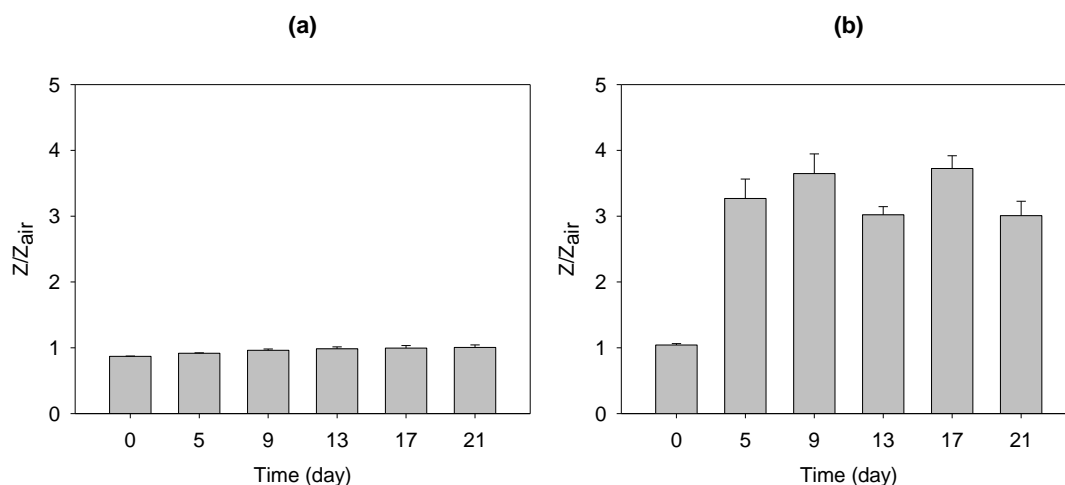


Figure 5.16. Ratiometric impedance response lifetime of the ammonia device to (a) 0 and (b) 1 mM ammonia exposure ($n = 3$) following storage in a desiccators for up to 21 days.

The response beyond day five was reproducibly above that of day 0. A larger sample size would need to be studied before a conclusive statement of ammonia determining behaviour on aging device could be made. These results show that waiting at least five days prior to impedimetrically determining ammonia with the device would result in higher response. A future study may be conducted to compare leaving the devices for five days in a desiccated storage prior to measurement with the current pre-calibration method used with the device.

5.3. CONCLUSIONS

The work presented and discussed in this chapter has shown that ammonia can be reliably determined in a PBS matrix at the clinically relevant range of 11 to 50 μM . This work has been validated using the Abcam® assay kit using calibrators (sample size 6 at $n = 2$) from the kit which resulted in a correlation of 0.9747, $p < 0.0001$, and a slope of 1.1526. Test samples were then prepared in-house and compared to the calibrator results. This was presented as statistical correlation (0.9679, $p < 0.0088$ with a slope of 0.7017) and Bland-Altman agreement which demonstrated a close agreement at low concentrations which decreased with concentration. Mean difference of the device (~9%) was better than the assay (21%) when comparing test samples with the calibrator samples.

Matrix studies showed ammonia could be successfully determined by the device in a simple protein matrix, albeit with associated errors and non-linearity. The assessment of ammonia in serum revealed that while common small molecule interferences present in serum did not affect the measurement, more complex protein and lipids did. The deterioration of the impedimetric ammonia response in increasing complex matrices was understood to be caused by the cleavage of protein due to the alkaline environment of the measurement and the lipid content. The Abcam® assay suffered from similar effects caused by proteins and lipids. It was necessary to remove both proteins and lipids in order to impedimetrically and spectrophotometrically measure ammonia.

This was achieved by attaining delipidated serum which was centrifuged using a 3 kDa spin filter column which removed proteins from the lipid free serum. A good correlation (0.9699, $p = 0.0001$ with a slope of 1.4472) was attained between impedance of the device and the spectrophotometric absorbance of the assay in response to ammonia in delipidated, deproteinated human serum (sample size 5 at $n = 3$). Correlation and Bland-Altman analysis between both methods was carried out. This demonstrated a correlation of 0.9642, $p < 0.7312$ and a slope of 1.1031 with disagreement between the methods increasing with ammonia concentration. Mean accuracy of the assay (71%) was worse than the device (52%) for human serum analysis. This demonstrated the developed device outperformed a commercial assay based on a robust spectrophotometric reaction for ammonia. The assay provided

acceptable standards required for a POC ammonia device. In order for the device to achieve these standards in whole serum, extensive matrix assessments and POC integrations are required. Microfluidic technologies have been exploited to integrate sample preparation on lab-on-a-chip systems (Labuz and Takayama, 2014). A blood based systems like the one developed in this study may be combined with a microvortex. The principles of microvortices are based on balanced sheer gradient and wall effect forces which creates vortices capable of trapping large particles in blood (Mach *et al.*, 2011). This technology may be incorporated into a blood ammonia device to remove protein and lipids prior to the impedimetric measurement of ammonia.

The lifetime of the devices did not change over a period of five months when stored in a desiccator. However, the response to ammonia was shown to change with aging devices. This study need to be repeated with increased number of devices over a longer period of time. It also indicated that devices should be stored in vacuum packed bags with added desiccant.

5.4. REFERENCES

Abcam Plc. (2016) *Ammonia Assay Kit - Modified Berthelot - (Colorimetric) (ab102509)*. Available from: <http://www.abcam.com/ammonia-assay-kit-modified-berthelot-colorimetric-ab102509.html>.

Arkray, I. (2016) *Blood Ammonia Meter PocketChem BA PA-4140*. Available from: <http://www.arkray.co.jp/english/products/pdf/pa4140.pdf>.

Baler, K., Martin, O.A., Carignano, M.A., Ameer, G.A., Vila, J.A. and Szleifer, I. (2014) Electrostatic Unfolding and Interactions of Albumin Driven by pH Changes: A Molecular Dynamics Study. *Journal of Physical Chemistry B*. 118 (4), pp.921-930.

Barberis, A., Spissu, Y., Fadda, A., Azara, E., Bazzu, G., Marceddu, S., Angioni, A., Sanna, D., Schirra, M. and Serra, P.A. (2015) Simultaneous amperometric detection of ascorbic acid and antioxidant capacity in orange, blueberry and kiwi juice, by a telemetric system coupled with a fullerene- or nanotubes-modified ascorbate subtractive biosensor. *Biosensors & Bioelectronics*. 67 pp.214-223.

Batra, B., Kumari, S. and Pundir, C.S. (2014) Construction of glutamate biosensor based on covalent immobilization of glutamate oxidase on polypyrrole nanoparticles/polyaniline modified gold electrode. *Enzyme and Microbial Technology*. 57 pp.69-77.

Beaumont, J.L., Carlson, L.A., Cooper, G.R., Fejfar, Z. and Fredrickson D S Srasser, T. (1970) Classification of Hyper Lipidemias and Hyper Lipo Proteinemias. *Bulletin of the World Health Organization*. 43 (6), pp.891-915.

Butterworth, R.F. (2003) Hepatic encephalopathy - A serious complication of alcoholic liver disease. *Alcohol Research & Health*. 27 (2), pp.143-145.

Derr, R.F. and Zieve, L. (1976) Effect of Fatty-Acids on Disposition of Ammonia. *Journal of Pharmacology and Experimental Therapeutics*. 197 (3), pp.675-680.

Dimeski, G. and Jones, B.W. (2011) Lipaemic samples: Effective process for lipid reduction using high speed centrifugation compared with ultracentrifugation. *Biochemia Medica*. 21 (1), pp.86-92.

Ellison, G., STRAUMFJORD, J.V.J. and Hummel, J.P. (1958) Buffer capacities of human blood and plasma. *Clinical Chemistry*. 4 (6), pp.452-61.

Erden, P.E., Kacar, C., Ozturk, F. and Kilic, E. (2015) Amperometric uric acid biosensor based on poly(vinylferrocene)-gelatin-carboxylated multiwalled carbon nanotube modified glassy carbon electrode. *Talanta*. 134 pp.488-495.

Fountoulakis, M. and Lahm, H.W. (1998) Hydrolysis and amino acid composition analysis of proteins. *Journal of Chromatography a*. 826 (2), pp.109-134.

Girousi, S.T., Pantazaki, A.A. and Voulgaropoulos, A.N. (2001) Mitochondria-based amperometric biosensor for the determination of L-glutamic acid. *Electroanalysis*. 13 (3), pp.243-245.

Good, N.E., Winget, G.D., Winter, W., Connolly, T.N., Izawa, S. and Singh, R.M. (1966) Hydrogen ion buffers for biological research. *Biochemistry*. 5 (2), pp.467-77.

Huizenga, J.R., Gips, C.H. and Tangerman, A. (1996) The contribution of various organs to ammonia formation: A review of factors determining the arterial ammonia concentration. *Annals of Clinical Biochemistry*. 33 pp.23-30.

Isabel Lopez, M., Pilar Callao, M. and Ruisancez, I. (2015) A tutorial on the validation of qualitative methods: From the univariate to the multivariate approach. *Analytica Chimica Acta*. 891 pp.62-72.

Kellum, J.A. (2000) Determinants of blood pH in health and disease. *Critical Care*. 4 (1), pp.6-14.

Kroll, M.H. and Elin, R.J. (1994) Interference with Clinical Laboratory Analyses. *Clinical Chemistry*. 40 (11), pp.1996-2005.

Labuz, J.M. and Takayama, S. (2014) Elevating sampling. *Lab on a Chip*. 14 (17), pp.3165-3171.

Liang, B., Zhang, S., Lang, Q., Song, J., Han, L. and Liu, A. (2015) Amperometric L-glutamate biosensor based on bacterial cell-surface displayed glutamate dehydrogenase. *Analytica Chimica Acta*. 884 pp.83-89.

Link, A.J. and LaBaer, J. (2011) Trichloroacetic acid (TCA) precipitation of proteins. *Cold Spring Harbor Protocols*. (8), pp.993-4.

Lodish, H., Berk, A., Zipursky, L., Matsudaira, P., Baltimore, D. and Darnell, J. (2000) *Molecular Cell Biology*. 4th ed. New York: W. H. Freeman.

Mach, A.J., Kim, J.H., Arshi, A., Hur, S.C. and Di Carlo, D. (2011) Automated cellular sample preparation using a Centrifuge-on-a-Chip. *Lab on a Chip*. 11 (17), pp.2827-2834.

Manabe, T. and Jin, Y. (2005) Alkaline cleavage of covalent bonds in chicken insulin and bovine alpha-lactalbumin analyzed by matrix-assisted laser desorption/ionization-mass spectrometry. *Electrophoresis*. 26 (1), pp.257-267.

Mohan, C. (2003) Buffers: A guide for the preparation and use of buffers in biological systems. *Calbiochem*.

Mundaca-Urbe, R., Bustos-Ramirez, F., Zaror-Zaror, C., Aranda-Bustos, M., Neira-Hinojosa, J. and Pena-Farfal, C. (2014) Development of a bienzymatic amperometric biosensor to determine uric acid in human serum, based on mesoporous silica (MCM-41) for enzyme immobilization. *Sensors and Actuators B-Chemical*. 195 pp.58-62.

Nikolac, N. (2014) Lipemia: causes, interference mechanisms, detection and management. *Biochemia Medica*. 24 (1), pp.57-67.

Norde, W. and Gage, D. (2004) Interaction of bovine serum albumin and human blood plasma with PEO-tethered surfaces: Influence of PEO chain length, grafting density, and temperature. *Langmuir*. 20 (10), pp.4162-4167.

Nuttall, S.L., Khan, J.N., Thorpe, G.H., Langford, N. and Kendall, M.J. (2003) The impact of therapeutic doses of paracetamol on serum total antioxidant capacity. *Journal of Clinical Pharmacy and Therapeutics*. 28 (4), pp.289-294.

Ortho-Clinical Diagnostics Inc. (2015) *Vitros Chemistry Products AMON Slides*. Available from: https://www.cmmc.org/cmmclab/IFU/AMON_MP2-90_EN_I.pdf.

Park, S. (2013) The Effects of High Concentrations of Vitamin C on Cancer Cells. *Nutrients*. 5 (9), pp.3496-3505.

Richards, P., Brown, C.L., Houghton, B.J. and Wrong, O.M. (1975) The incorporation of ammonia nitrogen into albumin in man: the effects of diet, uremia and growth hormone. *Clinical Nephrology*. 3 (5), pp.172-9.

Salvagno, G.L., Lippi, G., Gelati, M. and Guidi, G.C. (2012) Hemolysis, lipaemia and icterus in specimens for arterial blood gas analysis. *Clinical Biochemistry*. 45 (4-5), pp.372-373.

Sekisui Diagnostics (UK) Ltd. (2013) *Ammonia L3K®*. Available from: http://www.sekisuidiagnostics.com/writable/product_documents/files/Ammonia_L3K_SS_80-7440-00-02.pdf.

Shih, Y.T. and Huang, H.J. (1999) A creatinine deiminase modified polyaniline electrode for creatinine analysis. *Analytica Chimica Acta*. 392 (2-3), pp.143-150.

Sigma-Aldrich Co. LLC. (2015) *Ammonia Assay Kit*. Available from: <https://www.sigmaaldrich.com/content/dam/sigmaaldrich/docs/Sigma/Bulletin/aa0100bul.pdf>.

Spahr, P.F. and Edsall, J.T. (1964) Amino Acid Composition of Human and Bovine Serum Mercaptalbumins. *The Journal of Biological Chemistry*. 239 pp.850-4.

Sprinson, D.B. and Rittenberg, D. (1949) The rate of utilization of ammonia for protein synthesis. *The Journal of Biological Chemistry*. 180 (2), pp.707-14.

Sutariya, P.G., Pandya, A., Lodha, A. and Menon, S.K. (2016) A simple and rapid creatinine sensing via DLS selectivity, using calix[4]arene thiol functionalized gold nanoparticles. *Talanta*. 147 pp.590-7.

Svedberg, T. and Sjögren, B. (1930) The pH stability regions of serum albumin and of serum globulin. *Journal of the American Chemical Society*. 52 (7), pp.2855-2863.

Turner, A.P.F. (2013) Biosensors: sense and sensibility. *Chemical Society Reviews*. 42 (8), pp.3184-3196.

Voet, D. and Voet, J.G. (2004) *Biochemistry*. 3rd ed. USA: John Wiley & Sons, Inc.

Wang, J. (2006) Electrochemical biosensors: Towards point-of-care cancer diagnostics. *Biosensors & Bioelectronics*. 21 (10), pp.1887-1892.

Yadav, S., Kumar, A. and Pundir, C.S. (2011) Amperometric creatinine biosensor based on covalently coimmobilized enzymes onto carboxylated multiwalled carbon nanotubes/polyaniline composite film. *Analytical Biochemistry*. 419 (2), pp.277-283.

Yu, Z., Kastenmueller, G., He, Y., Belcredi, P., Moeller, G., Prehn, C., Mendes, J., Wahl, S., Roemisch-Margl, W., Ceglarek, U., Polonikov, A., Dahmen, N., Prokisch, H., Xie, L., Li, Y., Wichmann, H.-., Peters, A., Kronenberg, F., Suhre, K., Adamski, J., Illig, T. and Wang-Sattler, R. (2011) Differences between Human Plasma and Serum Metabolite Profiles. *Plos One*. 6 (7), pp.e21230.

Zheng, M., Wu, Y., Lu, L., Ding, K., Tang, F., Lin, Z. and Wu, X. (2011) Simultaneous analysis of acetaminophen, p-aminophenol and aspirin metabolites by hydrophilic interaction and strong anion exchange capillary liquid chromatography coupled to amperometric detection. *Journal of Separation Science*. 34 (16-17), pp.2072-2078.

CHAPTER 6

FUTURE DEVELOPMENTS

6.1. FURTHER DEVELOPMENTS OF THE BLOOD AMMONIA DEVICE

The device developed in this work facilitated the impedimetric measurement of ammonia in human serum over the physiologically relevant range. The device incorporated an inkjet-printed modified polyaniline sensor. Reliable measurements required reproducible sensors. This was assessed as inter-sensor variance which was seen to be 6.9% for $n = 15$. This was comparable with commercial sensors which typically possess 3 to 5% variation (DropSens, 2015). The sensor was used in conjunction with a gas-permeable membrane to aid the device in the determination of ammonia in an aqueous environment. The device included additional refinements to enhance its sensitivity. This included adjustment of the liquid sample pH to render it basic ($\text{pH} > 9$). Under such conditions, the equilibrium of ammonia and ammonium in liquid strongly favours the gaseous ammonia form. This increases the absolute mass of ammonia gas liberated from the liquid sample and so increases sensitivity. These characteristics, combined with careful optimisation of other aspects of the assay such as assay timings, have allowed for the effective detection of ammonia in a serum sample. Ammonia was determined in human serum across the clinically relevant levels of 25 to 200 μM with a calculated LOD of 12 μM , a coefficient of determination of 0.9984, slope of 0.0046 and an intercept of 1.1534 was generated for $n = 3$. Impedimetric device measurements were validated using a commercially available spectrophotometric assay kit for ammonia which resulted in excellent correlation (0.9699, $p < 0.0001$) with a slope of 1.4472 and an intercept of 0.5631 between both methods for $n = 3$.

The device has been fabricated in a simple and cost effective manner by combining laminar sheet processing combined with printed techniques. This simple, inexpensive and mass producible way of device production can be compared to earlier laboratory-based techniques available for the determination of blood ammonia which are expensive and involve complex instrumentation. Mass production of the devices would significantly reduce production costs. A factor that may also decrease manufacturing costs and improve throughput is miniaturisation of the device. Preliminary work has shown that the device may be reduced by 30% without impedimetric deterioration. A 50% reduction in polyaniline deposition, from ten layers to five, did not significantly change the response of the devices to

ammonia. Reducing the number of inkjet-printed polyaniline layers deposited onto electrodes is also a viable processing change in order to reduce printing time which is currently the most significant production bottleneck.

6.1.1. Reflections and lessons

6.1.1.1. Limitations

The main limitation of the developed ammonia device is matrix related interference. To compensate for this, the device incorporated an air purge to recover the sensor subsequent to sample exposure. Further work needs to be conducted to integrate this step as part of a simple device with a one-step-measurement. This may be carried by utilising a process called degas-driven flow. In this process, the air within a polymer sheet is removed by vacuum for storage. The device is brought to atmospheric conditions during use causing a pressure difference which drives the flow of air within the device (Dimov *et al.*, 2011). As opposed to recovering the device, another option for integration is to completely prevent the sensors response to water vapour. To do this, an absorbent layer may be attached to the gas headspace side of the PTFE membrane. While this might solve issues around matrix related water vapour interference, it may expose sensitivity issues. It is probable that ammonia may be retained in the absorbent layer as part of the water vapour. To overcome this, the absorbent layer may be impregnated with an alkaline reagent to encourage gaseous ammonia permeation. This has been demonstrated in the literature by impregnating the PTFE membrane with an alkaline reagent (Dobler *et al.*, 2006). The introduction of a means to change pH and prevent matrix related interferences *in situ* would reduce analysis time by 15 min. These concepts would aid complete integration of the device which is typically required for modern POC diagnostics.

6.1.1.2. Sensitivity and reproducibility

During the development of the printed polyaniline sensor it was evident that thinner inkjet-print films (< 5 layers) resulted in higher sensitivities. This is most apparent in Fig 3.18 insert, in which ten inkjet-print layers of polyaniline resulted in an increase of 1 k Ω upon exposure to 1 mM ammonia, whereas five layers increased by 2.5 k Ω upon exposure to the same concentration. Although thinner films resulted in higher sensitivities, they were also less reproducible. This is because the inkjet

printed films were not homogenous on the grainy silver electrode surface and therefore prone to variations in response. At the time of these studies, sensitivity was sacrificed for reproducibility. However, upon reflection, it is recommended to investigate smoothing of the silver electrode surface which would result in homogenous thin (< 5 layers) inkjet printed films with high sensitivity and reproducibility.

Sensitivity and reproducibility were affected during the pre-calibration process of the devices. Pre-calibration resulted in a 3.2 fold increase in sensitivity. However, this was accompanied with a reduction in device baseline reproducibility. The reason for this is not understood and further studies are recommended to examine the process of pre-calibration.

6.1.1.3. Optimisations

For the device to be commercially viable, further analytical and technological improvements are recommended. Improvements to the synthesis protocol of polyaniline nanodispersions are required to up-scale the process. Currently batches are polymerised on a 40 mL scale, up-scale may cause changes to the rate of the reaction and the homogeneity of the synthesis. Also, on a large scale, the post-synthesis processing of the dispersion such as centrifugation and dialysis may become unmanageable.

The synthesis protocol is also inherently prone to deviations. Use of the same synthesis parameters throughout this work resulted in considerable size variations of the polyaniline nanoparticles produced. These variations can also be compared to the diverse size of polyaniline nanoparticles reported in the literature using the same synthesis methodology (Han *et al.*, 2002, Moulton *et al.*, 2004, Ngamna *et al.*, 2007). These variations may have been caused during the centrifugation step of the synthesis. Subsequent to centrifugation, larger entities form a pellet. However, this pellet is not solid and leaks into the supernatant when decanting. This alters the average diameter of the nanoparticles and the overall concentration of the polyaniline nanodispersion. It remains unclear how this would be solved if commercialisation was to be realised. There are a number of alterations which could be implemented to improve the reproducibility of the devices. The use of a reaction chamber may be used to control the polymerisation process (temperature, pressure,

rate of the reaction). The ink may be optimisation with the use components such as surfactants, electrolytes, solvents and stabilisers. This would in turn improve the quality of the inkjet-print films deposited and reproducibility of the device. Further inkjet-print film assessments are recommended to examine rheology (surface tension and viscosity) and film formation (atomic force microscopy).

Analytical improvements include inter-sheet variation analysis. An extensive impedimetric baseline study on sheet to sheet device variations is required if the device is to be mass produced. In doing this, the statistical variations between devices may be established. This work has demonstrated that these variations occur during ink synthesis and/or the inkjet-print process.

A better understanding of the relevance of ζ -potential measurements for polyaniline-SDS colloidal suspension (DBSA/polyaniline nanoparticulate micelle is stabilised by a SDS micelle) is required. The issue of ζ -potential and stability may be more complex in a colloidal stabilised suspension, than in a single type of particle in a medium. Within the polyaniline dispersion, SDS micelles impart negative charges upon the DBSA/polyaniline micelles which create repulsion between the polyaniline nanoparticles and stabilises the dispersion. Further work is required in order to understand where the electrostatic surface potential (ζ -potential) of the micellar particles is being measured and what this value represents in this kind of system.

6.1.3. Further matrix and interference assessments

Proteins and lipids were seen to interfere with the impedimetric ammonia measurements using the devices. In order to fully evaluate this, higher concentrations of ammonia in serum should be analysed using the device. Although these higher concentrations may not be clinically relevant, they would allow assessment of the matrix effect of serum. It is possible that the device may be able to determine high concentration ammonia in serum.

In order for the device to achieve acceptable POC standards in serum, extensive matrix assessments and POC integrations are required. Compounds such as bilirubin, pyruvate and lactate are known to interfere with ammonia measurements and should be impedimetrically assessed using the device. Microfluidic technologies have accelerated lab-on-a-chip innovations (Labuz and Takayama, 2014). They have

facilitated *in situ* sample preparation, separation and combination on a miniaturised, disposable chip. In the case of the blood ammonia device, they may be utilised to produce delipidated and deproteinated serum samples using microvortices which trap large particles based on balanced sheer gradient and wall effect forces (Mach *et al.*, 2011).

6.2. INTEGRATED SENSING SYSTEMS

Sensors have achieved both academic and commercial success due to their accessibility and flexibility which make them ideal for use at the point of care. As modern healthcare moves towards decentralisation and personalised medicine, the demand for integrated sensors is ever increasing. Ideally, a fully printed POC device should be integrated into a system which consists of the sensing device, display, battery, measurement chip, communications chip, and a push button (Beni *et al.*, 2015). This device should have the capacity to be interfaced with a miniaturised potentiostat. Miniaturised potentiostats are being developed in parallel with sensor technologies to produce truly localised patient testing. The integration of the ammonia device developed in this work into a POC system will surpass current state-of-the-art POC technologies which require wet chemistry reactions, complex laboratory equipment, and trained personnel.

6.3. OTHER APPLICATIONS AND ALTERNATIVE TECHNIQUES

6.3.1. Wearable sensors

The next generation of POC sensing systems is targeting fully-integrated and wearable platforms. Wearable sensors provide real time non-invasive health information. There has been rising interest in fully integrated wearable sensors which combines textiles and electroanalysis (Windmiller and Wang, 2013). Fully printed smart patches may be fabricated utilising polyaniline for the determination of ammonia in sweat. Ammonia determination via a wearable sensor may be explored using polymers (Seesaard *et al.*, 2015).

6.3.2. Clinical and environmental gas-based ammonia measurements

The sensor technology developed in this work may be applied to gaseous ammonia determination for use in clinical and environmental testing. The clinical standard for measuring ammonia is through blood analysis. However, due to the challenges and complications associated with blood ammonia sampling, there has been a significant increase in interest in other sample matrices in which to measure ammonia. In particular, there has been major development in the field of breath ammonia measurement. Previous work in our group have applied a polyaniline sensor for breath ammonia measurements for the efficacy of haemodialysis and correlated them with blood urea nitrogen levels (Hibbard *et al.*, 2013). Ammonia gas based analysis also has application in the environment, these include farming emissions (Hristov *et al.*, 2011), automotive exhaust emissions (Moos *et al.*, 2002), refrigeration leaks (Lopes *et al.*, 2015), along with gas (Erisman *et al.*, 2001) and water (Costa and Guilhermino, 2015) pollution.

6.3.3. Enzymatic biosensors

The developed ammonia device platform may be combined with enzymes for further application of diagnostic value. Pathological illnesses such as renal dysfunction and muscular dysfunction may be identified utilising ammonia generating enzymes such as creatinine deaminase, glutamate dehydrogenase and urease (Fig. 7.1 (a), (b) and (c), respectively). The ammonia released during these enzymatic reactions is proportional to substrate blood levels and may be quantified using the ammonia device. Normal blood levels of creatinine (44 - 106 μM), glutamate (150 μM) and urea (2.5 – 7.9 mM) are within the detection capabilities of the developed ammonia device (Tietz, 1987).

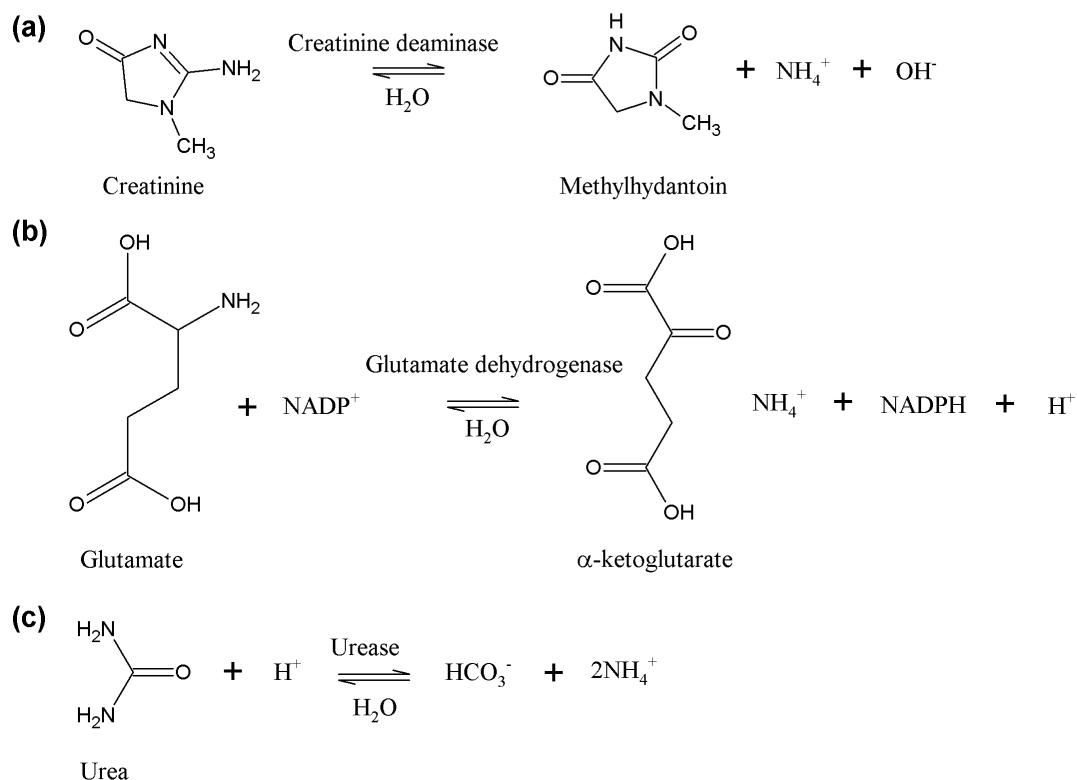


Figure 7.1. Enzymatic reactions which generate ammonia (a) creatinine deaminase, (b) glutamate dehydrogenase and (c) urease.

Polyaniline has been combined with these enzymes to produce sensors for the aforementioned illnesses (Zhybak *et al.*, 2016, Batra *et al.*, 2014, Suman *et al.*, 2011).

6.3.4. Alternative techniques to impedimetric ammonia analysis

The measurement of ammonia using polyaniline is an indirect measurement of the analyte, whereby deprotonation of the polymer backbone is proportional to analyte concentration. The measurement of this interaction may be carried out using amperometry and has been demonstrated by Crowley *et al.*, (2008) using an inkjet printed polyaniline sensor for aqueous ammonia in refrigerant waste water via an amperometric flow injection system. Combining the amperometric determination of ammonia demonstrated by Crowley *et al.* (2008) and the knowledge gained during the development of this thesis, an amperometric POC blood ammonia sensor may be realised using a gel electrolyte to regenerate the polyaniline sensor.

The Berthelot reaction has formed the basis of numerous POC ammonia technologies which utilise the spectrophotometric determination of ammonia (Arkray, 2016, Ortho-Clinical Diagnostics Inc., 2015, Abcam Plc., 2016). Spectrophotometric determinations of ammonia may also be conducted utilising the inherent colour change of polyaniline upon exposure to ammonia. This principle has been used by Florea *et al.*, (2013), micro-capillaries were coated with polyaniline nanofibres which were monitored upon exposure to ammonia and recovered with hydrochloric acid.

Polyaniline is an extremely versatile sensing material and its full capacity may be harnessed to produce an optical and electrochemical sensor. Frequency-resolved periodic optical (transmission) and electrical (impedance) responses of polyaniline films grown electrochemically on indium tin oxide electrodes has been studied (Kalaji and Peter, 1991). The device developed in this work was fabricated upon a transparent PET substrate and so it may be combined with an LED optical monitoring system (Cogan *et al.*, 2014).

6.4. REFERENCES

- Abcam Plc. (2016) *Ammonia Assay Kit - Modified Berthelot - (Colorimetric) (ab102509)*. Available from: <http://www.abcam.com/ammonia-assay-kit-modified-berthelot-colorimetric-ab102509.html>.
- Arkray, I. (2016) *Blood Ammonia Meter PocketChem BA PA-4140*. Available from: <http://www.arkray.co.jp/english/products/pdf/pa4140.pdf>.
- Batra, B., Kumari, S. and Pundir, C.S. (2014) Construction of glutamate biosensor based on covalent immobilization of glutamate oxidase on polypyrrole nanoparticles/polyaniline modified gold electrode. *Enzyme and Microbial Technology*. 57 pp.69-77.
- Beni, V., Nilsson, D., Arven, P., Norberg, P., Gustafsson, G. and Turner, A.P.F. (2015) Printed Electrochemical Instruments for Biosensors. *Ecs Journal of Solid State Science and Technology*. 4 (10), pp.S3001-S3005.
- Cogan, D., Cleary, J., Fay, C., Rickard, A., Jankowski, K., Phelan, T., Bowkett, M. and Diamond, D. (2014) The development of an autonomous sensing platform for the monitoring of ammonia in water using a simplified Berthelot method. *Analytical Methods*. 6 (19), pp.7606-7614.
- Costa, S. and Guilhermino, L. (2015) Influence of Long-Term Exposure to Background Pollution on the Response and Recovery of the Invasive Species *Corbicula fluminea* to Ammonia Sub-lethal Stress: a Multi-marker Approach with Field Estuarine Populations. *Water Air and Soil Pollution*. 226 (4), pp.95.
- Crowley, K., O'Malley, E., Morrin, A., Smyth, M.R. and Killard, A.J. (2008) An aqueous ammonia sensor based on an inkjet-printed polyaniline nanoparticle-modified electrode. *Analyst*. 133 (3), pp.391-399.
- Dimov, I.K., Basabe-Desmots, L., Garcia-Cordero, J.L., Ross, B.M., Ricco, A.J. and Lee, L.P. (2011) Stand-alone self-powered integrated microfluidic blood analysis system (SIMBAS). *Lab on a Chip*. 11 (5), pp.845-850.
- Dobler, L.J., Ibbons, J.M. and Evtodienko, V.Y. (2006) *Quick Acting Toxic Ammonia Test for Aqueous Samples* Hach Company US7033839 B1.
- DropSens (2015) *Innovative Technology for Miniturised Electrochemistry*. Available from: <http://www.dropsens.com/en/home.html>.
- Erisman, J.W., Otjes, R., Hensen, A., Jongejan, P., van den Bulk, P., Khlystov, A., Mols, H. and Slanina, S. (2001) Instrument development and application in studies and monitoring of ambient ammonia. *Atmospheric Environment*. 35 (11), pp.1913-1922.
- Florea, L., Diamond, D. and Benito-Lopez, F. (2013) Polyaniline coated micro-capillaries for continuous flow analysis of aqueous solutions. *Analytica Chimica Acta*. 759 pp.1-7.

Han, M.G., Cho, S.K., Oh, S.G. and Im, S.S. (2002) Preparation and characterization of polyaniline nanoparticles synthesized from DBSA micellar solution. *Synthetic Metals*. 126 (1), pp.53-60.

Hibbard, T., Crowley, K., Kelly, F., Ward, F., Holian, J., Watson, A. and Killard, A.J. (2013) Point of Care Monitoring of Hemodialysis Patients with a Breath Ammonia Measurement Device Based on Printed Polyaniline Nanoparticle Sensors. *Analytical Chemistry*. 85 (24), pp.12158-12165.

Hristov, A.N., Hanigan, M., Cole, A., Todd, R., McAllister, T.A., Ndegwa, P.M. and Rotz, A. (2011) Review: Ammonia emissions from dairy farms and beef feedlots. *Canadian Journal of Animal Science*. 91 (1), pp.1-35.

Kalaji, M. and Peter, L.M. (1991) Optical and Electrical Ac Response of Polyaniline Films. *Journal of the Chemical Society-Faraday Transactions*. 87 (6), pp.853-860.

Labuz, J.M. and Takayama, S. (2014) Elevating sampling. *Lab on a Chip*. 14 (17), pp.3165-3171.

Lopes, T.J., Barros, R., dos Santos, N.L., Costelli, M.C., da Silva, A. and Cancelier, A. (2015) Risk Analysis Applied to Industrial Refrigeration Installations that use Ammonia. *Revista Eletronica Em Gestao Educacao E Tecnologia Ambiental*. 19 (1), pp.160-166.

Mach, A.J., Kim, J.H., Arshi, A., Hur, S.C. and Di Carlo, D. (2011) Automated cellular sample preparation using a Centrifuge-on-a-Chip. *Lab on a Chip*. 11 (17), pp.2827-2834.

Moos, R., Muller, R., Plog, C., Knezevic, A., Leye, H., Irion, E., Braun, T., Marquardt, K.J. and Binder, K. (2002) Selective ammonia exhaust gas sensor for automotive applications. *Sensors and Actuators B-Chemical*. 83 (1-3), pp.181-189.

Moulton, S.E., Innis, P.C., Kane-Maguire, L.A.P., Ngamna, O. and Wallace, G.G. (2004) Polymerisation and characterisation of conducting polyaniline nanoparticle dispersions. *Current Applied Physics*. 4 (2-4), pp.402-406.

Ngamna, O., Morrin, A., Killard, A.J., Moulton, S.E., Smyth, M.R. and Wallace, G.G. (2007) Inkjet printable polyaniline nanoformulations. *Langmuir*. 23 (16), pp.8569-8574.

Ortho-Clinical Diagnostics Inc. (2015) *Vitros Chemistry Products AMON Slides*. Available from: https://www.cmmc.org/cmmclab/IFU/AMON_MP2-90_EN_I.pdf.

Seesaard, T., Lorwongtragool, P. and Kerdcharoen, T. (2015) Development of Fabric-Based Chemical Gas Sensors for Use as Wearable Electronic Noses. *Sensors*. 15 (1), pp.1885-1902.

Suman, O'Reilly, E., Kelly, M., Morrin, A., Smyth, M.R. and Killard, A.J. (2011) Chronocoulometric determination of urea in human serum using an inkjet printed biosensor. *Analytica Chimica Acta*. 697 (1-2), pp.98-102.

Chapter 6

Tietz, N.W. (1987) *Fundamentals of Clinical Chemistry*. 3rd ed. Philadelphia: WB Saunders.

Windmiller, J.R. and Wang, J. (2013) Wearable Electrochemical Sensors and Biosensors: A Review. *Electroanalysis*. 25 (1), pp.29-46.

Zhybak, M., Beni, V., Vagin, M.Y., Dempsey, E., Turner, A.P.F. and Korpan, Y. (2016) Creatinine and urea biosensors based on a novel ammonium ion-selective copper-polyaniline nano-composite. *Biosensors & Bioelectronics*. 77 pp.505-511.

CHAPTER 7

OVERALL CONCLUSIONS

7.1. CONCLUSIONS

This thesis describes the development of a device for facilitating the measurement of ammonia in blood. It is based on an impedance sensing principle and works in conjunction with a polyaniline nanoparticle based sensing material which is sensitive and selective towards ammonia. The polyaniline nanoparticles were synthesised using micellar polymerisation of aniline in the presence of APS in a DBSA micellar solution. This solution was dialysed against a surfactant forming an aqueous co-colloidal printable ink. Polyaniline nanodispersions were then inkjet print deposited onto a silver screen printed IDEs to form an ammonia sensor. This sensor was encapsulated into a device which facilitated the measurement of aqueous ammonia. The device was pre-calibrated which improved the reproducibility of the responses from 8.65 to 2.98% at ambient conditions. However, when stored in a desiccator, the pre-calibration procedure resulted in a 3.2 fold increase of the ammonia response.

Prior to ammonia sensing, characteristics of the polyaniline nanodispersions were analysed. Their impact on the sensing ability of the fabricated sensors was assessed. It was observed that nanoparticle size and ζ -potential varied between each batch. The variation in size has been demonstrated in literature with contradicting reports of size. This suggests that the micellar polymerisation method is prone to variations. Variations in ζ -potential may be explained by the nature of the polyaniline nanodispersion which is stabilised with surfactant micelles. Therefore, the measurement of the polyaniline nano-sized micelles may not be possible alone, rather the surfactant micelles may also be considered. The impact of size and ζ -potential on sensor impedance was assessed and there were no significant relationships observed. Thus, the measurement of size and ζ -potential are irrelevant with respect to sensor performance.

Early work of the thesis revealed water vapour from the matrix were interfering with the measurement, preventing the determination of the lowest levels of ammonia necessary for blood testing (11 to 50 μM). Therefore, additional means were introduced to remove the water vapour signal by forcing a controlled amount of air across the sensor. Ammonia gas has a high affinity for the sensor and so remained in contact. However, water vapour has only low affinity and is also liable to

evaporation from the surface and thus was quickly removed. This resulted in a final signal which was due to the presence of ammonia alone ($R^2 = 0.9868$, $n = 3$).

Matrix interference studies were conducted with ammonia associated compounds and electroactive species at clinically relevant concentrations. There was no interference observed with the measurement of ammonia (30 μM). This demonstrated the capability of the device to determine ammonia in a biological matrix. Prior to serum analysis, a protein matrix was evaluated. Ammonia was determined in protein, amongst challenges of non-linearity and reproducibility. These challenges were further complicated when human serum matrix was assessed. It appeared that both proteins and lipids interfered with the impedimetric measurement of ammonia. The human serum required the removal of lipids and proteins. This was achieved by centrifuging delipidated serum with a spin filter column.

Ammonia was determined in delipidated deproteinated human serum across the clinically relevant levels of 25 to 200 μM with a calculated limit of detection (LOD) of 12 μM , a coefficient of determination of 0.9984, slope of 0.0046 and an intercept of 1.1534 was generated for $n = 3$. Impedimetric device measurements were validated using a commercially available Abcam® spectrophotometric assay kit for ammonia which resulted in excellent correlation (0.9699, $p < 0.0001$) with a slope of 1.4472 and an intercept of 0.5631 between both methods for $n = 3$. The Abcam® assay also suffered similar, if not worse, interferences and inhibition from proteins and lipids. Therefore, it can be concluded that the developed blood ammonia device achieved minimum commercial requirements as set by the Abcam® assay kit. The reproducibility of the device for $n = 15$ was 6.9%. They were seen to be stable for up to five months.

7.2. CLOSING STATEMENT

This thesis has demonstrated that fabrication techniques such as screen and inkjet printing technologies may be used in combination with advanced materials such as polymer nanoparticles to produce low cost, disposable devices suitable for the determination of blood ammonia at the point of care. While further developments are required to make them viable for clinical use, significant proof of concept has

Chapter 7

been demonstrated, with routes to effective implementation identified. The inexpensive, low cost, printed and laminar nature of the devices make them highly compatible with existing commercial ammonia assays for the determination of blood ammonia.

LIST OF PUBLICATIONS AND PRESENTATIONS

1. SCIENTIFIC PUBLICATIONS

- **Brannelly, N.T.** and Killard, A.J. (2017) A Printed and Microfabricated Sensor Device for the Sensitive Low Volume Measurement of Aqueous Ammonia. *Electroanalysis*. 29 (1), pp.162-171.
- **Brannelly, N.T.** and Killard, A.J. (2017) Inkjet printable nanomaterials and nanocomposites for sensor fabrication in *Nanomaterials for 2D and 3D printing* (eds Shacham-Diamand, Y., Magdassi, S.) Germany:Wiley-VCH.
- **Brannelly, N.T.,** Hamilton-Shield, J.P. and Killard, A.J. (2016) The Measurement of Ammonia in Human Breath and its Potential in Clinical Diagnostics. *Critical Reviews in Analytical Chemistry*. 46 (6), pp.490-501.
- **Brannelly N.T.,** Killard, A.J. Fabrication of an aqueous ammonia sensor for potential blood ammonia determination (manuscript submitted to *Sensors and Actuators B*).
- **Brannelly N.T.** and Killard A.J. Optimisation and characterisation of polyaniline nanoparticle ink production and sensor fabrication (manuscript in preparation for *Journal of Materials Chemistry*).

2. ORAL PRESENTATIONS

- **Brannelly N.T.,** Hamilton-Shield, J.P., Killard A.J., *Printed polyaniline nanoparticle sensors for the determination of ammonia in an aqueous environment*
ESEAC 16 The Assembly Rooms, Bath, UK on June 12th to 16th, 2016
- **Brannelly N.T.,** Hamilton-Shield, J.P., Killard A.J., *Gaseous ammonia determination in an aqueous environment using printed polyaniline sensors*
GASG Rising Stars in Gas Sensing Cranfield University, UK on April 21st, 2016

Publications and presentations

- **Brannelly N.T.**, Hamilton-Shield, J.P., Killard, A.J., *Application of printed polyaniline for blood ammonia determination*
Electrochem 2015 Durham University, UK on September 13th, 2015*
*Santander Travel Bursary awarded
- **Brannelly N.T.**, Hamilton-Shield, J.P., Killard, A.J., *Impedimetric detection of ammonia using printed polyaniline-modified electrodes*
9th Postgraduate Research Topics Meeting in Electroanalysis Birkbeck, University of London, UK, on December 4th, 2014
- **Brannelly N.T.**, Hamilton-Shield, J.P., Killard, A.J., *Development of a point-of-care device for blood ammonia*
RSC Analytical Research Forum Burlington House, Piccadilly, London, UK on July 7th, 2014
- **Brannelly N.T.**, Hamilton-Shield, J.P., Killard, A.J., *Fabrication of a blood ammonia sensor*
Summer Sessions – Best of Faculty Fora Exhibition and Conference Centre, Bristol, UK on July 3rd, 2014
- **Brannelly N.T.**, Hamilton-Shield, J.P., Killard, A.J., *Determination of blood ammonia via a point-of-care printed device*
Centre for Research in Biosciences Seminar UWE, Bristol, UK on June 20th, 2014

3. POSTER PRESENTATIONS

- **Brannelly N.T.**, Hamilton-Shield, J.P., Killard A.J., *Development of a Point-of-Care Device for Measuring Blood Ammonia*
Sensors in Medicine 2016, DoubleTree by Hilton Docklands, London, UK on November 9th to 10th, 2016

Publications and presentations

- **Brannelly N.T.**, Hamilton-Shield, J.P., Killard A.J., *Optimisation and characterisation of polyaniline nanoparticle ink production and sensor fabrication*
ESEAC 16 The Assembly Rooms, Bath, UK on June 12th to 16th, 2016
- **Brannelly N.T.**, Hamilton-Shield, J.P., Killard, A.J., *Impedimetric assessment of polyaniline modified silver electrodes for blood ammonia sensing**
Sensors in Medicine 2015, Royal Geographic Society, Kensington, London on March 24th to 26th, 2015
*1st place poster presentation winner
- **Brannelly N.T.**, Hamilton-Shield, J.P., Killard, A.J., *Impedimetric assessment of polyaniline modified silver electrodes for blood ammonia sensing*
Sensors in Medicine 2014 Royal Geographic Society, Kensington, London on March 25th to 26th, 2014
- **Brannelly N.T.**, Hamilton-Shield, J.P., Killard, A.J., *Printed sensors for the determination of blood ammonia*
ESEAC 2014 Malmö University, Sweden on June 12th to 16th, 2014
- **Brannelly N.T.**, Hamilton-Shield, J.P., Killard, A.J., *Development of a point-of-Care diagnostic device for blood ammonia**
Postgraduate Research Conference UWE, Bristol, UK on June 27th, 2014
*1st place poster presentation winner
- **Brannelly N.T.**, Hamilton-Shield, J.P., Killard, A.J., *Development of a point-of-care device for blood ammonia*
Great Western Electrochemistry Meeting University of Bath, UK on June 3rd, 2013

Publications and presentations

- **Brannelly N.T.**, Hamilton-Shield, J.P., Killard, A.J., *Electrochemical sensor development for blood ammonia*
The 3rd International Conference on Bio-Sensing Technology Hotel Melia, Sitges, Spain on May 12th to 15th, 2013
- **Brannelly N.T.**, Hamilton-Shield, J.P., Killard, A.J., *The development of electrochemical sensors for blood ammonia*
Electrochem 2013 University of Southampton, UK on September 1st to 3rd, 2013

APPENDIX

Appendix

Appendix I. Inter- and intra-sensor differences accompanied with statistical information for $n = 15$.

Sensor	Mean	SD	RSD%
1	397.2	0.3	0.1
2	423.0	0.5	0.1
3	413.4	0.6	0.1
4	400.5	0.5	0.1
5	370.3	0.6	0.2
6	386.4	0.7	0.2
7	444.1	0.6	0.1
8	403.5	0.5	0.1
9	412.2	0.4	0.1
10	400.4	0.3	0.1
11	366.6	0.3	0.1
12	355.9	0.3	0.1
13	367.4	0.3	0.1
14	357.8	0.3	0.1
15	358.9	0.4	0.1
Mean	390.5	0.4	0.1

Appendix II. Statistical impedimetric data for increased inkjet-printed layers of polyaniline during the measurement of 1 mM ammonia as ammonium chloride ($n = 3$).

Inkjet-printed polyaniline layers	Z/Z_{air}	Z_{air}	Z
Mean			
1	4.81	23437.21	110746.91
5	3.89	863.78	3361.10
10	3.82	314.97	1198.25
20	2.44	209.87	511.99
40	1.00	269.50	269.13
SD			
1	1.87	2007.32	34072.54
5	0.39	30.80	412.36
10	0.33	28.32	97.75
20	0.19	3.56	32.10
40	0.02	19.15	17.32
%RSD			
1	38.82	8.56	30.77
5	10.14	3.57	12.27
10	8.65	8.99	8.16
20	7.77	1.70	6.27
40	1.85	7.11	6.43

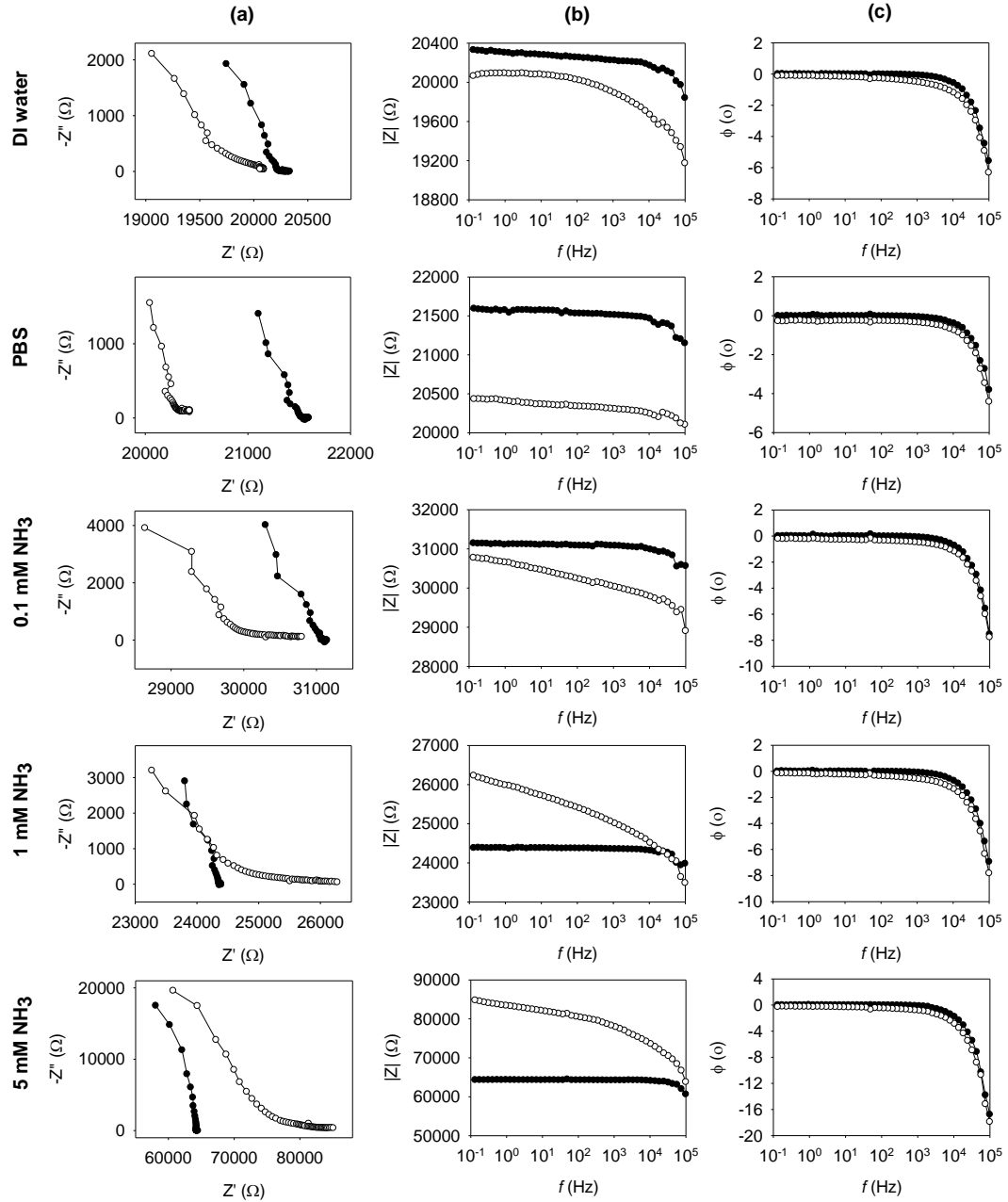
Appendix

Appendix III. The change in impedance of aqueous ammonia devices upon exposure to ammonia.

Concentration of NH ₃ (mM)	Z (Ω)	Z_{air} (Ω)	$Z-Z_{air}$ (Ω)	Z/Z_{air}
DI water	19909.74	20230.78	-321.04	0.98
0	20329.3	21508.65	-1179.36	0.95
0.1	30204.82	31046.05	-841.22	0.97
1	25278.78	24335.45	943.32	1.04
5	78871.15	64084.10	14787.05	1.23

Appendix

Appendix IV. Impedance spectroscopic analysis of the preliminary devices firstly in air (●) and secondly in DI water, PBS and 0.1, 0.5, 1 mM ammonia in PBS (○). Data is represented as (a) Nyquist, (b) Bode modulus, and (c) phase angle from 0.1 Hz to 100 kHz.



Appendix

Appendix V. Impedance response (Z/Z_{air}) results of ammonia concentrations in PBS pH 11.0 as determined by ammonia devices at $n = 3$.

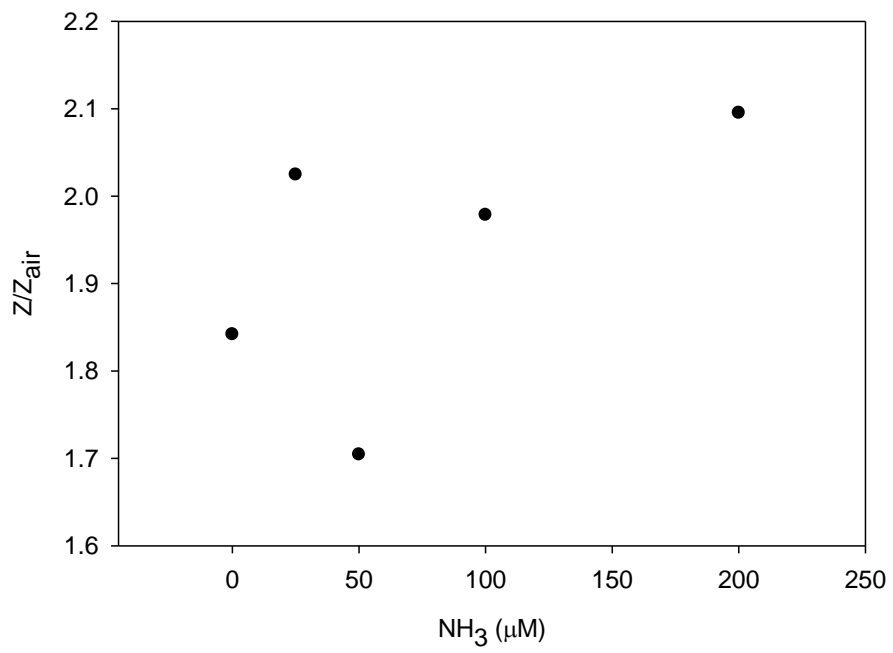
Ammonia (μM)	Average Z/Z_{air}	SD	%RSD
200	1.86	0.08	4.23
150	1.59	0.06	3.89
100	1.33	0.03	2.09
50	1.16	0.01	0.94
25	1.07	0.01	0.77
0	1.00	0.01	1.17

Appendix

Appendix VI. Statistical data of the ammonia device in response to ammonia in BSA (n = 3).

NH₃ (μM)	1	2	3	Mean	SD	%RSD
200	3.11	2.43	2.34	2.37	0.06	2.67
150	2.29	2.34	2.26	2.29	0.04	1.68
100	2.10	2.29	2.17	2.19	0.09	4.30
50	2.16	1.90	1.88	1.98	0.16	7.95
25	2.00	1.86	1.83	1.90	0.09	4.76
0	1.66	1.75	1.65	1.69	0.05	3.08

Appendix VII. Impedance response (Z/Z_{air}) results of ammonia concentrations in delipidated human serum as determined by ammonia devices.



Doras feasa fiafraí